NOTE TO USERS

This reproduction is the best copy available.

UMI

SCHWANN CELL APOPTOSIS IN AN IN VITRO MODEL OF DIABETIC NEUROPATHY: MITOCHONDRIAL DYSFUNCTION AND THE PERMEABILITY TRANSITION PORE

by

Hardy Joseph Rideout

Submitted in Partial Fulfillment of the Requirements for the
Degree of Doctor of Philosophy

at

Dalhousie University
Halifax, Nova Scotia

March 1999

0-612-49286-9

This thesis is dedicated to my parents
David and Patricia Rideout, and my sister Jodie

and to my wife Tracey

Table of Contents

List of Figures and Tables

Abstract

This thesis describes the development of a novel in vitro Schwann cell isolation method that results in the establishment of two populations of Schwann cells depending upon the age of the rat used. Schwann cells from PD15 rat sciatic nerve proliferate in vitro without the need for additional growth factor supplementation, whereas PD2 Schwann cells require further support to induce proliferation. These two populations were used to investigate the direct effects of high glucose on Schwann cell survival.

It was shown that exposure to high glucose leads to a dose- and time-dependent decrease in survival in both populations of Schwann cells. Significant cell death was observed at 2 hr following exposure to high glucose by counts of intact nuclei. Using two independent in situ markers of the nuclear changes associated with the final degradative phase of apoptosis, chromatin condensation and internucleosomal DNA fragmentation, a significant proportion of this cell loss was determined to be due to apoptosis. Dual staining revealed that while internucleosomal DNA fragmentation was not present at 2 hr following exposure to high glucose, significant changes in nuclear structure were evident, including the presence of nuclear blebs, which have been observed in other models of apoptotic cell death. In addition, the anti-apoptotic agents IGF-I, NAC, and DMD each prevented cell loss observed at 2 hr following exposure to 40 mM glucose, suggesting that the death observed at this time point was indeed apoptotic.

A central convergence point in many forms of apoptosis is the opening of a mitochondrial megapore, known as the permeability transition pore (PTP), coupled to the collapse of the voltage potential across the inner mitochondrial membrane ($\Delta\Psi_M$). It was shown here that exposure to high glucose induced a time-dependent decrease in $\Delta\Psi_M$ that was preventable by anti-apoptotic agents that improve Schwann cell survival. It was further shown that the PTP was involved in high glucose induced apoptosis. An agent that maintains PTP closure, cyclosporin A, maintained $\Delta\Psi_M$ and prevented the death of Schwann cells in high glucose media. Using confocal imaging it was determined that the localization of hexokinase at the PTP was dependent upon $\Delta\Psi_M$ and the conformation of the PTP, further implicating mitochondria in high glucose induced apoptosis. Western blot analysis of sub-cellular fractions confirmed the findings of others showing that the pro-apoptotic protein, Bax, was increased in enriched mitochondrial fractions of Schwann cells exposed to high glucose.

Taken together, these findings demonstrate for the first time that high glucose is toxic to Schwann cells in vitro, and that the cells die via apoptosis. It was further shown that this process involved a disruption of mitochondrial function at the PTP through a re-distribution of the proteins Bax and hexokinase.

Abbreviations and Symbols

AIF	Apoptosis initiating factors
ANT	Adenine nucleotide translocator
AraC	Cytosine arabinoside
ATP	Adenosine triphosphate
ATPase	Adenosine triphosphatase
ATR	Atractyloside
BDNF	Brain-derived neurotrophic factor
BH	Bcl-2 homology domain
BPE	Bovine pituitary extract
BrdU	Bromodeoxyuridine
cAMP	cyclic adenosine monophosphate
CMTMR	Chloromethyl-tetramethlyrosamine methyl ester
CMXRos	Chloromethyl-X-rosamine
ΣCMAP	Summated compound muscle action potential
CNPase	2',3'-cyclic nucleotide 3'-phosphodiesterase
CNS	Central nervous system
CNTF	Ciliary neurotrophic factor
CrK	Creatine kinase
CsA	Cyclosporin A
CT	Cholera toxin

DCCT	Diabetes Control and Complications Trial
DHAP	Dihydroxyacetone-phosphate
DiOC$_6$	3,3'-dihexyloxacarbocyanine iodide
DM	Diabetes mellitus
DMD	(-)-Desmethyldeprenyl
DMEM	Dulbecco's modified Eagle's medium
DNA	Deoxyribonucleic acid
DPN	Diabetic polyneuropathy
DRG	Dorsal root ganglion
$\Delta\Psi_M$	Mitochondrial membrane potential
ECL	Enhanced chemiluminescence
EDTA	Ethylene diamine tetracetic acid
ELISA	Enzyme-linked immunosorbent assay
FADH$_2$	Reduced flavin adenine dinucleotide
FBP	Fructose bisphosphate phosphatase
FBS	Fetal bovine serum
FITC	Fluorescein isothiocyanate
FIU	Fluorescence intensity units
FRET	Fluorescence resonance energy transfer
GalC	Galactocerebroside
GAP-43	Growth-associated protein-43
GAPDH	Glyceraldehyde 3-phosphate dehydrogenase

GFAP	Glial fibrillary acidic protein
GFP	Green fluorescent protein
GLUT	Glucose transporter
GSH	Reduced glutathione
GSSH	Oxidized glutathione
H_2O_2	Hydrogen peroxide
HBSS	Hank's buffered salt solution
HK	Hexokinase
H-reflex	Hoffmann's reflex
ICE	Interleukin converting enzyme
IDDM	Insulin-dependent diabetes mellitus
IFN-γ	Interferon-gamma
IGF	Insulin-like growth factor
IL	Interleukin
ISEL	In situ end-labeling
JC-1	5,5', 6,6'-tetrachloro-1,1',3,3'-tetraethybenzimidazol carbocyanine iodide
JNK	c-Jun N-terminal kinase
L-NIL	N^{6}-(1-iminoethyl)-L-lysine
LPS	Lipopolysaccharide
MAG	Myelin associated glycoprotein
MAPK	Mitogen-activated protein kinase

MBP	Myelin basic protein
MHC	Major histocompatibility class
MTG	MitoTracker green
NAC	N-acetyl cysteine
NADH	Reduced nicotinamide adenine dinucleotide
NADPH	Reduced nicotinamide dinucleotide phosphate
NAO	Nonyl acridine orange
NCAM	Neural cell adhesion molecule
NDS	Neurological disability score
NF	Neurofilament
NGF	Nerve growth factor
NIDDM	Non-insulin-dependent diabetes mellitus
NO	Nitric oxide
NOS	Nitric oxide synthase
NT	Neurotrophin
$\bullet O_2^-$	Superoxide anion
OONO$^-$	Peroxynitrite
PBS	Phosphate buffered saline
PBz	Peripheral benzodiazepine binding protein
PD	Postnatal day
PFK	Phosphofructokinase
PLP	Proteolipid protein

PMP22	Peripheral myelin protein-22
PNS	Peripheral nervous system
PPP	Pentose phosphate pathway
PTP	Permeability transition pore
P_0	Protein zero
RDNS	Rochester Diabetic Neuropathy Study
RNA	Ribonucleic acid
ROS	Reactive oxygen species
SDS	Sodium dodecyl sulfate
SMTC	S-methyl thiocitrulline
SNAP	S-nitroso acetylpenicillamine
ΣSNAP	Summated sensory nerve action potential
SOD	Superoxide dismutase
STZ	Streptozotocin
TCA	Tricarboxylic acid (cycle)
TdT	Terminal deoxynucleotidyl transferase
TMRM	Tetramethylrhodamine methyl ester
TNF-α	Tumor necrosis factor-alpha
VDAC	Voltage dependent anion channel (porin)
WD	Wallerian degeneration

Acknowledgements

I would like to express my thanks and gratitude to my supervisor Dr. Nadine Tatton for the past 4 years of unending support, faith, and encouragement. I will take with me not only the skills that she has taught me, but also a greater enthusiasm for science and an appreciation for the enjoyment of the process.

I would also like to thank Dr. William Tatton for the guidance and advice given during the past 4 years, and for the introduction into the world of mitochondria and apoptosis. I would also like to thank him for the expert instruction on the confocal microscope, and for invaluable scientific feedback.

I would like to thank my co-supervisor, and graduate co-ordinator Dr. Theo Hagg for his support and guidance, especially during the move to New York. I also thank the members of my advisory committee, Dr. Howard H. Ellenberger, Dr. Ivar Mendez, and Dr. Catherine B. Lazier for their help and feedback during this work.

I thank my friends and colleagues in the lab, Sai Shankar, Graeme Carlile, Katherine Borden, Ruth Chalmers-Redman, Chen Meng, Teena Chase, Molly Mammen, and Andrew Fraser for support, advice, friendship, and much-needed feedback on the thesis. As well, I would like to thank my friends and fellow graduate students back at Dalhousie, Matt, Anne Marie, Krista, Leticia, Nicole, and so many others.

I would also like to thank my family and friends back in Nova Scotia and Ontario for always being there with their support and kindness. And also to my parents, David and Patricia, and my sister, Jodie for their love.

Finally, I am grateful to my wife Tracey, without whose love and support I would not have been able to finish this.

I. Introduction

Diabetes mellitus (DM) is a metabolic disorder characterized by abnormal carbohydrate metabolism. Two distinct manifestations have been identified with different etiologies and interventions, Type I (insulin dependent diabetes mellitus) and Type II (non-insulin dependent diabetes mellitus). Type I DM is caused by an autoimmune-mediated destruction of pancreatic β-cells, and therefore requires insulin treatment. Type II DM is a non-autoimmune disease associated with degrees of insulin resistance or attenuated insulin release. Estimates of the incidence of DM have ranged between 2-3% of the population in the United States. The percentage of people with DM varies greatly with age; approximately 10% of people over age 64 develop DM while only 0.8% of people less than 45 years of age develop DM (Porte and Halter, 1999). The major complications associated with DM, in addition to neuropathy, include arteriosclerosis, particularly coronary artery disease which is the most common cause of death in diabetics. Arteriosclerosis in the lower legs, often leads to gangrenous ulcers and amputation. The development of kidney disease is also common in diabetics, and two nephropathic syndromes have been identified, nodular glomerulosclerosis and tubular nephrosis. One of the most characteristic findings in diabetic patients is retinopathy, manifested by edema, microaneurysms, and hemorrhages or retinitis proliferans. The developments of cataracts, which has been attributed to accumulation of sorbitol in the lens (Beyer-Mears and Cruz, 1985), is also a common presentation in diabetic patients.

Approximately 50% of patients develop some form of diabetic polyneuropathy (DPN) during the course of their disease (Dyck and Dyck, 1999), of whom 15-30% develop symptomatic neuropathy (Dyck et al., 1991; Dyck et al., 1993; Dyck and Dyck, 1999). DPN is a progressive disease, worsening with increased duration of DM. In both Type I and Type II DM, it usually develops after several years of chronic, or unrecognized, hyperglycemia. It has been estimated that the incidence of DPN ranges from approximately 35% in patients with DM less than 10 years, to approximately 50% between 10 and 20 years of DM, to almost 75% in patients with DM greater than 20 years (Dyck and Dyck, 1999). Present treatments include intensive insulin therapy, which has yielded the most promising results (Ginsberg and Mazze, 1994), or treatment with aldose reductase inhibitors (see below), which have yielded only modest improvements in nerve function.

Although the pathogenesis of DPN is not completely understood, there is a good correlation between the extent of neuropathy and the degree of hyperglycemia, as well as the duration of Type I or Type II diabetes (Tesfaye et al., 1996). Controversy exists concerning whether the observed functional abnormalities are due to axonal degeneration or to Schwann cell dysfunction (Dyck and Giannini, 1996). Pathological observations suggest that Schwann cells may be involved in the pathogenesis of the disease. At present, however, there are no studies that examine the direct effects of high glucose on Schwann cell function, or whether the observed changes in Schwann cell function and morphology are indirectly due to the metabolic consequences of diabetes. Given

the importance of Schwann cells in normal peripheral nerve development, function, and regeneration, it is necessary to ask the question whether high glucose is directly toxic to Schwann cells.

An in vitro model system was developed using primary rat Schwann cells to examine the effects of high glucose concentrations (17.5-50 mM, or 315-900 mg/dl) on Schwann cell function. In humans, diabetes is diagnosed once fasting blood glucose rises above 140 mg/dl. The range of glucose concentrations examined in this study was chosen to approximate the levels of hyperglycemia seen in animal models of diabetes induced by streptozotocin (STZ), where blood glucose levels range between 30 and 50 mM (Fernyhough et al., 1995).

I.a Peripheral Nerve Development and Anatomy

The glial cells of the peripheral nervous system, the Schwann cells, are derived from the neural crest, along with neuronal precursor cells (Stemple and Anderson, 1992). Early precursor Schwann cells are first identified at embryonic day (E) 14. They are distinguished from immature and differentiated adult Schwann cells by two factors: 1) their inability to survive in vitro under culture conditions in which Schwann cells isolated from older nerves would normally survive, and 2) that they do not demonstrate detectable levels of expression of the Ca^{++} binding protein S100, which is ultimately expressed by both types of adult Schwann cells (myelin forming and non-myelin forming) (Mirsky and Jessen, 1996). At E14, the rat peripheral nerves consist of tight bundles of axons associated with rapidly dividing Schwann cell precursors. At this stage of

development, the Schwann cell precursor/axon unit lacks a basal lamina, which is present in the adult nerve (Jessen and Mirsky, 1991). In addition the Schwann cell precursors do not express any of the markers unique to neuronal precursors, in particular, growth-associated protein (GAP)-43 (Jessen and Mirsky, 1991; Jessen et al., 1994). By E15-16, expression of S100 is detectable, and proliferation of the immature Schwann cells in vivo continues at a fast rate (Jessen and Mirsky, 1991) mediated by axonal signals at all stages of development, and in regeneration.

Between E15-20, continuing Schwann cell proliferation is accompanied by the segregation of axons into discrete axon-Schwann cell units. Larger axons within these units segregate further and become isolated within "troughs" in the Schwann cell cytoplasm. During this period, prior to the establishment of single axon-Schwann cell associations, the Schwann cells assemble a basal lamina (Webster et al., 1973); a transition which is crucial to the subsequent development of myelinated peripheral nerves. If basal lamina deposition is disrupted, subsequent myelination is blocked (Bunge, 1987).

Schwann cell proliferation peaks approximately at about E19 (Stewart et al., 1993), which coincides with the first detectable signs of myelination. Double labeling experiments have demonstrated that Schwann cells expressing the major myelin protein, protein zero (P_0) did not show bromodeoxyuridine (BrdU) incorporation which is used to provide an index of DNA synthesis and proliferation (Jessen and Mirsky, 1992). From E20 onward, there is a marked reduction in the amount of Schwann cell proliferation (Jessen and Mirsky, 1992),

and a significant increase in the number of apoptotic Schwann cells is detected in the developing nerve (Jessen et al., 1994). This may be caused by a reduction in the amount of available Schwann cell mitogens in the developing peripheral nerve, or the presence of soluble or membrane-bound growth inhibitory factors.

A number of molecules regulate Schwann cell survival and proliferation in vivo. One such molecule is glial growth factor, one of 12 splice variants belonging to the neuregulin family of growth factors (Lemke, 1996). This survival factor is found in high levels on peripheral axons, and can prevent the apoptotic death of Schwann cell precursor cells in vitro (Dong et al., 1995) or differentiating Schwann cells deprived of trophic support in vitro (Syroid et al., 1996). The survival-promoting action of glial growth factor was shown to be mediated via a heterodimeric complex between the ErbB2 and ErbB3 receptors (Syroid et al., 1996). Recently, Syroid and colleagues (Syroid et al., 1999) also demonstrated that insulin-like growth factor-I (IGF-I) promoted Schwann cell survival in vitro. IGF-I was shown to stimulate Schwan cell proliferation (Sondell et al., 1997; Syroid et al., 1999), but also to prevent the apoptotic death of Schwann cells deprived of trophic support without stimulating DNA synthesis (Syroid et al., 1999), suggesting the involvement of separate signaling pathways. However it should be noted that unusually high concentrations of IGF-I were employed (up to 50 ng/ml); whereas at lower concentrations (1-5 ng/ml), approximately one-half of the cell death was prevented at 72 hr.

Differentiation of the Schwann cell precursors into mature myelin forming and non-myelin forming Schwann cells occurs in response to specific signals,

both membrane-bound and soluble, derived from the associated axon. Primary Schwann cells in vitro in the absence of neurons, do not normally express myelin proteins such as P_0, however they can be induced to do so under specific culture conditions. Morgan and co-workers demonstrated an up-regulation of P_0 when Schwann cells were grown in serum-free medium containing cholera toxin or forskolin, both of which elevate intracellular cAMP levels (Morgan et al., 1991). This up-regulation of the expression of P_0 was accompanied by down-regulation of glial fibrillary acidic protein (GFAP), neural cell adhesion molecule (NCAM), and the low-affinity nerve growth factor receptor, p75. It was determined from these experiments that cAMP plays an important role in both differentiation and proliferation of Schwann cells. When grown in serum-free conditions, Schwann cell proliferation was stopped, and elevation of cAMP induced expression of P_0; however, in growth-promoting conditions where serum is present, elevation of cAMP potentiates the proliferative effects of serum and other Schwann cell mitogens (Morgan et al., 1991). Bolin and Shooter demonstrated that neurons induce the down-regulation of p75 and the up-regulation of the major peripheral myelin protein P_0 through diffusible molecules (Bolin and Shooter, 1993). However, the axon-derived signals responsible for elevating Schwann cell cAMP and inducing differentiation have yet to be characterized.

Both Schwann cell types can be identified in vivo by the presence of specific proteins unique to each phenotype. The myelin forming Schwann cells express the major myelin proteins: P_0, myelin associated glycoprotein (MAG), myelin basic protein (MBP), proteolipid protein (PLP), and peripheral myelin

protein 22 (PMP22). Conversely, the non-myelin forming Schwann cells express GFAP, p75, NCAM, and the adhesion molecule, L1. Both cell types share the expression of the calcium binding protein S100, as well as galactocerebroside (GalC). These Schwann cell phenotypes also differ with respect to their association with axons. Myelin forming Schwann cells and their associated axons form a 1:1 relationship; while the non-myelin forming Schwann cells, ensheath several axons at once.

Myelinating Schwann cells are associated with the Type Aα motor axons innervating skeletal muscle, Type Aγ motor nerves innervating muscle spindles, the larger sensory nerves serving the skin (Type Aβ, Type Aδ) and preganglionic Type B autonomic fibres. Unmyelinated peripheral nerves include postganglionic autonomic fibres and smaller Type C sensory nerves mediating temperature and pain perception (see Table 1).

In the mature PNS, each nerve is organized and segregated by a series of connective tissue sheaths (see Figure 1). As the nerve roots emerge from the spinal cord, successive layers of connective tissue enclose them as they pass through each of the meningeal layers. Enclosing the entire nerve is a thick sheath of loose connective tissue known as the epineurium, which is continuous with the dura. Enclosed within the epineurium are bundles of fibers or fascicles of varying size. Each fascicle is in turn enclosed by a connective tissue sheath known as the perineurium. The fascicles repeatedly divide and anastomose along the course of the fiber. Fine strands of connective tissue known as the endoneurium penetrate each fascicle extending inward from the perineurium.

Table 1. Peripheral nerve fiber classification.

Fiber Class	Function	Size (μm)	Conduction Velocity (m/sec)
Aα	▫ Motor efferents to skeletal muscle ▫ Proprioception, stretch, muscle spindle afferents	12-22	70-120
Aβ	▫ Discriminitive touch, pressure, joint rotation ▫ Secondary muscle spindle afferents ▫ Golgi tendon organ afferents	5-12	30-70
Aγ	▫ Muscle spindle efferents (intrafusal)	2-8	15-30
Aδ	▫ Touch and discriminitive pain	1-5	5-30
B	▫ Preganglionic autonomic axons (afferent & efferent)	< 3	3-15
C	▫ Inflammatory or visceral pain, temperature	0.1-1.5	0.6-2.0
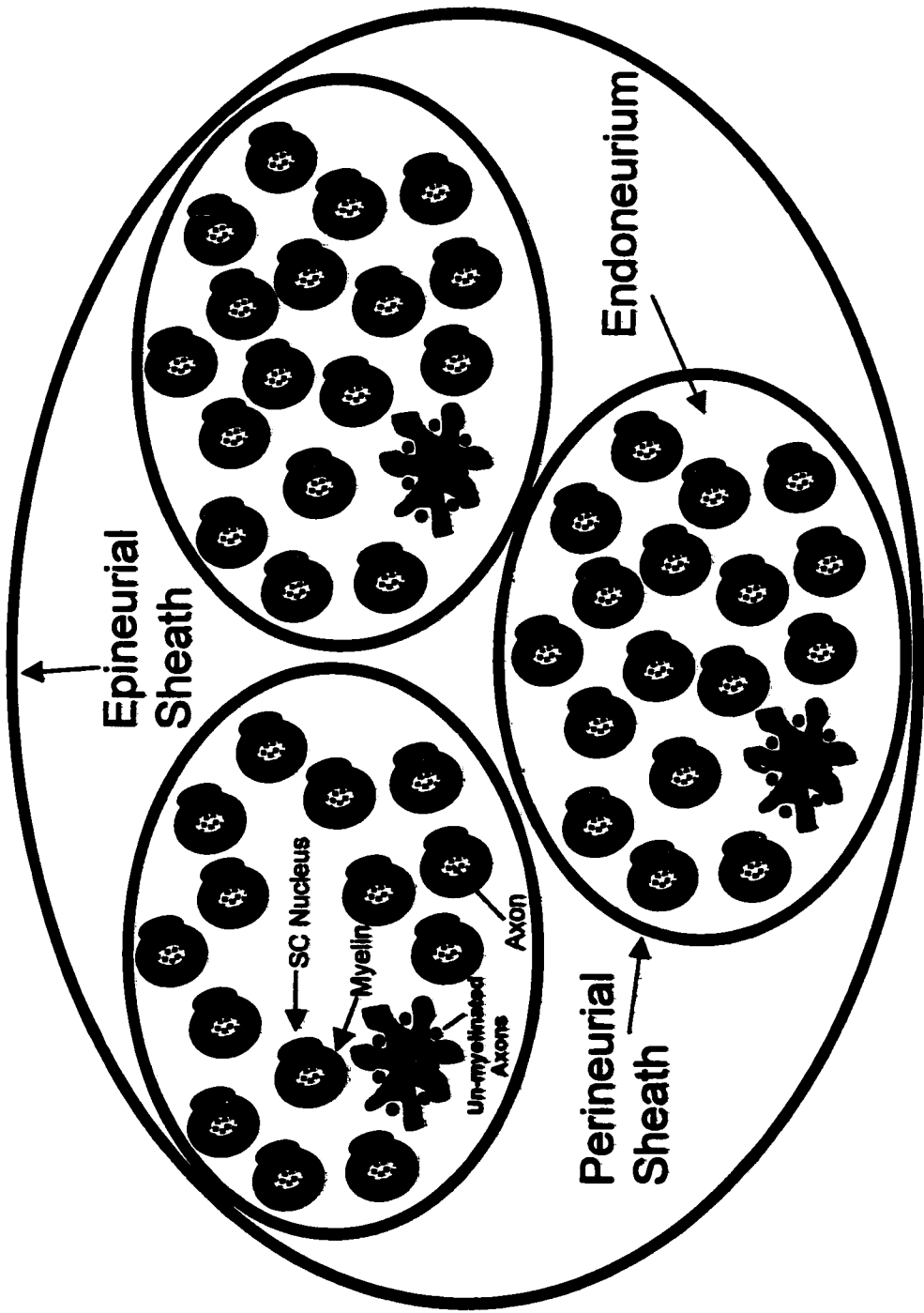
Figure 1. Schematic showing cross-section of peripheral nerve

In addition to providing structural support for the peripheral nerves, these sheaths also comprise the initial level of the blood-nerve barrier. The first barrier is established by the perineurium, within which the perineurial cells are arranged and joined by tight junctions. The permeability of the perineurium is greatest during development and at the sites of vascular penetration in the adult nerve. The second barrier is provided by the vasculature. The capillaries within the perineurium are considerably more permeable to circulating factors due to the fenestrated endothelium; however, the capillaries of the endoneurium resemble those in the CNS with tight junctions between endothelial cells (Giannini and Dyck, 1994).

The cell bodies of the afferent sensory nerve fibers are located in spindle shaped swellings on the dorsal root known as the spinal ganglion (or dorsal root ganglion, DRG). These pseudo-unipolar neurons each give rise to a single process that divides into a peripheral and central branch. In the human, distal to the DRG, the dorsal and ventral roots merge to form a mixed nerve. This common nerve trunk divides into four branches or rami: the dorsal ramus, ventral ramus, meningeal ramus, and the ramus communicans. The larger ventral ramus innervates the ventrolateral portion of the body wall and all the extremities. The ventral rami from several spinal segments in the cervical, lumbar, and sacral regions anastomose and divide repeatedly forming a plexus of fibers (see Figure 2 for example of human lumbosacral plexus compared to rat). The dorsal ramus innervates the deep muscles and skin of the back. The spinal cord is connected to the sympathetic ganglia via the rami communicans,

which are divided into myelinated preganglionic (Type B) fibers (white communicating ramus) which project from the spinal cord to the sympathetic ganglion, and unmyelinated fibers (grey communicating ramus) projecting from the ganglion back into the spinal nerve and then out to the body. In addition, the white ramus contains afferent fibers from the viscera with those cell bodies located within the sympathetic ganglia. The meningeal ramus re-enters the intervertebral foramen and supplies the meninges, blood vessels, and vertebral column.

I.b Axoglial Interactions

The most obvious axoglial interaction in the peripheral nervous system is that of myelination. The myelin sheath is a highly organized structure consisting of a radially arranged repeating unit of membrane. Ultrastructurally, the myelin sheath consists of the apposition of the two inner cytoplasmic faces of the plasma membrane, forming the major dense line, interspersed between the abutment of the external surfaces of the plasma membrane, known as the intraperiod line. The myelin sheath is interrupted at intervals of up to 1000-2000 μm by unmyelinated regions of axon known as the node of Ranvier, where high concentrations of ion channels (Na^+, K^+, etc.) that facilitate action potentials are located.

A. Human Lumbosacral Plexus

L4
L5
S1
S2
S3

Sciatic N.

Common Peroneal N.

Tibial N.

B. Rat Sciatic Nerve

L2

Lat. Cutaneous N.

Femoral N.
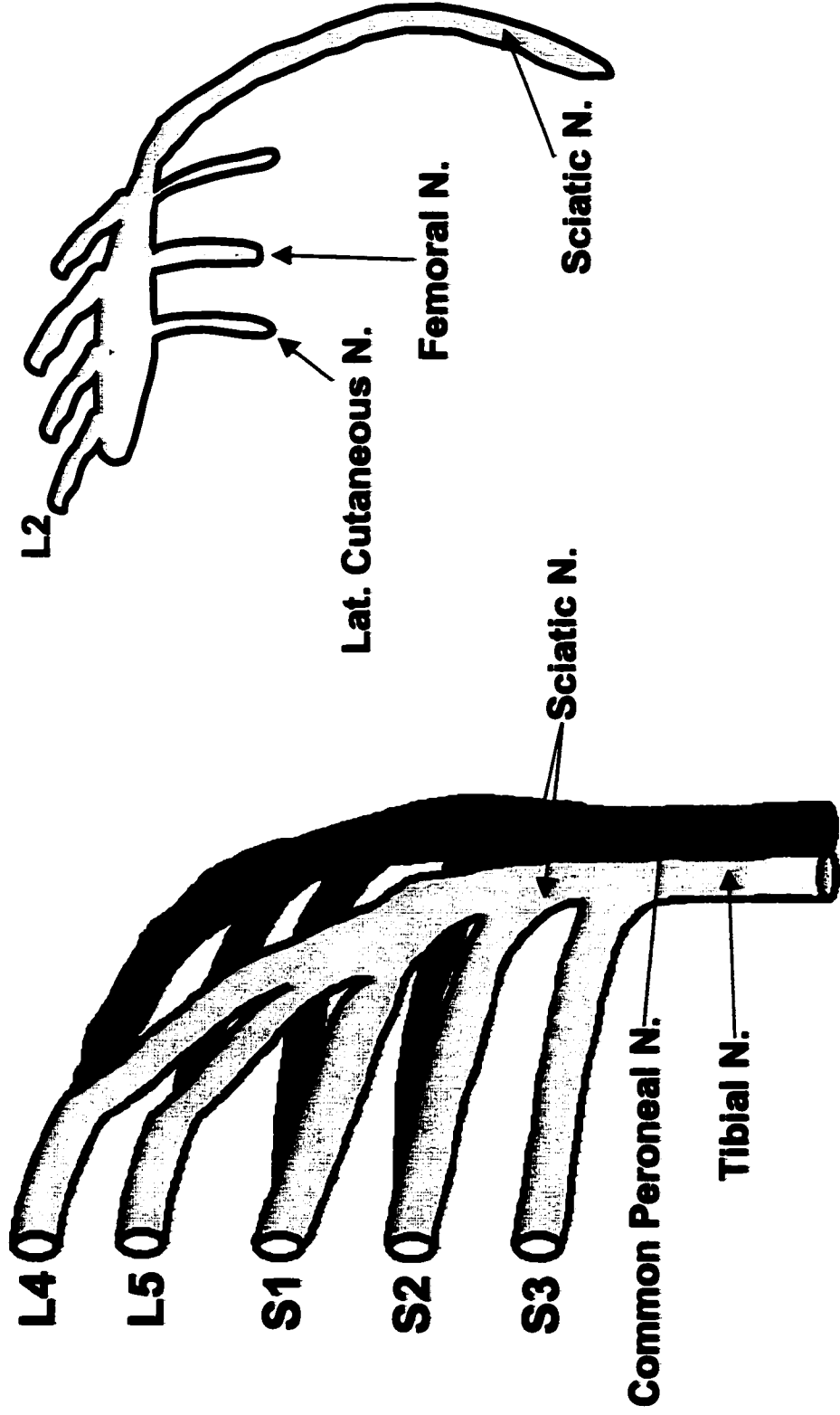
Sciatic N.

Figure 2. Schematic diagram of human (A) and rat (B) sciatic nerve

Signals from the peripheral axon ultimately determine the differentiation state of the adult Schwann cell, directing it to invest the axon with a myelin sheath, or simply to ensheath it within a cytoplasmic recess. Myelinating Schwann cells, in turn, in addition to mediating fast saltatory conduction, also influence final axonal diameter and the clustering of Na^+ ion channels at the node of Ranvier.

It has been established, both in vitro (Starr et al., 1996; Windebank et al., 1985) and in vivo (de Waegh and Brady, 1991; de Waegh et al., 1992) that myelination enhances the phosphorylation of the tail domains of the 160 kDa and 200 kDa subunits of neurofilaments (NF-M and NF-H respectively), and the subsequent extension of lateral side arms resulting in increased axonal diameter. In areas that are unmyelinated (e.g. at the node of Ranvier), or areas of demyelination, axonal diameter is reduced and the density of neurofilaments appears greater in ultrastructural analyses due to the reduction of interfilamental space caused by the attenuation of side arm projections (see de Waegh et al., 1992). Additionally, it has been demonstrated that demyelination reduces the rate of slow axonal transport, mediated by neurofilaments, within the axon by almost 20% (de Waegh and Brady, 1990; de Waegh et al., 1992). Therefore, in addition to the disruption of nerve conduction, pathological demyelination, either secondary to axonal injury or as the result of Schwann cell insult, can induce structural changes in the associated axon that have implications for normal nerve function.

Myelinating Schwann cells also influence the clustering of Na^+ channels at the node of Ranvier. Vabnick et al. examined the clustering of Na^+ channels in

the developing rat sciatic nerve (Vabnick et al., 1996). In the rat, at early stages of axonal development before myelination begins, clustering of Na^+ channels is completely absent. By the end of the first post-natal week, sites of Na^+ channel clustering are highly focal and always associated with myelinating Schwann cells (Vabnick et al., 1996). In peripheral axons that have been demyelinated by an injection of 1% lysolecithin, clustering of Na^+ channels is absent (Dugandzija Novakovic et al., 1995), as in the early developing nerve prior to myelination. If Schwann cell proliferation is prevented in the demyelinated nerve, which subsequently prevents remyelination, reformation of Na^+ channel aggregates is blocked. Ultrastructural analysis revealed that Na^+ channel aggregates were localized just beyond the site of axon-Schwann cell contact (Dugandzija Novakovic et al., 1995), suggesting that an inhibitory signal present on the surface of the Schwann cells prevents the ion channels from migrating into the internodal regions or that there is a diffusible signal released by Schwann cells that sequesters Na^+ channels at the nodal region.

Evidence concerning the nature of the myelin-induced modulation of both axonal diameter (Starr et al., 1996; de Waegh and Brady, 1990; de Waegh et al., 1992) and Na^+ channel clustering (Vabnick et al., 1996; Dugandzija Novakovic et al., 1995) suggests the participation of MAG. MAG, which is a membrane spanning molecule comprising approximately 0.1% of total myelin protein in the peripheral nervous system (Trapp et al., 1989), has been localized to the periaxonal Schwann cell membrane. It is speculated to be involved in the initial adhesion of the Schwann cell to the axon during myelination as it is first detected

in myelin forming Schwann cells that have encircled an axon 1-2 times (Trapp et al., 1989). MAG may act as a ligand for a putative axolemmal receptor coupled to an intra-axonal protein kinase. When bound, the kinase is activated and induces phosphorylation of the carboxy terminal domains of the medium and heavy subunits of neurofilament protein (NF-M and NF-H) (de Waegh and Brady, 1990; de Waegh et al., 1992). Na^+ channel aggregation may also be influenced by Schwann cell expression of MAG. A graded density of Na^+ channel aggregation toward Schwann cells with the greatest amount of MAG expression has been observed (Vabnick et al., 1996) at nodes of Ranvier.

MAG may provide a molecular link between putative Schwann cell dysfunction in diabetic neuropathy and the observed morphological sequelae of prolonged hyperglycemia in human and experimental models. Segmental and paranodal demyelination as well as reduced axonal diameter and slowed axonal transport are reported in the human disease and prolonged experimental diabetes. Reduced levels of periaxonal Schwann cell MAG could serve as the signal leading to the reduction in axonal diameter and the disruption of Na^+ channel aggregates.

Schwann cells play a crucial role in the repair of injured peripheral nerves. In Wallerian degeneration (WD), axons distal to the site of injury degenerate, while those proximal to the lesion survive and retain the capacity to regenerate. A coordinated series of changes in gene expression regulating differentiation and proliferation in the surviving Schwann cells occur that enhance the regrowth of injured axons. There is a detectable increase in the mRNA levels for nerve

growth factor (NGF) and neurotrophin (NT)-4 within 6-12 hr following peripheral

nerve injury. This is followed by a more gradual increase in the mRNA and

protein levels of IGF-I and brain derived neurotrophic factor (BDNF) over the first

48h. Expression of IGF-II is also up-regulated but at a slower rate, and at sites

more distal than IGF-I. There is a large drop in the expression of NT-3 mRNA

within 6 hr following injury to approximately 10% of pre-injury levels, followed

also by a drop in ciliary neurotrophic factor (CNTF) levels after 3 days (Friedman

et al., 1992; Seniuk et al., 1992; Funakoshi et al., 1993; Ishii et al., 1994).

I.c Diabetic Neuropathy

Peripheral sensorimotor neuropathy (or diabetic polyneuropathy, DPN) is

the most predominant form of the neuropathies affecting diabetic patients.

Abnormalities of nerve conduction or attenuation of the heartbeat response to

deep breathing are the first signs of peripheral nerve dysfunction in diabetes

(Dyck and Dyck, 1999). The first clinical signs are greater vibration thresholds in

the toes, and decreased ankle reflexes (Dyck and Giannini, 1996). In more

severe cases, diabetic patients can develop sensory loss of the toes, feet and

distal legs, a prickling sensation or pain in the feet or legs, muscle stretch reflex

dysfunction, autonomic dysfunction, and muscle weakness in the feet and ankles

(Dyck and Dyck, 1999).

Dyck and Giannini (1996) described a proposed staging classification for

the clinical changes seen in DPN. Stage 1 is asymptomatic and involves distal

sensory loss in the feet and decreased ankle reflexes. Stage 2A patients

develop distal neuropathic symptoms, but are able to walk on their heels; there are clinical and pathological findings of distal polyneuropathy. In Stage 2B, sensory loss is greater than in the previous stage, and the patients can no longer walk on their heels. In Stage 3, the symptoms have become disabling. The Rochester Diabetic Neuropathy Study (RDNS) published in 1993 found only approximately 15% of diabetic patients with DPN develop symptoms, however estimates of symptomatic DPN have been as high as 20% (Harris et al., 1993) to 25% in patients with DM longer than 20 years (Dyck and Dyck, 1999). These differences likely reflect underlying differences in data collection between the studies and variation in the neurological assessment of subject patients.

The results of the Diabetes Control and Complications Trial (DCCT), suggested that glycemic control was a crucial factor in the prevention or delay of development of peripheral neuropathy. Evidence of DPN, suggested by abnormal clinical or autonomic examinations, or abnormalities of nerve conduction was significantly reduced by almost half in Type I diabetic patients who received intensive insulin therapy for a period of 5 years (Ginsberg and Mazze, 1994). Additionally, Tesfaye et al. reported a strong correlation between the extent of neuropathy and the degree of hyperglycemia, as well as the duration of Type I or Type II DM (Tesfaye et al., 1996). Studies of somatosensory evoked potentials such as Hoffmann's reflex (H-reflex) conduction velocity, which can be used to show abnormal proximal nerve function (Daube, 1999), revealed that a significant component of nerve conduction abnormalities is attributable to metabolic derangements (Troni et al.,

1984). Within 48 hr of commencement of intensive insulin therapy, resulting in significantly reduced blood glucose levels, there was a mean increase of approximately 1.7 m/sec in H-reflex conduction velocity.

Sugimura and Dyck (1982) and Dyck et al. (1986) systematically surveyed pathological changes in patients with DPN compared to controls. Proximal to distal frames at the levels of the fifth lumbar (L5) ventral and dorsal roots, segmental nerve, proximal and distal sciatic nerve, and the tibial, peroneal, and sural nerves were examined using electron microscopy. They reported focal and multifocal fiber loss in proximal sections and a more severe diffuse fiber loss distally and attributed the pattern to discrete ischemic insults. Further, Dyck and colleagues reported that the abnormality associated with axonal degeneration and regeneration was greater compared to that associated with segmental demyelination and remyelination (Dyck et al., 1986). They concluded, together with the findings of focal and mutifocal fiber loss, that axonal degeneration was the primary event in DPN. Other authors have reported a symmetrical "dying-back" (Said et al., 1994; Watkins et al., 1995) axonal degeneration affecting both myelinated and non-myelinated fibers (Bradley et al., 1995).

Evidence of primary (segmental) and secondary demyelination and remyelination has been reported by Said et al. (1994). They additionally reported individual fibers with proximal segmental demyelination together with axonal degeneration in the more distal aspects. This suggests that the two processes may develop independently. Pathological observations from human sural nerve biopsies have demonstrated myelin ovoids and segmental demyelination

adjacent to intact axons, variable internode lengths, and onion bulbs suggestive of repeated demyelination and remyelination (Dyck and Giannini, 1996).

Although the loss of both myelinated and unmyelinated fibers is consistently observed in peripheral nerve biopsies of diabetic patients, (Dyck et al., 1986; Llewelyn et al., 1991), clinical presentations have suggested the possibility of a selective vulnerability of large and small sensory, or autonomic nerves (Dyck and Giannini, 1996). Guy et al. (1985) compared thermal and vibration sensitivity in diabetic patients and suggested that there may be a selective early loss of small unmyelinated fibers mediating thermal sensation. Dyck and co-workers however did not report clustering of cases with small or large fiber loss that would suggest potential fiber class vulnerability (Dyck et al., 1986). Further, it has been cautioned that the presentation of sensory loss of the toes and feet in the absence of muscle weakness does not necessarily indicate a selective vulnerability of sensory versus motor fibers. In this case, it may represent involvement of a length-dependent process affecting sensory innervation of the skin of the toes earlier than the motor fibers innervating the same area which terminate in the upper third of the leg (Giannini and Dyck, 1999).

In contrast to the human disease, animal models of DPN do not show evidence of segmental demyelination. Abnormalities of nerve conduction and paranodal structure are however consistently observed. Rats injected with STZ or alloxan have shown decreases in sensory and motor nerve conduction velocity, paranodal demyelination, and increased myelin wrinkling (Sagara et al.,

1996). In STZ-treated animals, reductions in mean myelinated fiber number and size and increased axonal atrophy have been reported (Yagihashi, 1995) along with a reduction in slow axonal transport and decreases in both sensory and motor nerve conduction velocity (Moore et al., 1980; Weis et al., 1995). In the spontaneously diabetic BB/W rat, a 20% decrease in nerve conduction velocity, compared to non-diabetic littermates, has been observed (Cherian et al., 1996). Elias and colleagues developed a transgenic mouse overexpressing a major histocompatibility complex (MHC) class 1 protein in pancreatic β-cells (Elias et al., 1998). These mice became hyperglycemic within 2 months of age. There was a significant decrease in proprioceptive (Aα fibers) sensory nerve conduction velocity following 2 months of hyperglycemia, whereas motor nerve conduction velocity was not decreased until 5 months after the onset of hyperglycemia. Morphologically, both myelinated and unmyelinated fiber loss was evident, as were abnormally thin myelin sheaths (Elias et al., 1998). The reduction in myelin sheath thickness is consistent with remyelination of a region of axon, and may be indicative of segmental demyelination. This particular transgenic model involves the auto-immune mediated destruction of pancreatic β-cells similar to human Type I DM, and in this regard may be a more appropriate model for human DPN showing similar morphological and functional abnormalities in peripheral nerve function.

I.d Schwann Cell Pathology in Diabetic Polyneuropathy

Several authors have suggested that sural nerve myelinated fiber density (the number of myelinated fibers/mm^2 cross-sectional area) can be a useful tool

in evaluating the progression or severity of DPN (e.g., Dyck et al., 1985; Sima et al., 1993). Russell et al. (1996) correlated changes in three different clinical measures with changes in myelinated fiber density in sural nerve biopsies from diabetic patients and non-diabetic controls. The patients were evaluated according to the Neurological Disability Score (NDS; Dyck et al., 1989), which grades the patients' strength, muscle reflexes, and sensation, yielding a summated NDS value from 0-8. On this scale, a change of 2 points is considered the minimally detectable clinical change (Russell et al., 1996). Nerve conduction studies were also performed, measuring the summated compound muscle action potential (ΣCMAP) for the ulnar, peroneal, and tibial nerves, and the summated sensory nerve action potential (ΣSNAP) for the ulnar and sural nerves. Nerve conduction tests were normalized to percentile scales from a database of normal individuals with no history of neuropathy.

Significant associations were found between myelinated fiber density and all three measures of clinical and electrophysiological function (Russell et al., 1996). Specifically, a 2 point change in the NDS was associated with a change in myelinated fiber density of approximately 200 fibers/mm^2, a 1mV change in ΣCMAP amplitude was associated with a change of 160 fibers/mm^2, and a 1 μV change in ΣSNAP amplitude with a change of 70 fibers/mm^2. Taken together, these are useful in that it allows the determination of whether or not an observed change in myelinated fiber density, which is consistently observed in DPN, is associated with a meaningful clinical change.

The question of whether there is direct injury to Schwann cells in human

DPN has not been completely resolved. Sima and colleagues (1986; 1988) suggested that the phenomenon of axoglial dysjunction, which is the disappearance of discrete associations between terminal myelin loops and the paranodal axolemma (known as transverse bands), is a widespread finding in human DPN. Although the retraction of terminal loops early in WD prior to axonal degeneration is observed, the extent of axoglial dysjunction in diabetic polyneuropathy reported by Sima and colleagues has not been confirmed by other laboratories (Thomas et al., 1996). Further, the morphological techniques and criteria used to define axoglial dysjunction have been called into question by other groups (Dyck and Giannini, 1996; Giannini and Dyck, 1996; Thomas et al., 1996).

A recent study by Mizisin et al. (1998) reported significant Schwann cell injury in spontaneous feline diabetes, including degenerative changes such as myelin splitting and the dissolution of Schwann cell cytoplasm at the inner glial loop. Thinly myelinated axons surrounded by proliferating Schwann cells were also observed, suggesting regions of demyelination and re-myelination. Of particular importance was the observation of intact axons surrounded by degenerating Schwann cells (Mizisin et al., 1998), which suggests a direct involvement of Schwann cells, independent of axonal atrophy in feline diabetic neuropathy.

Increases in NF density have been observed in peripheral nerve biopsies of diabetic patients (Medori et al., 1988); however, colocalization of focal regions of increased NF density and regions of segmental demyelination have not been

reported. Increased NF density per unit area is indicative of a reduction in lateral extension of side arms of NF-H and NF-M subunits. This may be due in part, to reduced signaling from associated myelin-forming Schwann cells (de Waegh and Brady, 1991; de Waegh et al., 1992). Increased turnover of the myelin proteins P_0 and MBP has been reported in alloxan treated diabetic rats (Conti et al., 1996; Conti et al., 1993), which is suggestive of disrupted axoglial interactions in diabetic nerve. Paranodal demyelination and increased myelin wrinkling (Sagara et al., 1996) have also been demonstrated in experimental diabetes, indicating a link between Schwann cell pathology and observed nerve conduction abnormalities.

The galactose intoxication model of galactosemia has been utilized to study DPN because galactose metabolism relies on the polyol pathway; which has been implicated in the pathogenesis of the disease (Sima, 1996; see below). Degenerative changes in Schwann cells have been observed in this model, including retraction of the cytoplasm from the myelin sheath, and enlargement of mitochondria, followed by the ultimate disintegration of Schwann cell cytoplasm (Forcier et al., 1991; Mizisin and Powell, 1997; Kalichman et al., 1998). In STZ induced diabetes, hyperglycemia in young rats leads to an increased propensity for demyelination induced by consumption of tellurium compared to non-diabetic rats (Jaffey and Gelman, 1996). This would suggest an increased vulnerability of Schwann cells to injury in hyperglycemic conditions.

The ability of Schwann cells to respond to axonal signals during WD and establish an environment that supports the damaged axon is crucial to the

success of axonal regeneration. A significant delay in the recruitment of macrophages to the site of nerve crush was reported in spontaneously diabetic BB/W rats (Kamijo et al., 1996) along with a delay in the initiation of WD. In STZ-induced diabetic rats, seven days following sciatic nerve crush, total sensory nerve regeneration was reduced by approximately 20% compared to non-diabetic animals, as estimated by the pinch-reflex assay (Ishii and Lupien, 1995; Zhuang et al., 1996). Ekstrom reported a 14% decrease in the rate of sensory nerve regeneration with the greatest difference at six days following nerve crush (Ekstrom et al., 1989). Prolonged hyperglycemia may directly affect the regenerative capacity of Schwann cells. The extent of sensory nerve regeneration was estimated by functional recovery only, and was not verified by morphological techniques, and can therefore not conclusively determine to what extent the deficit in nerve regeneration was attributable to Schwann cell dysfunction.

Expression of NGF and NT-4 is increased in normo-glycemic distal Schwann cells following crush or transection of the sciatic nerve (see above). However, in the sciatic nerve of diabetic rats, expression of NT-4 transcripts were decreased by 29% (Rodriguez-Pena et al., 1995). NGF levels (Hellweg and Hartung, 1990), and NGF retrograde transport (Hellweg et al., 1994) in peripheral nerve were reduced by approximately 50% in diabetic animals and were found to inversely correlate with high blood glucose levels. Localized administration of NGF (Whitworth et al., 1995), IGF-I, or IGF-II (Ishii and Lupien, 1995; Zhuang et al., 1996) via osmotic mini-pumps reduced the hyperglycemia-induced disruption

of sensory nerve regeneration as assessed by the tail-flick test. This suggests that the trophic environment normally established by Schwann cells in the injured nerve is deficient in the diabetic rat and that it is necessary in order for peripheral nerve regeneration to occur.

I.e Glucose Metabolism

The glycolytic pathway is utilized by all tissues for the breakdown of glucose in order to provide energy in the form of ATP and intermediates for other metabolic pathways. In both Type I and Type II DM, carbohydrate metabolism is disrupted by the inability of most tissues to adequately metabolize available glucose. Since essentially all sugars, derived from either the diet or from other catabolic reactions, can be converted to glucose, glycolysis is a central metabolic pathway. The highly regulated glycolytic pathway yields 2 molecules each of ATP, NADH, and pyruvate for each molecule of glucose. The steps of the pathway are presented in Figure 3. The ultimate fate of pyruvate within the cell is linked to the net formation of NADH and the presence of an adequate supply of oxygen resulting in the generation of lactate in anaerobically respiring cells or acetyl coenzyme A which enters the citric acid cycle in aerobically respiring cells. The first step in the metabolism of glucose is its phosphorylation by hexokinase (HK); the activity of which is greatest when bound to mitochondria (see below, and Weiler et al., 1985). This is also the first of two steps requiring the
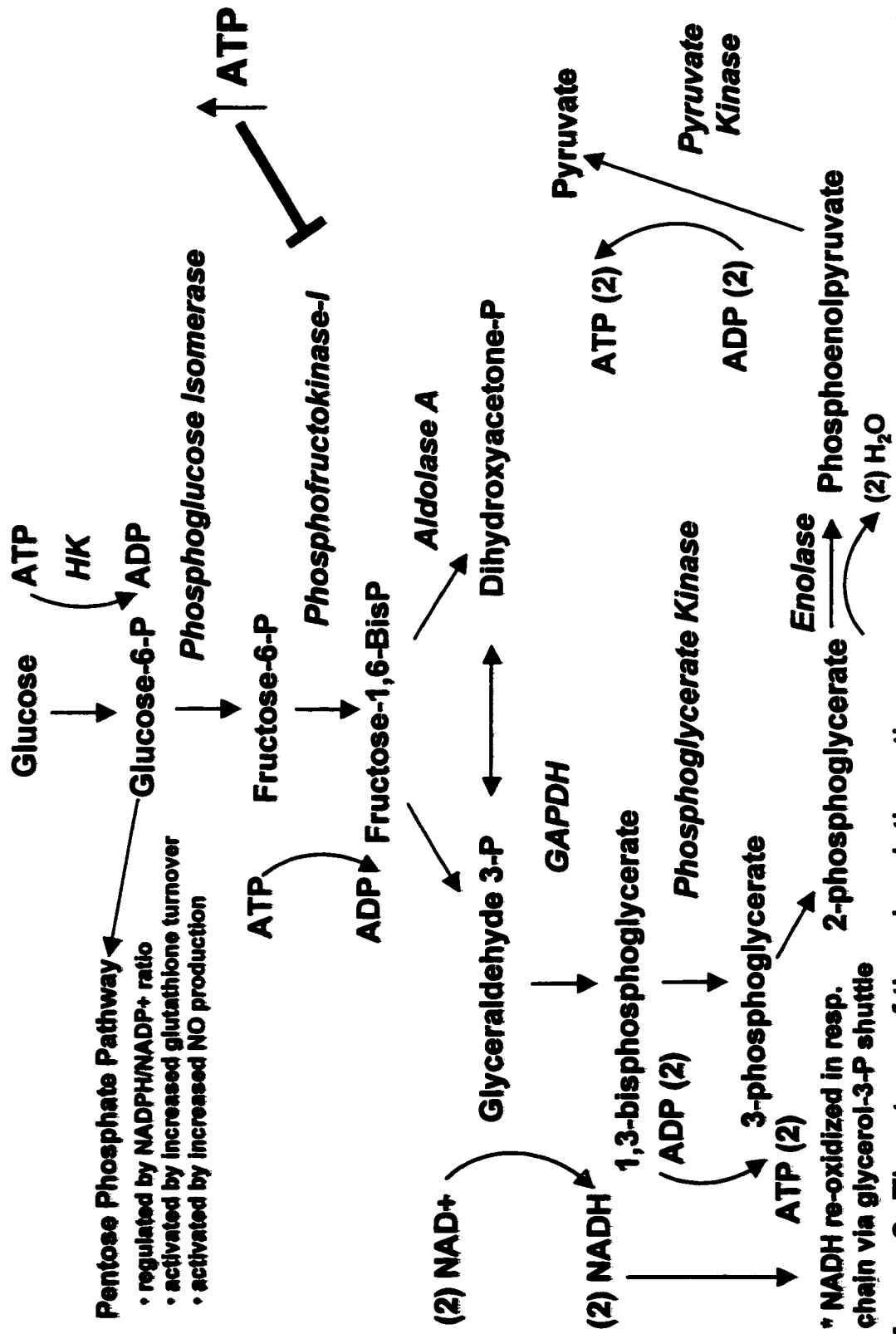
Figure 3. The steps of the glycolytic pathway

expenditure of ATP. The second occurs during the phosphorylation of fructose-6-phosphate by phosphofructokinase-I (PFK-I). This reaction is the rate-limiting step in glycolysis. The activity of PFK-I is inhibited by high levels of ATP and citrate, but activated by high levels of AMP. Additionally fructose-2,6-bisphosphate is a potent activator of PFK-I, with a reciprocal inhibition of fructose-1,6-bisphosphatase, thereby inhibiting the rate of gluconeogenesis while glycolysis is continuing.

During a well-fed state where there are high levels of insulin and low levels of glucagon, cAMP and active protein kinase A levels are reduced. This favours the dephosphorylated, active form of the phosphofructokinase-2/fructose bisphosphate phosphatase-2 (PFK-2/FBP-2) complex. Increased activity of PFK-2 leads to the formation of fructose-2,6-bisphosphate, which in turn, increases the activity of PFK-I.

The triose phase begins with the conversion of fructose-1,6-bisphosphate to glyceraldehyde-3-phosphate and dihydroxyacetone-phosphate (DHAP) by aldolase A. DHAP is freely converted to glyceraldehyde-3-phosphate (by triose phosphate isomerase), to which a second phosphate group is added by glyceraldehyde-3-phosphate dehydrogenase (GAPDH) during the oxidation of glyceraldehyde-3-phosphate. This reaction is coupled to the reduction of 2 molecules of NAD^+ to NADH. The cytoplasmic NADH is re-oxidized to NAD^+ in aerobically respiring cells in the mitochondrial respiratory chain. Since NADH cannot cross the impermeable inner mitochondrial membrane, its electrons are transferred to the matrix via the glycerol-3-phosphate shuttle (or also via the

malate-aspartate shuttle). Matrix glycerol-3-phosphate dehydrogenase donates the electrons obtained from cytosolic NADH to Complex II of the respiratory chain, bypassing Complex I. Therefore, the glycerol-3-phosphate shuttle results in the formation of 2 molecules of ATP per molecule of NADH oxidized; whereas the malate-aspartate shuttle does not bypass Complex I of the respiratory chain and therefore yields 3 molecules of ATP per molecule of oxidized NADH.

The two molecules of 1,3-bisphosphoglycerate generated by GAPDH are converted to 3-phosphoglycerate by phosphoglycerate kinase in the first of two sites of glycolytically produced ATP. The second site of ATP generation in the glycolytic pathway occurs during the production of pyruvate from phosphoenolpyruvate catalyzed by pyruvate kinase. In cells with few or no mitochondria such as red blood cells, and in skeletal muscle during periods of high activity, pyruvate is converted by lactate dehydrogenase to lactate in the cytosol. This reaction utilizes the NADH produced during the oxidation of glyceraldehyde-3-phosphate, resulting in no net formation of NADH during anaerobic glycolysis. Alternatively, the oxidative decarboxylation of pyruvate by pyruvate dehydrogenase produces acetyl coenzyme A for the TCA cycle in the mitochondrial matrix which in turn provides high energy electrons in the form of 3 molecules of NADH, and 1 molecule of $FADH_2$ for oxidative phosphorylation in the respiratory chain.

Following the phosphorylation of glucose to glucose-6-phosphate, metabolism of the hexose may be redirected to alternative metabolic pathways such as the pentose phosphate pathway (PPP, also known as the hexose

monophosphate pathway). This pathway yields 2 molecules of NADPH for each molecule of glucose-6-phosphate, and thus provides a large proportion of the cell's supply of this reductant. The activity of this pathway is regulated in part by the intracellular demands for NADPH. The PPP is also important in the synthesis of nucleotides as it produces ribose-phosphate.

The first two reactions in this pathway are part of the irreversible oxidative phase of the PPP, and are the sites of NADPH production. The activity of glucose 6-phosphate dehydrogenase is inhibited by high intracellular ratios of NADPH/NADP$^+$. However, during situations of increased demand for NADPH, this ratio falls, and activity of glucose 6-phosphate dehydrogenase increases. For example, during the reduction of molecular oxygen, a series of reactive oxygen intermediates are produced, such as superoxide ($\bullet O_2^-$), hydrogen peroxide (H_2O_2), and hydroxyl radical ($\bullet OH^-$). The reduction of H_2O_2, which forms oxidized glutathione (GSSG) from reduced glutathione (GSH) via glutathione peroxidase, is part of the cell's internal anti-oxidant mechanism. The production of GSH from GSSG is catalyzed by glutathione reductase and requires NADPH as a source of reducing electrons. Therefore, under situations of increased oxidative stress, there is increased turnover of glutathione and increased demand for NADPH.

Another requirement for NADPH is in the synthesis of nitric oxide (NO). Arginine, O_2, and NADPH are substrates for NO synthase, producing citrulline and NO. There are two families of NO synthase: a Ca^{++}-dependent, constitutive isoform present in neural tissue (cNOS or bNOS) and endothelial cells (eNOS),

and a Ca^{++}-independent inducible form (iNOS). The effects of NO are wide-ranging, and include: vasodilation, neurotransmission, and inhibition of platelet aggregation (Bolanos et al., 1997). Additionally, high levels of NO have been shown to induce cell death in several cell systems (see below). Activity of NOS is enhanced by a number of molecules including tumor necrosis factor-α (TNF-α), and interleukin-1 (Bolanos et al., 1997). Redirection of glucose-6-phosphate to the PPP might therefore be increased during situations that increase the production of NO.

I.f Schwann Cell Metabolism

Little is known about the control of carbohydrate metabolism in Schwann cells in normal and in diabetic nerve. The non-insulin-dependent transport of glucose into Schwann cells is facilitated through specific isoforms of the glucose transporter. In young rats, the GLUT1 isoform has been detected in the membrane and cytoplasm of myelin-forming Schwann cells (Magnani et al., 1996). In mature rats, in addition to GLUT1, the GLUT3 isoform has also been detected (Magnani et al., 1996). Expression of GLUT1 has also been confirmed in isolated Schwann cells in vitro (Muona et al., 1992). Asada et al. (1998) provided the first evidence of expression of the GLUT5 isoform in both Schwann cells and axons in the rat sciatic nerve, and demonstrated that levels of this protein were increased in STZ treated diabetic rats. However, they were unable to determine whether the increase was due to upregulation of GLUT5 in axons or Schwann cells. It has been suggested that central nervous system glia function

as a passive conduit for glucose from the capillaries to the nerve cell (e.g., Kacem et al., 1998). Similarly, Schwann cells may also serve this same function for peripheral nerve axons (Magnani et al., 1996).

Greene and Winegrad (Greene and Winegrad, 1979) utilized an in vitro preparation of the rabbit tibial nerve to investigate metabolic activity in the peripheral nerve. A nerve fascicle preparation was obtained by removing the epineurial sheath, while an endoneurial preparation was obtained by also removing the perineurial membrane. An endoneurial preparation permits the separation of indices of metabolic activity of Schwann cells plus nerve axon from the cellular components of the epineurial and perineurial sheaths (namely, fibroblasts). It was determined from these preparations that the normal nerve utilizes glucose as its primary metabolic substrate, and that the majority of glucose is oxidized to carbon dioxide (Greene and Winegrad, 1979). The addition of insulin to the incubation medium did not alter glucose consumption (energy metabolism), as determined by intensity of fluorescence reaction products in the isolated nerve preparations. This indicates that glucose uptake into this preparation was not insulin-dependent. However, it cannot be determined from this preparation what proportion of glucose uptake was directed to Schwann cells and what proportion to the nerve axon. Control endoneurial preparations from normoglycemic animals in this study did not show reductions in the rate of energy utilization when exposed to high glucose conditions (20 mM) for 2 hr, suggesting that prolonged hyperglycemia may be required to alter the energy metabolism of peripheral nerve. In contrast, the rate of glucose

consumption was compromised in the endoneurial preparations from alloxan-diabetic animals.

Because insulin is not required for the uptake of glucose into Schwann cells (Greene and Winegrad, 1979), during periods of hyperglycemia, a large amount of glucose may enter these cells. It has been proposed that during periods of uncontrolled hyperglycemia, the excess intracellular glucose activates the enzyme aldose reductase which in turn produces a significant amount of sorbitol. In those cells in which sorbitol dehydrogenase levels are low or absent, the accumulation of sorbitol (which cannot pass easily through plasma membranes) presumably leads to osmotic stress and the depletion of myo-inositol. The depletion of myo-inositol is thought to disrupt activity of a Na^+/K^+ ATPase which can lead to altered nerve conduction (see Sima, 1996 for review).

Utilizing a schwannoma-derived Schwann cell line (JS1), Mizisin et al. (Mizisin et al., 1996) investigated the effects of high glucose on polyol pathway constituents. It was reported that the activity levels of aldose reductase did not significantly increase following 5 days of exposure to high glucose medium. Further, the levels of sorbitol and myo-inositol in JS1 Schwann cells exposed to high glucose did not differ from normo-glycemic controls; that is, an accumulation of sorbitol was not observed and myo-inositol was not depleted. Conversely,. (Karihaloo et al., 1997) recently demonstrated reduced uptake of labeled myo-inositol in primary rat Schwann cells exposed to 30-50 mM glucose over a 14-day period. However, clinical trials of diet supplementation with myo-inositol or aldose reductase inhibitors have yielded only modest improvements in nerve

conduction velocity (Sima, 1996; Pfeifer and Schumer, 1995).

The involvement of the polyol pathway in the development and/or progression of diabetic neuropathy has been inferred partly from the success of aldose reductase inhibitors in improving nerve conduction and structural abnormalities in experimental diabetes. However, the extent of myo-inositol depletion and sorbitol accumulation in human diabetic patients is not as profound as it is in experimental diabetes (e.g., Dyck et al., 1988). This would suggest that the polyol pathway might only contribute to nerve pathophysiology at the onset of hyperglycemia rather than throughout the course of the disease. Alternately, the polyol pathway may simply not be as prominent a metabolic pathway in humans as it is in rodents.

Compared to brain, endogenous anti-oxidant levels are reduced in the peripheral nervous system (Romero et al., 1990; Romero et al., 1991), suggesting that the peripheral nervous system may be particularly vulnerable to oxidative stress in diabetes. For example, sciatic nerve levels of glutathione GSH, glutathione reductase, and glutathione peroxidase are approximately 10% of levels measured in brain (Romero et al., 1991). In diabetic rodents, Cu/Zn-superoxide dismutase (SOD1) and glutathione peroxidase levels were significantly reduced in sciatic nerve compared to non-diabetic controls (Low and Nicklander, 1991; Hermenegildo et al., 1993). Hermenegildo and colleagues used regression analysis to predict that for each 1 mM increase in blood glucose, there was an approximate 10% decrease in glutathione peroxidase activity in sciatic nerve. This is in contrast to evidence of increased activity of glutathione

peroxdiase activity in cultured endothelial cells exposed to high glucose (Ceriello et al., 1996). It is not known whether high glucose has an effect on anti-oxidant enzyme activity levels in Schwann cells.

I.g Apoptotic Cell Death

Apoptosis, or programmed cell death, occurs following exposure to specific death-inducing stimuli or the withdrawal of survival factors. The wide range of apoptosis-inducing events converge on a few characteristic signaling pathways and gene changes within the cell that mediate apoptotic death. This is in contrast to necrotic cell death, which involves the lysis of the cell often followed by an inflammatory reaction (see Table 2). The sequence of morphological changes in cells undergoing necrotic cell death include minimal clumping of loosely organized chromatin, marked swelling and dissolution of the mitochondrial matrix, the rupture of nuclear, organelle, and plasma membranes, and the swelling of the nucleus and cytoplasm. In contrast, cells undergoing apoptotic cell death demonstrate marked nuclear chromatin condensation, overall shrinkage of the nucleus and cytoplasm, but maintenance of organelle structure (Wyllie et al., 1980).

The apoptotic cascade has been divided into three phases (see Table 3). The induction phase, during which, the cell encounters lethal insults which can include treatment with mitochondrial toxins such as MPP+ (Basma et al., 1992); (Cobuzzi et al., 1994) or rotenone (Wolvetang et al., 1994), the withdrawal of trophic support (e.g., Wadia et al., 1998), or the addition of TNF-α (Polla et al.,

Table 2. Characteristics of Apoptotic and Necrotic Cell Death

Apoptosis	Necrosis
□ Developmental and pathological.	□ Pathological only.
□ Margination of densely compacted chromatin.	□ Margination of loosely aggregated chromatin that disappears with nuclear membrane.
□ Convolution of nuclear membrane, eventual separation of nuclear protuberances, membrane pores adjacent to loosely aggregated chromatin remain while pores adjacent to condensed chromatin lost, eventual disruption of membrane continuity and fragmentation of dense chromatin bodies.	□ Swelling of nucleus and cytoplasm components, rupture of membranes and destruction of organelles, densities with mitochondrial matrix. □ Inflammatory reaction.
□ Condensation of cytosol, organelles retain integrity, blebs on surface of plasma membrane separate to form apoptotic bodies that may or may not contain condensed chromatin.	
□ No inflammatory reaction.	

1996). Additionally, early changes in mitochondrial function are evident, such as the movement of the pro-apoptotic protein Bax from the cytosol to the mitochondria (Hsu et al., 1997; Wolter et al., 1997). In certain forms of apoptotic cell death, such as that elicited by the FAS ligand, the apoptotic cascade involves the activation of specific interleukin-converting ezyme- (ICE) like proteases associated with the Fas receptor complex, and also caspase 3 prior to mitochondrial changes.

During the effector phase, changes in gene expression occur as the death-signal is transduced within the cell. There is a down-regulation of the anti-apoptotic proteins Bcl-2 and Bcl-X_L (Tatton et al., 1997); and an up-regulation and translocation (Ishitani et al., 1997; Ishitani et al., 1998; Saunders et al., 1997) of GAPDH to the nucleus where it is suspected to induce changes in transcription/translation (Tatton et al., personal communication). This phase represents the point-of-no-return in the apoptotic cascade. It involves the opening of the mitochondrial permeability transition pore and the collapse of the mitochondrial membrane potential ($\Delta\Psi_M$), which irreversibly commits the cell to die.

The final degradation phase follows with the observed morphological changes in the cell, such as chromatin condensation and nuclear blebbing, followed by the fragmentation of genomic DNA. Wyllie et al. (1980) used electron microscopy to characterize the time course of morphological changes, particularly of the nucleus, in a variety of cells exposed to apoptosis-inducing insults. One of the earliest changes in the degradative phase involving nuclear

Table 3. Phases of the apoptotic cell death process.

Phase	Features
Initiation	▫ heterogeneous apoptosis-triggering stimuli (ligation of Fas/TNF receptor, withdrawal of survival factors, toxins) ▫ intracellular signaling molecules and proteins converge on mitochondria (ROS, NO, Ca^{++}, Bax)
Effector	▫ decision point in apoptotic cascade ▫ mitochondrial failure (opening of PTP, collapse of $\Delta\Psi_M$, release of CytC and AIF into cytosol) ▫ activation of cytosolic caspases by mitochondrial proteins ▫ upregulation, and translocation of GAPDH to the nucleus (transcriptional changes)
Degradation	▫ exposure of phosphatidylserine residues on plasma membrane ▫ overproduction of reactive oxygen species by mitochondria ▫ continued activation of caspase pathway; feedback amplification of mitochondrial dysfunction ▫ degradation of cytosolic and nuclear structural proteins ▫ condensation of nuclear chromatin and activation of nuclear endonucleases resulting in systematic fragmentation of DNA

structure involves the aggregation of chromatin into compact granular clumps along the nuclear membrane (Wyllie et al., 1980). This is followed by abnormalities of the nuclear membrane, including indentation and blebbing, and the formation of discrete fragments of nuclear material. The cytoplasm begins to condense as well, along with the early nuclear changes, and the formation of membrane enclosed "buds" or protuberances appears on the cell surface. Coinciding with the condensation of cytoplasm, is the increased density of organelles that maintain their integrity, unlike that seen in necrosis. The nucleus proceeds to fragment into discrete membrane-enclosed bodies containing condensed chromatin. In addition, the protrusions on the extracellular surface of the plasma membrane begin to pinch off into apoptotic bodies, which do not necessarily contain nuclear fragments (Wyllie et al., 1980). Resident cells eventually phagocytose the apoptotic bodies.

I.h Mitochondria and Apoptosis

It has been shown that one of the earliest detectable events in the apoptotic process is a drop of $\Delta\Psi_M$ (e.g., Wadia et al., 1998; Zamzami et al., 1995). Moreover, it has been shown that the maintenance of $\Delta\Psi_M$ is closely tied to the state of the mitochondrial permeability transition pore (PTP). PTP's occupy approximately 7-15% of the total outer membrane surface area (Rassow et al., 1989) and are made up of several proteins that form a channel across the outer mitochondrial membrane and normally impermeable inner membrane. These proteins include the voltage-dependent anion channel (VDAC, also known

as porin), the adenine nucleotide translocator (ANT), and the peripheral benzodiazepine binding protein (PBz) (Zoratti and Szabo, 1995).

Putative functions for the PTP under normal conditions include 1) the creation of microcompartments in which specific kinases gain preferential access to mitochondrially derived ATP (Nicolay et al., 1990; Gerbitz et al., 1996), and 2) the site of $\Delta\Psi_M$ dependent protein transport into the mitochondria (Nicolay et al., 1990; Pfanner et al., 1990). Early in the apoptotic cascade, the PTP opens in response to specific pro-apoptotic signals (e.g., the collapse of $\Delta\Psi_M$, the overproduction of oxidative radicals, the accumulation of Ca^{++} within mitochondria). Figures 4 and 5 present schematics of the PTP and its associated proteins, as is currently understood, in the closed or open conformation respectively. In light of evidence suggesting involvement of the PTP in functions not only concerned with the death of the cell (e.g. protein transport), for the purposes of this discussion, reference to the open versus closed conformation of the PTP will only be made with respect to its involvement in apoptosis.

In the closed conformation, based on co-immunoprecipitation analysis, fluorescence resonance energy transfer (FRET) image analysis, and functional characteristics (Beutner et al., 1998; Mahajan et al., 1998; Marzo et al., 1998; Zamzami et al., 1998; Zoratti and Szabo, 1995), a hypothetical model of the PTP can be re-constructed as follows. The ANT localized within the inner mitochondrial membrane and the VDAC in the outer membrane span the intermembrane space along with creatine kinase (see Figure 4).
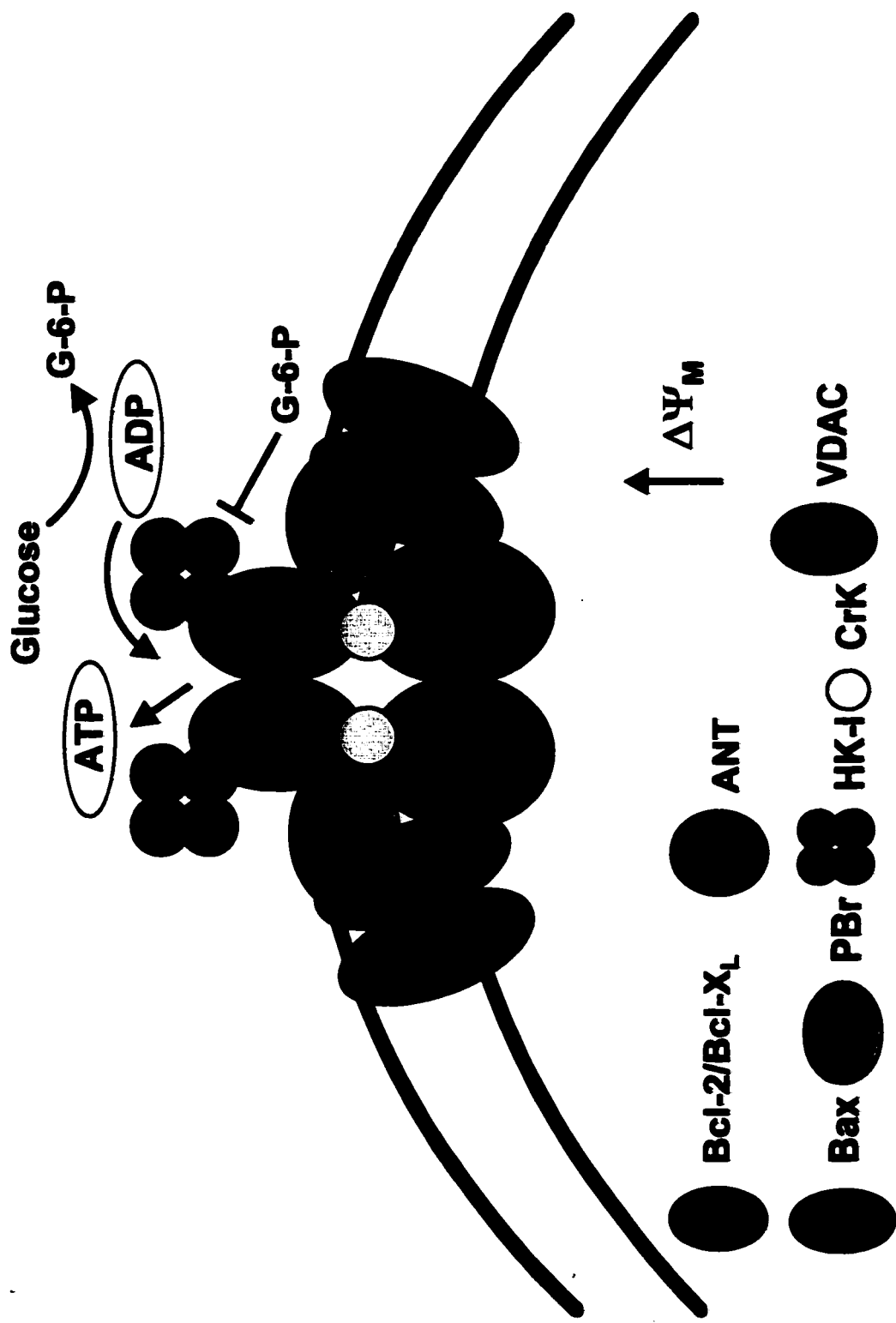
Figure 4. Schematic diagram of the PTP in its closed conformation
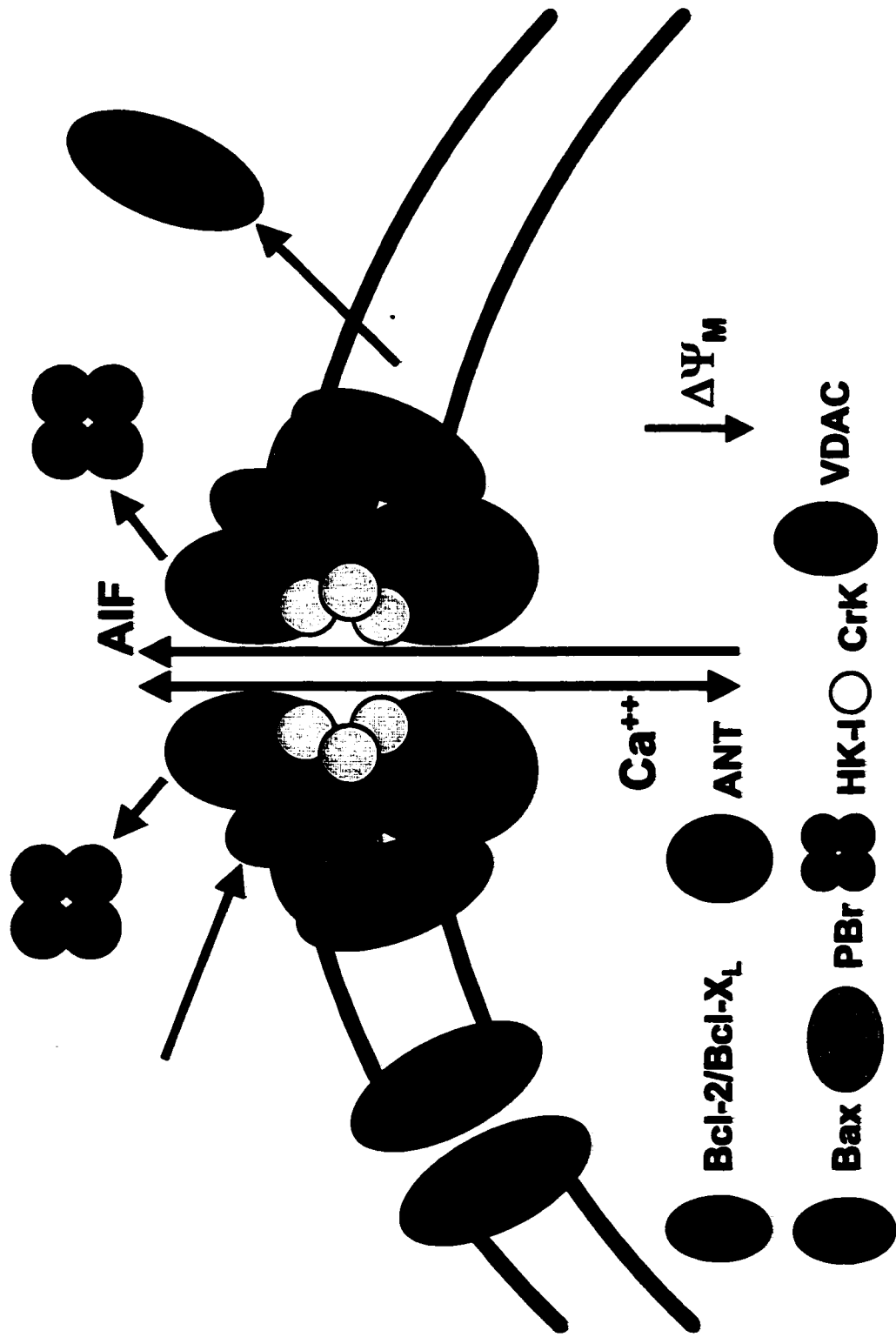
Figure 5. Schematic diagram of the PTP in its open conformation

Bcl-2/Bcl-X$_L$

Bax   PBr   HK-I○ CrK

ANT

VDAC

$\Delta\Psi_M$

Ca^{++}

AIF

The PBz has been co-immunoprecipitated along with the VDAC and ANT (McEnery et al., 1992), however its location within the intermembrane space or outer mitochondrial membrane has not been confirmed. The pro-apoptotic protein Bax has been shown in several systems to co-purify with PTP complexes (Marzo et al., 1998), and specifically with the ANT (Marzo et al., 1998), as well as with the anti-apoptotic protein Bcl-2 (Mahajan et al., 1998).

In contrast, several changes in the localization of specific components of the PTP in the open conformation have been proposed. It has been shown that there is increased Bax co-localization with mitochondria, either specifically with the PTP (e.g., Marzo et al., 1998) or independently as a pore-forming complex (e.g., Eskes et al., 1998), and a decreased association between Bax and Bcl-2 has been reported (Mahajan et al., 1998). Although the re-distribution of the PBz has not been observed, it can participate in permeability transition through an interaction with protoporphyrin IX (a ligand of the PBz) (Zamzami et al., 1998). Additionally, activity of creatine kinase has been shown to modulate conformation of the PTP (Beutner et al., 1998; O'Gorman et al., 1997), and provision of substrate for this enzyme has been shown to be neuroprotective (Matthews et al., 1998).

The opening of this pore allows the release of solutes present in the mitochondrial matrix that are less than 15 kDa (termed apoptosis initiating factors, AIF) (e.g., Susin et al., 1996). Agents that impair functioning of the mitochondrial respiratory chain (e.g. rotenone, 3-nitroproprionic acid, antimycin A, etc.), and cause the PTP to open (e.g. atractyloside), significantly reduce $\Delta\Psi_M$

(Marchetti et al., 1996) and cause the apoptotic death of fibroblasts (Wolvetang et al., 1994), thymocytes (Zamzami et al., 1996) and neuronally differentiated PC12 cells (Tatton et al., personal communication).

There has been considerable work done on the involvement of members of the Bcl-2 family of oncoproteins (e.g., Bcl-2, Bcl-X_L, Bax, Bak, etc.) in PTP/mitochondrial - dependent apoptosis. For example, knock-out studies using mice deficient in the anti-apoptotic protein Bcl-2, have shown marked degeneration of motor, sympathetic, and sensory neurons in early post-natal development (Michaelidis et al., 1996) and increased propensity of cultured cerebellar granule neurons to die via apoptosis (Tanabe et al., 1997). Conversely, deletion of the pro-apoptotic protein Bax leads to increased overall numbers of neurons in cervical ganglia and facial motor nucleus as well as enhanced survival of axotomized facial motor neurons (Deckwerth et al., 1996).

Sequence and structural analyses of members of the Bcl-2 family have revealed up to 4 Bcl-2 homology (BH1-4) domains and a transmembrane insertion domain common to each (see Zamzami et al., 1998). These BH domains have been implicated in the heterodimerization between members of this family; particularly, Bcl-2, Bcl-X_L, and Bax. It has been suggested that the BH3 domain of Bax forms a ligand that interacts with the apposition of the BH1, BH2, and BH3 domains of Bcl-2 or Bcl-X_L (Sattler et al., 1997). Deletion of any or all of these domains yields proteins with reduced pro- or anti-apoptotic properties (Zamzami et al., 1998). It has further been demonstrated that deletion of the transmembrane insertion domain in Bcl-2, which prevents the association

of Bcl-2 with mitochondria, attenuates or abolishes its anti-apoptotic properties (Zhu et al., 1996), stressing the importance of mitochondria in some forms of apoptosis.

Both Bcl-2 (Krajewski et al., 1993; Riparbelli et al., 1995) and Bax (Marzo et al., 1998a; Marzo et al., 1998b) have been co-localized at contact sites between the inner and outer mitochondrial membranes (i.e., at the PTP). Using FRET analysis of green fluorescent protein (GFP) fusions with both Bax and Bcl-2, Mahajan et al. demonstrated a co-localization between Bcl-2 and Bax at the mitochondria, which confirms the structural analysis predicting an interaction between Bcl-2 and Bax (Mahajan et al., 1998). The significance of the interaction between Bcl-2 and Bax is controversial. It was once believed that the intracellular ratio between Bcl-2 and Bax was critical in the regulation of apoptosis (e.g., Korsmeyer et al., 1993). However, it has been recently shown that Bax alone can induce mitochondrial changes that signal apoptotic cell death (Marzo et al., 1998b; Narita et al., 1998) through an interaction with the PTP in isolated mitochondria or reconstructed PTP complexes. Also, preliminary data reported by Mahajan et al. using FRET analysis indicate a reduced interaction between Bcl-2 and Bax in cells undergoing apoptosis (Mahajan et al., 1998).

The specific effects of Bcl-2 on cell survival are extremely wide ranging and are concentrated at different sites in the initiation and effector phases of mitochondrially dependent apoptosis. Bcl-2 has been shown to inhibit generation of reactive oxygen species (ROS; Kane et al., 1993), and increase levels of catalase, SOD and GSH (Ellerby et al., 1996). In the mitochondria, Bcl-2 can

prevent the disruption of $\Delta\Psi_M$ (Kroemer et al., 1995) and the $\Delta\Psi_M$ - dependent generation of ROS during the effector phase (Zamzami et al., 1995). Additionally, the enhanced influx of Ca^{++} into mitochondria (Baffy et al., 1993), and the release of cytochrome c from the intermembrane space into the cytosol is also prevented by Bcl-2 (Kluck et al., 1997; Yang et al., 1997).

The importance of the interaction of Bax with mitochondria, and specifically with the PTP, has recently been illustrated. A specific, and requisite, interaction between Bax and the ANT was demonstrated by Marzo et al. (Marzo et al., 1998b). Bax and the ANT co-immunoprecipated with each other in isolated PTP complexes and the interaction was confirmed using the yeast two-hybrid system. Additionally, in PTP complexes isolated from Bax deficient mice or in vesicles that had been immunodepleted of Bax, the pore opening agent atractyloside was unable to induce release of $DiOC_6$ that had been previously loaded into vesicles containing the PTP complexes (Marzo et al., 1998b). The requirement for Bax was also demonstrated by the inability of atractyloside to induce $\Delta\Psi_M$ loss in isolated mitochondria from Bax deficient mice.

Narita et al. (1998) showed that recombinant Bax, or pro-apoptotic Bak, added to isolated mitochondria was incorporated into the PTP and co-immunoprecipitated with the VDAC. Further, it was shown that Bax induced a rapid collapse of $\Delta\Psi_M$, induction of permeability transition, and release of cytochrome c from mitochondria that was prevented by co-incubation with Bcl-2 or Bcl-X_L. The correlation between loss of $\Delta\Psi_M$ and cytochrome c release, which is controversial (see Kluck et al., 1997; Yang et al., 1997; Bossy-Wetzel et al.,

1998), was also addressed by these authors. Isolated mitochondria were incubated in a hypotonic medium in order to disrupt the outer mitochondrial membrane and deplete cytochrome c, which is localized in the intermembrane space. These mitochondria were no longer capable of maintaining $\Delta\Psi_M$ until purified cytochrome c was added into the incubation medium (Narita et al., 1998), indicating that electron transport had been restored. Addition of recombinant Bax in the presence of added cytochrome c still induced the loss of $\Delta\Psi_M$, suggesting to the authors that Bax induced disruption of $\Delta\Psi_M$ occurs independently of cytochrome c release (Narita et al., 1998). However, the integrity of the PTP, which spans both inner and outer mitochondrial membranes, was not verified; nor was the ability of Bax to induce permeability transition in those mitochondria with disrupted outer membranes, making the interpretation of these data difficult.

Given the close relationship between mitochondrial function and many forms of apoptotic cell death, and the association between glucose metabolism and mitochondria, the link between glucose metabolism and apoptotic cell death may contribute to the pathogenesis of DPN.

I.i Glucose Metabolism and Apoptosis

Recent evidence suggests that high glucose conditions may be toxic to various cell types in vitro and in vivo. High glucose media as well as the glucose analogue 3-O-methyl-glucose (30 mM for 48-72 hr) induces apoptosis in human endothelial cells in vitro (Baumgartner Parzer et al., 1995; Du et al., 1998). Using cultured human neuroblastoma cells, Gandhi et al. reported that 20 mM glucose

is toxic to neurons over a 24 hr period, and that treatment with insulin-like growth factor I (IGF-I) prevents this cell death (Gandhi et al., 1995). Using the same model system, Cheng and Feldman have demonstrated that exposure to high glucose induced tyrosine phosphorylation of the mitogen-activated protein kinases (MAP kinase), p38 kinase, and c-Jun N-terminal kinase (JNK) in a dose- and time-dependent manner (Cheng and Feldman, 1998). It was also shown that treatment with IGF-I prevented the activation of JNK. This confirms the observation that withdrawal of NGF from cultures of differentiated PC12 cells, which leads to apoptotic cell death, is preceded by induction of both p38 kinase and JNK activity (Xia et al., 1995). The high glucose induced increases in p38 kinase and JNK phosphorylation occurred within 15 min after exposure, which significantly precedes the time at which the peak cell death is observed in these cells (24 hr), and correlates with the time course of kinase activation and cell death reported in PC12 cells.

Increased oxidation of glucose, in hyperglycemic conditions may result in the overproduction of oxidative radicals (Hunt et al., 1988; Kashiwagi et al., 1994). Elevated glucose levels have been shown to up-regulate mRNA levels as well as activity of the antioxidant enzymes SOD-1, catalase, and glutathione peroxidase (Ceriello et al., 1996) in endothelial cells, suggesting that these cells may be responding to increased oxidative radical production induced by exposure to high glucose. Treatment with exogenous SOD (Du et al., 1998) has been shown to prevent endothelial cell death following exposure to both high glucose and high 3-O-methyl-glucose. Glutathione depleted FRTL5 cells (a rat

thyroid cell line) die via apoptosis when exposed to 10 mM glucose, while 20 mM glucose invokes necrotic cell death (Donnini et al., 1996).

It has been reported previously that there is enhanced production of tumour necrosis factor-alpha (TNF-α) in spontaneously and STZ treated diabetic rats challenged with systemic lipopolysaccharide (LPS) (Tanaka et al., 1992; Sagara et al., 1996). In the central nervous system, certain cytokines (e.g., interleukin 6, IL-6; IL-1; and TNF-α) and LPS can induce the expression of iNOS in astrocytes (Bolanos et al., 1995). This is followed by increased production of NO, which can be toxic to central neurons. Knock-down of SOD-1 levels with antisense oligonucleotides leads to the apoptotic death of PC12 cells via the reaction of $\bullet O_2^-$ with NO to form peroxynitrite (ONOO-), which at low concentrations, induces the apoptotic death of PC12 cells (Estevez et al., 1995). Treatment of PC12 cells with TNF-α and LPS also stimulates the expression and activity of iNOS leading to the apoptotic death of these cells. The NOS inhibitor N-monomethylarginine, and aminoguanidine can block this cell death (Heneka et al., 1998).

It is not clear whether Schwann cells exposed to hyperglycemic conditions in vivo increase the production of NO. Cultured Schwann cells can secrete significantly greater amounts of the NO metabolite nitrite (NO$_2$) in a dose dependent manner when exposed to TNF-α and interferon-gamma (IFN-γ) (Gold et al., 1996; and see below). In vivo, Schwann cells upregulate the mRNA and protein levels of TNF-α and interleukin (IL)-6 following peripheral nerve crush; while in vitro, mRNA and protein levels of IL-6 and the IL-6 receptor increase

following TNF-α or trophic withdrawal in cultured Schwann cells (Wagner and Myers, 1996; Bolin et al., 1995). Prolonged hyperglycemia in vivo may induce Schwann cell upregulation of TNF-α and IL-6, which may, in turn, act in an autocrine manner (Bolin et al., 1995), stimulating iNOS. Alternatively, there may be a more direct link between glucose metabolism in hyperglycemic conditions and apoptotic cell death.

Recent evidence demonstrating co-localization of the glycolytic enzyme hexokinase with contact sites between the inner and outer mitochondrial membranes provides a potential link between glucose metabolism and apoptosis. Hexokinase (Type I; HK-I) forms a tetrameric structure (Xie and Wilson, 1990) upon binding to the mitochondrial PTP complex at the contact sites between the outer and inner mitochondrial membranes (Fiek et al., 1982; Linden et al., 1982; Krueger, 1991; McEnery et al., 1992). Sequence analysis has determined that the COOH terminus contains a mitochondrial insertion domain that specifically targets HK-I to the VDAC (Wilson, 1997).

It has been observed that the activity of hexokinase is increased 5 to 10 fold when bound to the VDAC (Weiler et al., 1985) and intact mitochondria that have maintained $\Delta\Psi_M$. This has prompted others to suggest that increases in $\Delta\Psi_M$ change the pore structure, which then increases binding affinity for hexokinase (Brdiczka and Wallimann, 1994). Binding of hexokinase to the VDAC-ANT complex in the presence of physiological concentrations of glucose (5 mM) promotes closure of the PTP (Beutner et al., 1997). In vitro studies have shown that re-constituted hexokinase-VDAC-ANT complexes in vesicles loaded

with ATP or malate were utilized to investigate the mechanics of hexokinase modulation of the VDAC-ANT pore complex (Beutner et al., 1997). ATP or malate release from these vesicles was used as an estimate of opening of the artificial PTP complex. Spontaneous ATP or malate release from these in vitro pore complexes was prevented by the addition of physiological (5 mM) concentrations of glucose suggesting a possible regulatory role of hexokinase activity or binding on PTP conformation (Beutner et al., 1997). In other words, in intact cells, events that would precipitate the liberation of hexokinase from its PTP binding sites may lead to the opening of the PTP and the beginning of the mitochondrially controlled apoptotic cascade.

Lynch et al. (1991) utilized confocal imaging and hexokinase immunofluorescence to examine the association between hexokinase and mitochondria under different metabolic conditions. Hexokinase was localized to mitochondria using an antibody raised against a protein derived from the inner mitochondrial membrane (Lynch et al., 1991). Image analysis determined that in primary cultured astrocytes, approximately 70% of total hexokinase was localized to mitochondria. When glucose was replaced with 2-deoxyglucose, a four-fold increase in the amount of gluocse-6-phosphate was detected, and a 35% reduction of mitochondrial bound hexokinase was observed within 1 hr (Lynch et al., 1991). The metabolic control of hexokinase localization to mitochondria was confirmed in smooth muscle cells microinjected with purified hexokinase conjugated with a fluorochrome (rhodamine X succinimidyl ester; Lynch et al., 1996). Exposure to 2-deoxyglucose in these cells caused a significant drop in

the ratio of mitochondrial bound hexokinase to free cytosolic hexokinase within 15 min. Treatment with 3-O-methyl-glucose also caused a significant drop in this ratio following 15-30 min exposure (Lynch et al., 1996).

Under normal conditions, hexokinase is inhibited (and solubilized) by its reaction product glucose-6-phosphate (Wilson, 1997; Lynch et al., 1996). Excessive phosphorylation of glucose by hexokinase may lead to the accumulation of glucose-6-phosphate within the cell, which in turn can solubilize and inhibit hexokinase thus altering the conformation of the mitochondrial PTP and favoring the open state. This notion is supported by the recent observation of apoptotic death of human endothelial cells exposed to high 3-O-methyl-glucose, a glucose analogue that is phosphorylated by hexokinase but not further metabolized by the cell (Du et al., 1998). Presumably, in these cells there is an accumulation of phosphorylated 3-O-methyl-glucose which might inhibit and release hexokinase from its binding site at the mitochondrial PTP, and in turn alter the conformation and permeability of the PTP.

I.j Hypothesis and Specific Aims

An examination of the effects of high glucose on Schwann cell survival is necessary in order to determine the role of Schwann cell dysfunction in the pathogenesis of DPN. Consequently, an in vitro model was chosen which would eliminate the influence of other cells such as endothelial cells which are known to increase nitric oxide production following exposure to high glucose. Schwann cells were obtained from postnatal day 2 (PD2) and postnatal day 15 (PD15) rats

to test the following hypotheses,

H_o1: that high glucose concentrations are directly toxic to Schwann cells

H_o2: that exposure to high glucose media can induce apoptotic cell death in Schwann cells in vitro that is accompanied by mitochondrial dysfunction

Specific Aims:

1. The effects of a range of glucose concentrations (5.5-50 mM) on Schwann cell survival will be examined by counts of intact nuclei in order to determine whether there is a dose-dependent effect on PD2 and PD15 cells. Counts will be made at 0, 2, 12, 24 and 48h after addition of the glucose test concentrations in media.

2. In situ end-labeling and YOYO-1 staining will be used to determine whether Schwann cell nuclei display fragmented DNA with free 3'-OH ends and condensed chromatin respectively, which are considered morphological hallmarks of apoptosis.

3. Anti-apoptotic agents, (-)-desmethyldeprenyl, IGF-1 and N-acetyl cysteine will be used to prevent Schwann cell apoptosis in high glucose, using counts of intact nuclei to assess cell survival.

4. Levels of nitrite in the media will be used to determine whether high glucose induces increased nitric oxide production in Schwann cells. Specific NOS inhibitors will be used to determine whether increased NO leads to decreased Schwann cell survival in high glucose media. TNF-α will also be measured by ELISA to determine if changes in Schwann cell NO production are due to

increased TNF-α signaling.

5. Changes in mitochondrial membrane potential ($\Delta\Psi_M$) following exposure to high glucose for 2, 6, and 24 hr; and the ability of the anti-apoptotic agents (-)-desmethyldeprenyl, N-acetyl cysteine, or IGF-I to prevent any changes will be measured using the potentiometric fluorescent dye CMTMR. Changes in $\Delta\Psi_M$ following inhibition of NO production in high glucose will also be examined using CMTMR.

6. The involvement of the PTP in high glucose induced Schwann cell apoptosis will be examined using immunofluorescence imaging of specific protein localized to the PTP. The sub-cellular distribution of hexokinase using confocal laser microscopy will be observed in relation to the changes in $\Delta\Psi_M$. The relationship between $\Delta\Psi_M$ and hexokinase binding in high glucose and in response to modification of PTP conformation will be assessed in order to determine whether their relationship can reflect the status of the PTP.

7. Changes in the sub-cellular distribution of hexokinase and Bax in high glucose will be examined using Western blot analysis of enriched mitochondrial, cytoplasmic, and nuclear fractions.

II. Materials and Methods

II.a Post-Natal Day 2 and Post-Natal Day 15 Schwann Cell Cultures

Litters from timed-pregnant Sprague-Dawley rats (Charles River; Montreal, Quebec or Taconic Farms, New York) were used at post-natal day 2 (PD2) or PD15. Following decapitation under deep anesthesia, a 10-15 mm segment of sciatic nerve distal to the sciatic notch was quickly removed and placed in ice-cold Dulbecco's modified Eagle's medium (DMEM; Sigma) containing 5.5 mM D-glucose, 25 mM HEPES, penicillin (20 U/ml) and streptomycin (20 □g/ml). The nerves were separated into fascicles, cleaned free of the epineurial and perineurial sheaths, and cut into 1 mm long segments. The nerve fragments were incubated in 0.0125% trypsin-EDTA/0.03% Type I collagenase in Hank's buffered salt solution (HBSS, Gibco) for 45 min at 37° C. The fragments were then washed in DMEM/10% fetal bovine serum (FBS, Gibco) and seeded onto 75 cm^2 tissue culture flasks (PD15) or 25 cm^2 (PD2) (Nunc) coated with poly-L-lysine (0.1 mg/ml; Sigma). The cells were maintained at 37° C in a 5% CO_2 atmosphere. Over the next 5 days, Schwann cells migrated out of the nerve pieces and adhered to the plastic surface. On day 5, the fragments were removed, and the remaining adherent cells maintained in DMEM/10% FBS with 500 µg/ml bovine pituitary extract (Upstate Biotechnology) and 0.5 µg/ml cholera toxin (Research Biochemicals) for PD2 Schwann cells, or DMEM/10% FBS only for PD15 Schwann cells until confluency was reached.

When confluent (day 10) the cells were harvested with 0.05% Trypsin-EDTA, and plated onto poly-L-lysine coated glass coverslips (12 mm, thickness

0; Carolina Biological Supply) at a density of 12,000 cells per coverslip, or onto poly-L-lysine coated 24 well plates (Nunc) for cell counting, at a density of 12,000 cells per well. Twenty-four hr after secondary plating, the medium was replaced with DMEM/5% FBS. Cells were allowed to stabilize in the new media for 24 hr before being placed in DMEM/2% FBS at 0 hr.

II.b Immunocytochemical Identification of Schwann Cells

Cells plated on coverslips were rinsed in phosphate buffered saline (PBS: 9 g NaCl, 3.2 g sodium phosphate monobasic, 10.9 g sodium phosphate dibasic/liter distilled H_2O) and then fixed in ice-cold 4% paraformaldehyde for 10 min. After rinsing in PBS, cells were blocked in 10% normal goat serum or normal horse serum, followed by overnight incubation with primary antisera against: MAG (1:20, Boehringer Mannheim), MBP (1:100, Sternberger Monoclonals), 2',3'-cyclic nucleotide 3'-phosphodiesterase (CNPase; 1:200, Sigma), L1 (1:20, Boehringer Mannheim), GFAP (1:800, Sigma), Thy 1.1 (hybridoma supernatant, ATCC), S100 (1:400, Dako), or ciliary neurotrophic factor (CNTF; 1:250, antiserum was kindly provided by Dr. Peter Richardson, Montreal General Hospital). Following PBS rinses, coverslips were incubated with biotinylated secondary antibodies (1:300, Vector Labs), fluorescein isothiocyanate (FITC) conjugated goat anti-rabbit IgG (1:250; Molecular Probes), or Texas Red (TR) conjugated goat anti-mouse IgG (1:200; Molecular Probes). Coverslips incubated with biotinylated secondary antibodies were rinsed in PBS, incubated for 30 min in avidin-horseradish peroxidase (Elite kit, Vector Labs) and

then incubated with (1.2 mg/ml) diaminobenzidine (Sigma) mixed 1:1 (v:v) with 0.01% hydrogen peroxide for chromogenic detection. Coverslips incubated with fluorescently labeled secondary antibodies were mounted in glycerol/PBS or Aquamount (VWR) and examined under epifluorescence with TR or FITC filter sets equipped with a Leica true confocal scanning (TCS) microscope.

II.c Assessment of Schwann Cell Proliferation in Baseline Glucose Media

Post-natal day 2 and PD15 Schwann cells grown in 24 well plates or on glass coverslips were maintained in the base medium containing 2% FBS and 5.5 mM glucose for the indicated time points (0, 2, 12, 24, and 48 hr). The cells were harvested and counts of intact nuclei (see below for description of counting method) were used to estimate proliferation. Additionally, Schwann cells grown on coverslips in base medium were fixed in 4% paraformaldehyde for 10 min and stained with an antibody raised against the Ki67 nuclear antigen. Fixed cells were briefly permeabilized with methanol for 30 sec at $-20°$ C, followed by blocking in 10% normal goat serum for 30 min at room temperature. Coverslips were incubated overnight at $4°$ C with a monoclonal antibody raised against the Ki67 nuclear antigen (1:200, Novocastra). Following PBS rinses, coverslips were incubated with a biotinylated anti-mouse secondary antibody (1:250, Vector Labs) for 40 min at room temperature, followed by PBS rinsing and a further 30 min incubation with avidin-horseradish peroxidase (Elite Kit, Vector Labs). Chromogenic detection was performed in the presence of diaminobenzidine (1.2 mg/ml; Sigma) mixed 1:1 (v:v) with 0.01% hydrogen peroxide. Coverslips were

then mounted in Aquamount. Cells that displayed no immunoreaction product were considered to be in the G_0 phase of the cell cycle and therefore not actively cycling. Cells in the G1-S phase showed Ki67 immunoreactivity associated with the nucleolus, while cells in the G2-M phase displayed intense patches of nuclear immunoreactivity, as well as increasing Ki67 immunodensity in the nuclear matrix (see (Braun et al., 1988)). Cells were counted at 0, 12, and 24 hr in randomly determined grids created on a schematic of the 12 mm round coverslip. The random numbers were generated by the Origin™ (Microcal) software package and corresponded to coordinates representing individual 40X microscope fields. The data represent the percentage of the total number of cells per 40X field in G_0.

II.d Assessment of Schwann Cell Survival in High Glucose Media

Cells were harvested at 0, 2, 12, 24, and 48 hr after the addition of DMEM/2% FBS with increasing glucose content (5.5, 17.5, 30, 40, or 50 mM). Other cells were treated with either 5.5 mM glucose or 40 mM glucose with the simultaneous addition of IGF-1 (1 ng/ml), DMD (10^{-9} M), or NAC (10^{-7} M) and harvested at 2 or 24 hr. Additionally, cells exposed to 5.5 or 40 mM glucose were also treated with the inducible nitric oxide synthase (iNOS) specific inhibitor N^δ-(1-iminoethyl)-L-lysine (L-NIL; 10^{-4} M, Molecular Probes), the NO donor S-nitroso-acetyl-penicillamine (SNAP; 1, 10, 100 μM, Sigma) cyclosporin A (CsA; 10^{-7} M, Sigma) or atractyloside (ATR; 10 mM, Sigma) and harvested at 24 hr. Cells were lightly digested with 0.05% trypsin-EDTA for 1 min, to remove them

from the 24 well plates and the contents of each well (including those cells that were detached from the substrate and floating in the medium) centrifuged at 600 x g for 5 min. The supernatant was removed and the pelleted cells resuspended in 200 μl of lysis buffer containing 10% Zapoglobin-II (Coulter Electronics). Nuclei with a completely intact, smooth membrane enclosing visible nuclear material (under phase contrast microscopy) were counted on a haemocytometer. This counting method is effectively a sensitive measure of nuclear fragility (see Wadia et al., 1998 for details) and can provide an accurate estimate of cell survival. Mean values shown are taken from a minimum of 12 duplicate wells obtained from 3 or more litters.

II.e Detection of Apoptotic Nuclei

In situ end labeling (ISEL) was used to detect free 3'-OH ends of endonuclease digested nuclear DNA, considered to be a characteristic feature of the final degradative phase of apoptosis. Schwann cells grown on glass coverslips treated with 5.5, 17.5, or 40 mM glucose were fixed with cold 4% paraformaldehyde for 10 min at 2, 12, and 24 hr. Following a 1 min permeabilization with methanol at -20° C, the coverslips were treated with DNAse-free RNAse A (100 μg/ml, Boehringer Mannheim) for 10 min at 37° C. Coverslips were then incubated with terminal deoxynucleotidyl transferase (TdT) reaction buffer (Boehringer Mannheim) for 15 min at room temperature. The reaction buffer was removed and replaced with fresh buffer containing 12.5 units TdT (Boehringer Mannheim) and 10 μM BODIPY/fluorescein-conjugated dUTP

(Molecular Probes) for 60 min at 37° C. The reaction was terminated by several rinses with 2X SSC (0.03 M sodium citrate, 0.3 M sodium chloride) at 37° C. The coverslips were mounted in glycerol/PBS or Aquamount and observed with a FITC filter set on a Leica inverted microscope with epifluorescence.

The nucleic acid-specific cyanine dye YOYO-1 (Molecular Probes) was used to visualize chromatin condensation which is also considered to be a characteristic feature of the degradative phase of apoptosis (Tatton et al., 1998; Tatton and Kish, 1997). Fixed cells were briefly permeabilized with methanol (-20° C) for 30 sec and washed with PBS, followed by incubation with 1 mM YOYO-1 (diluted in PBS) at room temperature for 30 min. The coverslips were then washed several times with PBS and mounted in Aquamount for confocal imaging.

Other identically treated coverslips were dual stained with BODIPY/TR-dUTP and YOYO-1 to reveal ISEL and chromatin condensation. When visualized under epifluorescence and confocal microscopy (see below), it was determined that all ISEL positive cells also demonstrated classic chromatin condensation. Therefore counts were made of ISEL positive cells to provide an estimate of Schwann cell apoptosis. Using a 40X objective, ISEL-positive cells (round, bright green nucleus, pale cytoplasm) in each of 10 sample areas per coverslip were counted. This procedure was repeated on 3 coverslips from each treatment, resulting in a total of approximately 3000 cells counted per group.

II.f Measurement of NO Production by Schwann Cells Exposed to High Glucose

To determine if Schwann cells exposed to high glucose upregulated their production of NO, the Greiss reagent (N-(1-naphthyl)ethylenediamine and sulfanilic acid) was used to measure levels of the NO metabolite NO_2^- released by the cells in the culture medium, as an estimate of NO production. The reaction is based on the conversion of sulfanilic acid to diazonium salt, in the presence of NO_2^-, which when combined with N-(1-naphthyl)ethylenediamine produces an azo colour product which can then be measured spectrophotometrically. Since NO_2^- is rapidly metabolized to NO_3, total NO_2^- was estimated by reducing NO_3 to NO_2^- with nitrate reductase, followed by incubation with the Griess reagent. PD2 and PD15 Schwann cells were seeded in 24 well plates at approximately 100,000 cells per well. Forty-eight hr later the cells were washed twice and replaced with DMEM/2% FBS containing 5.5 or 40 mM glucose. Other cells exposed to 40 mM glucose were treated with the iNOS inhibitor L-NIL (10^{-4} M), the cNOS inhibitor SMTC (10^{-4} M), or DMD (10^{-9} M). As a positive control, cells in base media were treated with 100U of TNF-α/IFN-γ which has been shown previously to increase NO production by Schwann cells (Gold et al., 1996).

Following a 24 hr incubation, an aliquot of medium was removed from each of 6 replicate wells per group and centrifuged at 2000 rpm for 5 min to pellet any floating cells. The supernatant was removed and incubated with 200 μM FAD, 2 U/ml nitrate reductase, and 2mM NADPH for 1 hr at room temperature.

This reaction was stopped by quenching excess NADPH by adding 210 mM pyruvate and 400 µg/ml lactate dehydrogenase in 0.1 M PBS. Equal volumes of the reduced sample were then mixed with the Griess reagent and incubated at room temperature for 1 hr. The absorbance was read in a plate reader (Molecular Devices) at 540 nm.

II.g Measurement of TNF-α Release From Schwann Cells Exposed to High Glucose

To determine if Schwann cells exposed to high glucose upregulated production and release of the cytokine TNF-α, an ELISA measuring TNF-α released into the media was performed. PD2 Schwann cells were seeded in 24 well plates at approximately 100,000 cells per well. Forty-eight hr later the cells were washed twice and replaced with DMEM/2% FBS containing 5.5 or 40 mM glucose, or with 40 mM glucose plus DMD (10^{-9} M). Following a 24 hr incubation, an aliquot of media was removed from each of 6 replicate wells per group and centrifuged at 2000 rpm for 5 min to pellet any floating cells.

Each sample was incubated on ELISA plates pre-coated with anti-rat TNF-α capture antibody (Biosource International) together with a second biotinylated anti-rat TNF-α antibody for 90 min at room temperature. Each well was washed 4 times with the supplied wash buffer according to the manufacturer's instructions, and then incubated with streptavidin-horseradish peroxidase for 45 min at room temperature. The wells were washed again 4 times and incubated with tetramethylbenzidine as a chromogen for 30 min at room temperature.

Following addition of stop solution, the absorbance of each well was read in a plate reader against a chromogen reference (Molecular Devices) at 450 nm.

II.h Confocal Imaging

High-resolution laser confocal imaging techniques provide the opportunity to directly visualize the sub-cellular distribution of specific proteins, allowing us to reconstruct the time course of pro-apoptotic signaling events. For example, the level of detail provided by confocal microscopy allows individual mitochondria to be resolved enabling the measurement of fluorescence of dyes that estimate mitochondrial membrane potential (see Wadia et al., 1998 for examples). Epifluorescent microscopy cannot resolve many of these sub-cellular localization questions because of the background haze of fluorescence that results from those portions of the cell outside of the observed focal plane. Laser confocal imaging is based on the reduction of out of focus haze through the use of a series of pinholes of varying aperture which are placed in the path of the light exciting the sample and also, most importantly, in the path of emitted light coming from the sample. These pinholes dramatically reduce the contribution made by signals arising from out of focus elements to the final image resulting in improved resolution. There is still, however, an appreciable amount of background "noise" in the confocal image that is not eliminated by the pinhole (see Shaw, 1994). This can be further reduced by deconvolution algorithms that mathematically subtract the signal from above and below the optical plane of interest, resulting in a depth of resolution approaching 50 nm. This is particularly

useful when establishing the co-localization of specific proteins within the cell.

II.i Analysis of Mitochondrial Membrane Potential ($\Delta\Psi_M$)

As has been previously reported in a number of models of apoptosis (Wadia et al., 1998; Zamzami et al., 1995), apoptotic cell death is often preceded by a fall in mitochondrial membrane potential ($\Delta\Psi_M$). To determine if the observed Schwann cell death was also accompanied by a fall in $\Delta\Psi_M$, Schwann cells were incubated with the potentiometric fluorescent dye, chloromethyl-tetramethlyrosamine methyl ester (CMTMR; Molecular Probes, 130 nM for 15 min at 37°C). This lipophilic cationic dye is preferentially taken up by mitochondria in proportion to $\Delta\Psi_M$ where it irreversibly binds to protein thiol groups within the mitochondrial matrix and is retained following aldehyde fixation. The irreversible interaction between CMTMR and matrix thiols occurs with respect to $\Delta\Psi_M$ and is not influenced by mitochondrial volume (Metivier et al., 1998). The CMTMR fluorescence intensity therefore represents the highest level of negativity difference (ie. the greatest $\Delta\Psi_M$) in the mitochondria during the period of dye exposure prior to fixation.

A Leica confocal microscope was used to image the cells. A pinhole aperture setting of 20 was maintained with constant laser and photo-detector power settings and an excitation wavelength of 568 nm and a bandpass emission filter of 600/30 nm. Each image was scanned using an oil-immersion, 100X, 1.4 N.A. objective at 512 by 512 by 8 bits per pixel resolution, background offset of -1 and line averaged 32 times. The confocal images were saved as tagged image

file format (TIFF) files for analysis. The Metamorph™ (Universal Imaging, Ltd.) image analysis system for Windows was used to measure the intensity of CMTMR fluorescence in individual mitochondria. In each mitochondrion, no fewer than two regions were defined by a box each measuring 9 pixels square. The average intensity per pixel within each defined region is measured and automatically logged to a Microsoft Excel spreadsheet for analysis. The intensity measured ranged from 0 (no fluorescence) to 255 (maximum fluorescence) and are referred to as fluorescence intensity units (FIU). The data represent images of approximately 10 cells per coverslip on 3 coverslips, with approximately 20-30 intensity measurements obtained from each cell.

Maintaining constant pinhole aperture, laser power, image size, and photo-detector voltage settings for each image allows the direct comparison of CMTMR fluorescence intensity between groups in a single experiment without necessitating the use of ratiometric dyes such as 5,5', 6,6'-tetrachloro-1,1', 3,3'-tetraethybenzimidazol carbocyanine iodide (JC-1), or the ratio between intramitochondrial CMTMR and adjacent cytoplasmic or nuclear CMTMR background fluorescence. Baseline differences in CMTMR fluorescence intensity between PD2 and PD15 Schwann cells precluded the direct comparison of $\Delta\Psi_M$ across the two populations of Schwann cells. In this case, only relative comparisons of the magnitude of high glucose induced changes in $\Delta\Psi_M$ can be made.

II.j The Relationship Between $\Delta\Psi_M$ and the Sub-cellular Distribution of Apoptosis-Related Proteins

In experiments where the localization and intensity of specific

mitochondrial and other proteins (e.g., hexokinase) are correlated with estimates

of $\Delta\Psi_M$, duplicate confocal images in the same focal plane are obtained for

CMTMR and the immunofluorescence signal. For each of the defined CMTMR

regions within mitochondria, the corresponding pixel co-ordinates are obtained

using the Metamorph™ software package and the regions are then superimposed

on the alternate immunofluorescence image. Since the corresponding images

are obtained simultaneously by separate detectors, the co-ordinates obtained by

the software package correspond to the exact pixel location on each image from

which the fluorescence intensity is measured. It is necessary to make

measurements from the original black and white confocal images. During the

digital re-colourization process for printing using Northern Eclipse™, low-end

intensity values can sometimes be lost. Quantitative measurements are

therefore made from the original black and white confocal digital images.

Schwann cells were treated with 5.5 or 40 mM glucose or an agent that

maintains the PTP in an open state (atractyloside, 1 mM; Zamzami et al., 1996).

At the end of the indicated time point, treated Schwann cells were incubated with

CMTMR for 15 min at 37° C, fixed with ice-cold 4% paraformaldehyde for 30 min,

and processed for the immuncytochemical co-localization of HK Type I to

mitochondria. The fixed coverslips were then permeabilized with 0.02% Tween

20 for 25 min at room temperature and then blocked for 1 hr with 10% normal

donkey serum to minimize non-specific binding, and incubated with a mouse

monoclonal antibody raised against HK-I (Chemicon; 1:500) overnight at 4°C.

Coverslips were washed in PBS and incubated with a Cy5 conjugated second

antibody (Jackson ImmunoResearch) at a dilution of 1:250 for 1 hr at room

temperature. Coverslips were then washed with PBS and mounted with

Aquamount.

In order to make reliable estimates of immunofluorescence intensity from

the confocal images; several steps were taken to insure that any differences

observed were not due to differences within the immunostaining procedure.

First, all coverslips were stained in parallel using common antibody and dye

reagent stocks, carefully controlling for the incubation time. Second, during the

acquisition of the CMTMR/HK image pairs, dual-fluorochrome images were

obtained simultaneously using two independent detector channels and constant

laser power, pinhole, and detector voltage settings.

II.k Western Blot Analysis of the Sub-cellular Distribution of Apoptosis-Related Proteins

To further quantify and confirm changes in the sub-cellular distribution of

certain proteins throughout the apoptotic cascade, western blots of cytoplasmic,

mitochondrial, and nuclear compartments were performed. PD2 Schwann cells

were harvested in ice-cold PBS and centrifuged at 2000 rpm for 6 min. The

pellet was resuspended in a lysis buffer containing: sucrose, 250 mM; DTT, 1

mM; EDTA, 1 mM; EGTA, 1 mM; MgCl$_2$, 1.5 mM; KCl, 10 mM; and HEPES, 20

mM with 1 mM each of the following protease inhibitors: leupeptin, pepstatin A,

chemostatin, aprotinin, antipain, and 5 mM benzamidine. The cells were

homogenized in a tight-fitting Dounce homogenizer and centrifuged at 800 rpm

for 10 min at 4°C to pellet the nuclei. The supernatant was collected and the

pellet was resuspended in lysis buffer to disrupt any remaining unbroken cells

and centrifuged again at 700 rpm for 10 min at 4°C. The resulting nuclear pellet

was resuspended in 50 μl of lysis buffer. The supernatant was then centrifuged

at 10,000 rpm for 15 min at 4°C resulting in a crude mitochondrial pellet and

cytoplasmic supernatant. The mitochondrial pellet was resuspended in 50 μl of

lysis buffer and all samples were stored at -30°C until use.

For sodium-dodecyl-sulfate polyacrylamide gel electrophoresis (SDS-

PAGE), 12% acrylamide mini-gels (Biorad) were run at approximately 100mV for

1.5 hr or until the dye front reached the bottom of the gel. The protein was then

transferred to nitrocellulose membranes (Pierce), which were then blocked with

10% non-fat milk for 1 hr, and incubated overnight with antibodies raised against

HK-I (1:500), or Bax (1:250). The membranes were then incubated with

horseradish peroxidase-conjugated second antibodies for 1 hr and visualized

with an enhanced chemiluminescence (ECL) kit (Pierce).

II.I Data Analysis

For estimation of cell survival, counts of intact nuclei are presented as the

number of intact nuclei per ml or the percentage of intact nuclei relative to control

(5.5 mM glucose). Cell cycle estimation and counts of ISEL-positive Schwann cells are presented as the percentage of total cells per 40X microscope field. CMTMR fluorescence intensity data are presented as frequency histograms representing the percentage of mitochondria with a given fluorescence intensity on a scale of 0-255. In this way, subtle changes in small populations of individual mitochondria, particularly at early time points, that may be obscured by parametric analysis only (i.e. comparing sample means), can be identified. All data were analyzed using the non-parametric Mann-Whitney U test since the assumptions of normality and homogeneity of variance were not met.

III. Results

III.a Characterization of PD2 and PD15 Schwann Cells

This study describes a novel method for isolating rat Schwann cells from post-natal sciatic nerve, that results in the establishment of two distinct Schwann cell populations that differ in the proteins that they synthesize and their proliferation rates. In contrast to previous methods that enzymatically and mechanically dissociate the sciatic nerve into a cell suspension containing primarily Schwann cells and fibroblasts, nerve fragments were plated directly onto a plastic surface. Over the first 5 days in vitro, cells migrate out from the nerve fragments and adhere to the poly-L-lysine coated plastic flask. Figure 6A illustrates a low power, phase contrast image of a nerve fragment 2 days after the initial plating showing presumptive Schwann cells emerging from the nerve fragment. These cells remained adherent after the nerve fragments were removed by washing after 5 days in vitro. Figure 6B and 6C illustrate the remaining adherent cells from the PD2 and PD15 sciatic nerve fragments respectively at approximately 5 days in vitro, prior to secondary plating. Note that the PD2 cells tend to be spindle-shaped with long processes, whereas PD15 cells have a more polygonal cell soma with either very short or no processes. Following removal of the nerve fragments, PD2 cells required additional mitogenic supplements (BPE and CT) to reach confluency while the PD15 cells required no further supplements in addition to 10% FBS (see below). After 10 days in vitro, cells were subplated into wells or onto glass coverslips, and the FBS content reduced from 10% to 2% over the next 48 hr.

Figure 6. Migration of PD2 and PD15 cells from nerve fragments. Phase

contrast photomicrograph showing novel isolation method of Schwann cells from

PD2 and PD15 rat. A. Low power image (100X mag.) of cells migrating out of

sciatic nerve fragment from PD2 rat shown at day 2 in vitro. B. Higher

magnification (400X mag.) image showing appearance of adherent cells

remaining following removal of nerve fragments at day 5 in vitro from PD2 rat;

note spindle morphology and phase bright appearance of PD2 cells. C.

Appearance of PD15 cells (250X mag.) after removal of nerve fragments at day 5

in vitro; note here that cells have flattened onto plastic surface and have few, if

any, extended processes.

Figure 6.

In vivo, the calcium-binding protein S-100 is first detectable in both myelinating and ensheathing Schwann cells by embryonic day 15-16 (Jessen and Mirsky, 1991). Myelination typically begins during the first post-natal day, while differentiation of ensheathing Schwann cells proceeds through the second and third weeks after birth (Jessen and Mirsky, 1992). In vivo, myelinating Schwann cells characteristically express the myelin proteins MAG, MBP, P_0, PLP, PMP-22 among others. In contrast, ensheathing Schwann cells express GFAP, the immunoglobulin superfamily adhesion molecule, L1, NCAM and p75, but do not express any of the myelin associated proteins. CNPase is a myelin associated enzyme, whose expression is shared by both myelin-forming Schwann cells in the PNS and oligodendrocytes in the CNS. CNPase levels are increased following exposure to insulin (Jung-Testas et al., 1994).

Antisera to S100, GFAP, CNTF, CNPase, MAG, MBP and L1 were used to identify Schwann cells from the PD2 and PD15 sciatic nerves. Both groups were immunopositive for S100, CNTF, and GFAP. Only PD2-derived cells expressed the cell adhesion antigen L1, while only PD15-derived cells expressed MBP. Neither group showed detectable immunoreactivity following incubation with MAG or CNPase antiserum. Figure 7 illustrates immunofluorescent images obtained either on an epifluorescent microscope or from a confocal laser microscope. Figure 7A1 and 7A2 show S100 immunopositive Schwann cells from PD2 and PD15 nerves respectively at 10 days in vitro. Figure 7B1 and 7B2 show GFAP immunopositive Schwann cells from PD2 and PD15 nerves respectively at 10 days in vitro. Figure 7C1 depicts L1 immunopositive Schwann

Figure 7. Immunocytochemical Identification of PD2 and PD15 Schwann cells. Fluorescence photomicrograph showing immunocytochemical identification of Schwann cells from PD2 and PD15 rat following secondary plating onto glass coverslips after 10 days in vitro. Confocal or epifluorescence images showing shared expression of S100 (A1, A2) and GFAP (B1, B2) by PD2 and PD15 Schwann cells. C1. confocal image of PD2 Schwann cell showing expression of the adhesion molecule L1. C2. confocal image of PD15 Schwann cells reacted with antibody raised against MBP. Scale bar = 10 μm.
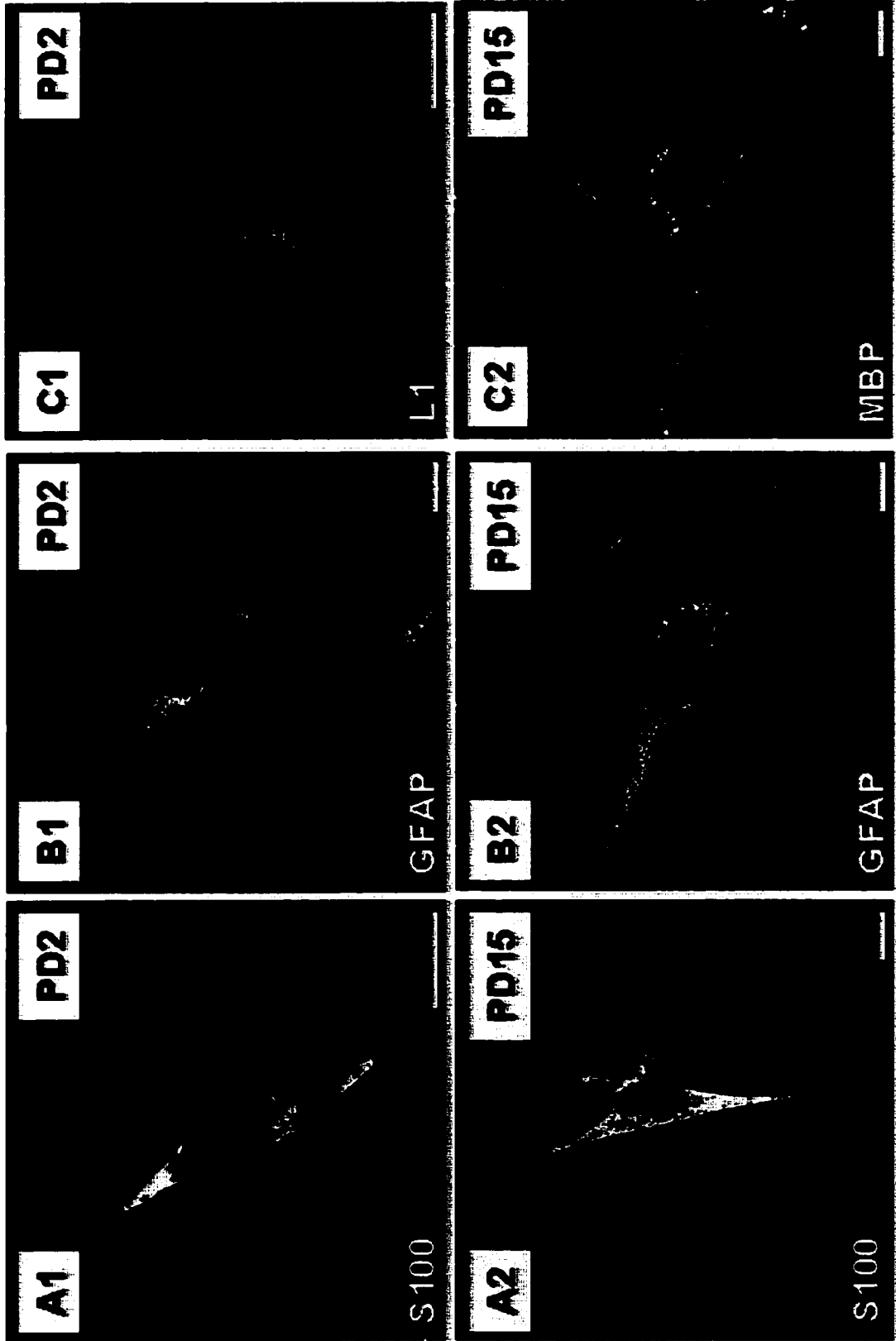
Figure 7.

cells from a PD2 culture, while Figure 7C2 shows MBP immunopositive Schwann cells from a PD15 culture.

Both PD2 and PD15 cells were examined to determine the proportion of contaminating fibroblasts using antiserum to Thy1.1, which specifically identifies fibroblasts (Brockes et al., 1979). The proportion of contaminating fibroblasts ranged between 2 and 5% using this method of obtaining Schwann cells. This compares well with other methods in the literature, reporting greater than 95% purity, which employ immunopanning, complement mediated lysis or cytosine arabinoside (AraC) to remove contaminating fibroblasts (e.g., Assouline et al., 1983). Having determined that two morphologically distinct populations of cells could be obtained from PD2 and PD15 nerve, it was then decided to observe their proliferative characteristics in 2% FBS media.

The absence or presence of proliferation in PD2 and PD15 Schwann cells was compared using 2 independent methods: counts of intact nuclei and counts of Schwann cells in the G_0 phase of the cell cycle (Figure 8). Counts of intact nuclei (n=12 wells) from PD2 Schwann cells taken at 0, 2, 12, 24 and 48 hr did not significantly increase over the 48 hr period in base media (5.5 mM glucose) with 2% FBS (Figure 8A). Conversely, counts of intact nuclei from PD15 Schwann cells over the same period showed a steady increase of approximately 20% during the 48 hr in base media with 2% FBS (Figure 8A). Importantly, these counts also revealed that there was no cell loss in base media over this time period.

Figure 8. Proliferation of PD2 and PD15 Schwann Cells. A. Schwann cells

maintained in base media at an initial seeding density of 12,000 cells per well in

24 well plates were harvested 2 d later at 0, 2, 12, 24, and 48 hr and lysed with

10% Zapoglobin. Intact nuclei were counted on a hemocytometer from 12-14

replicate wells. Counts of PD2 Schwann cells (open squares) indicated no

change, whereas counts of PD15 Schwann cells (open circles) showed a gradual

increase over 48 hr. B. Counts of Schwann cells that were Ki67 negative were

made at 0, 12, and 24 hr. The proportion of G_0 cells was unchanged over 24h for

PD2 cultures (open square). The proportion of G_0 cells declined over 24h for

PD15 cultures (open circle) suggesting that cells were entering the cell cycle.
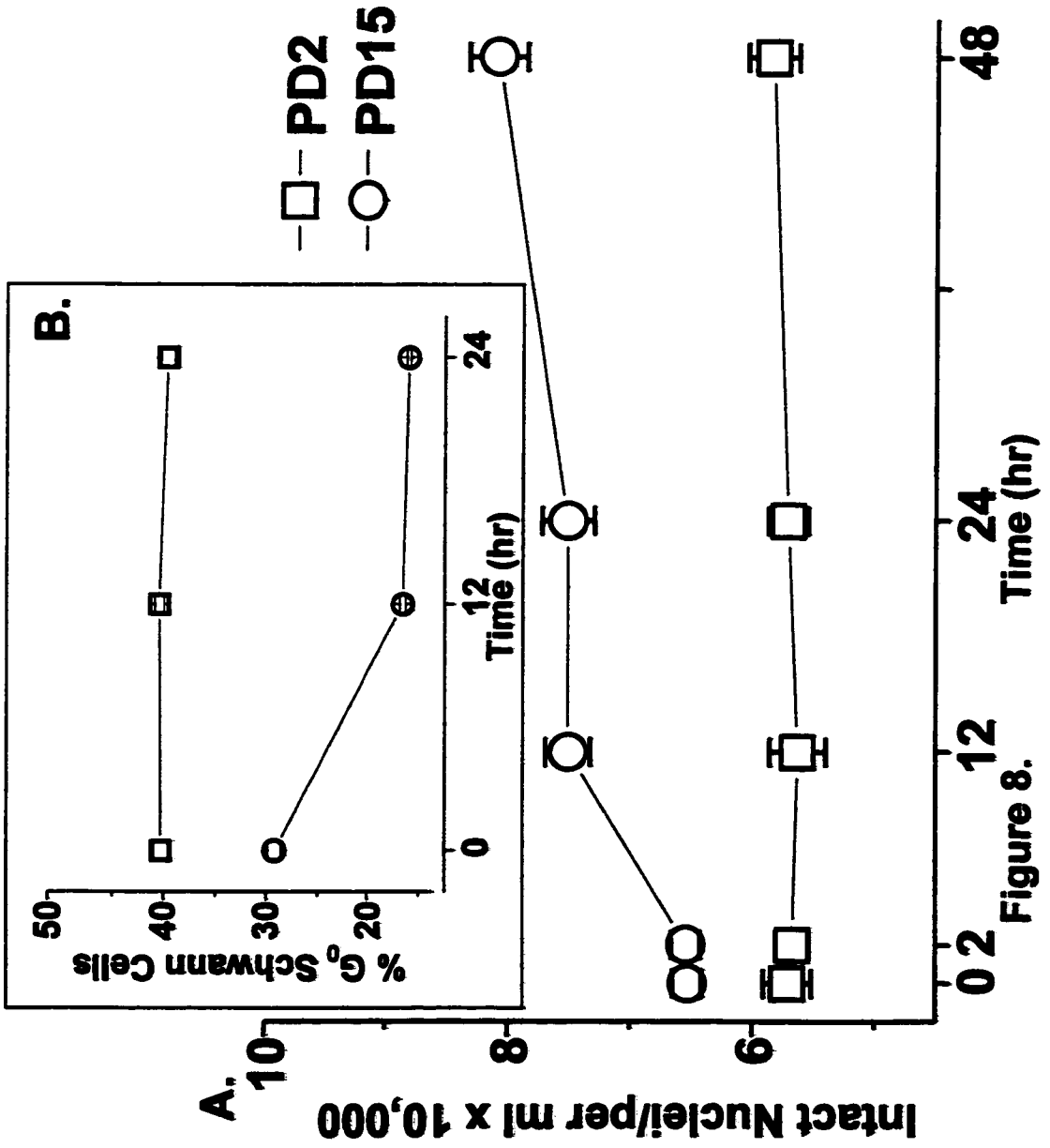
Figure 8.

Identically treated cells grown on glass coverslips were incubated with antiserum to the Ki67 antigen and visualized via an immunoperoxidase method. Ki67 immunoreactivity is generally used to grade the histopathology of cancerous tissue. Cell nuclei that are immunonegative for Ki67 are in the G_0 phase of the cell cycle (Braun et al., 1988). The number of G_0 (Ki67 immunonegative) cells were counted at 0, 12 and 24 hr for both PD2 and PD15 Schwann cells grown in base media for a total of about 3000 cells from 3 individual coverslips (see Figure 8B, inset). The percentage of PD2 cells in G_0 remained constant at approximately 40% over 24hr in base media, indicating a non-proliferating population. In contrast, the percentage of PD15 cells in G_0 declined from 29% to about 16% over 24hr in base media, suggesting that cells were leaving G_0 and entering the cell cycle.

III.b Dose-Dependent Cell Death of Schwann Cells in High Glucose Media

The effect of high glucose on the survival of both populations of Schwann cells was determined. PD2 and PD15 Schwann cells were exposed to glucose concentrations of 5.5, 17.5, 30, 40 or 50 mM for a period of 48 hr. Counts of intact nuclei were made at 0, 2, 12, 24, and 48 hr to quantitate cell survival. Counts of intact PD2 Schwann cell nuclei are shown in Figure 9A. Each point represents the mean and standard error obtained from 12-14 individual wells. There was a significant dose-dependent cell loss observed at 2 hr following washing ranging between 13-26% for cells exposed to 17.5-50 mM glucose. Statistical analysis revealed that the assumption of normality had not been met

FIGURE 9. Dose-dependent death of Schwann cells in high glucose media.

A. Counts of intact nuclei of PD2 Schwann cells were used to determine cell

survival in 5.5 (square), 17.5 (circle), 30 (up triangle), 40 (down triangle) and 50

(diamond) mM glucose showed a dose-dependent loss of Schwann cells at 2 hr,

and a gradual time-dependent decrease in survival between 12-48 hr. B. An

initial dose-dependent cell death was observed in the first 2 hr exposure to high

glucose media. This was followed by a slower rate of cell loss, as compared to

PD2 cells, which may be due to ongoing proliferation of PD15 cells.

A.

B.

Hours
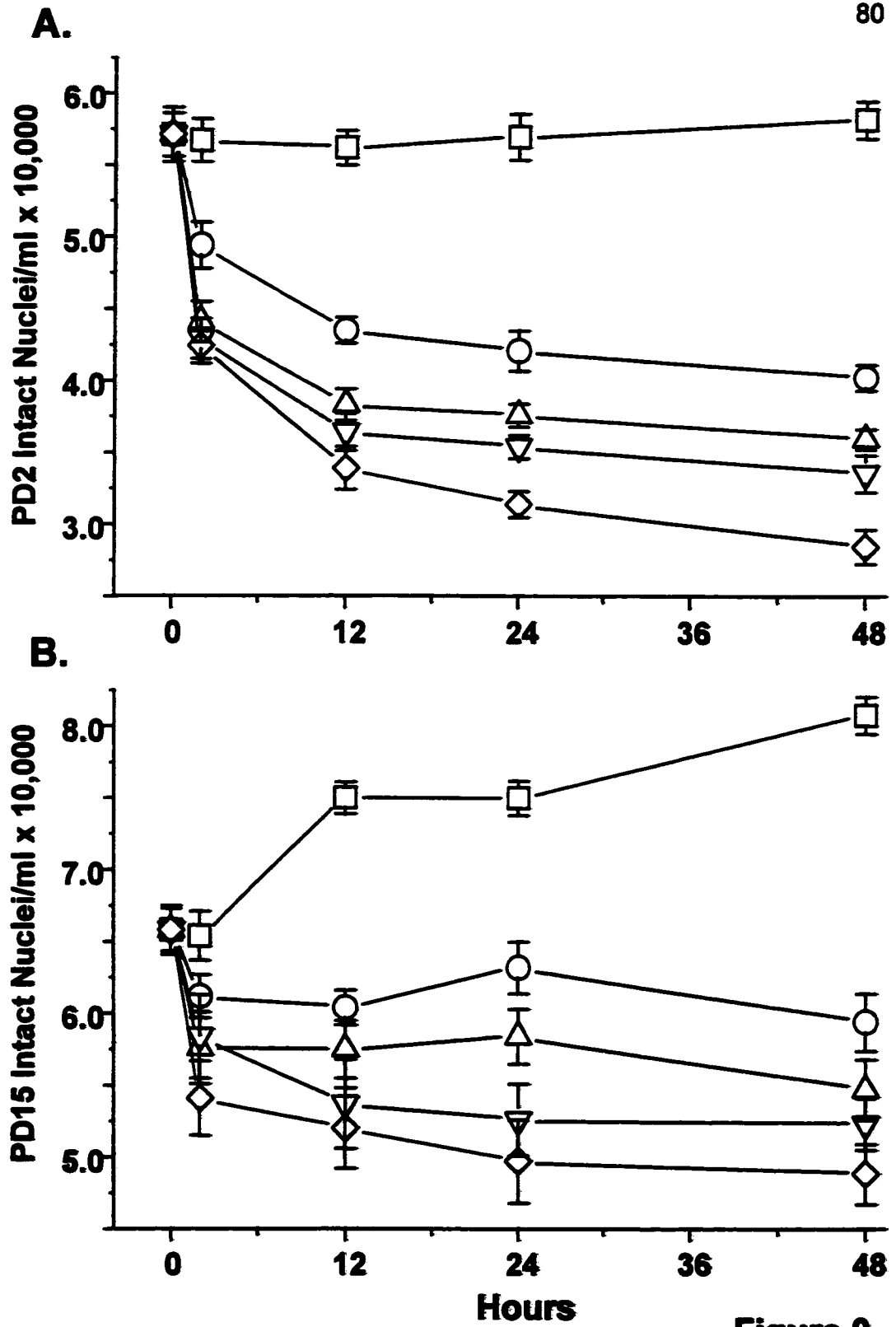
Figure 9.

(Chi Square test, p's < 0.01), therefore non-parametric tests which do not require assumptions regarding the underlying distribution of the data were used. Pair-wise comparisons, using the Mann-Whitney U test, of each concentration of glucose with base media containing 5.5 mM glucose revealed significant differences at each concentration of glucose (all p's < 0.01; see Table 4, Appendix B). Counts of intact PD15 Schwann cell nuclei were decreased by 7-18% during the first 2 hr of exposure to 17.5-50 mM glucose (all p's < 0.05, see Figure 9B).

In PD2 Schwann cells, the greatest rate of decline in cell survival over the remaining 2-48 hr period occurred between 2-12 hr for all concentrations of glucose (17.5-50 mM), followed by a steady decline in survival between 12-48 hr. Conversely, there was a more gradual decline in cell survival of PD15 Schwann cells over the entire 2-48 hr period. The extent of cell loss in PD2 Schwann cells ranged between 29-50% for cells exposed to 17.5-50 mM glucose by 48 hr (Figure 9A). The extent of PD15 Schwann cell loss, however, ranged between 10-26% over 17.5-50 mM glucose between 2 and 48 hr (Figure 9B). Mann-Whitney U tests revealed significant decreases compared to 5.5 mM glucose in both populations over the range of glucose concentrations tested between 12 and 48 hr (all p's < 0.001).

The initial decline in nuclear counts between 0-2 hr for PD2 and PD15 Schwann cells cannot be attributed to pretreatment washes prior to their placement in the different glucose media. Cells in base media subjected to the same wash treatment did not experience any decline in numbers. Also, this

initial wave of cell loss was glucose dose-dependent for both cell populations. It is possible that a subset of Schwann cells may be uniquely sensitive to decreased trophic support with 2% FBS. However, given the findings presented in Figure 8, it would seem more likely that there is a subset of Schwann cells that are particularly sensitive to changing glucose concentrations. Total PD15 cell loss over 48 hr appeared to be about half that of PD2 Schwann cells over the same time period. PD2 cells may be more susceptible to glucose toxicity; however, it is possible that ongoing proliferation of PD15 Schwann cells could account for this difference, since there is an average increase of about 20% in PD15 cell numbers in base media between 0 and 48 hr.

III.c High Glucose Induces Apoptosis in PD2 and PD15 Schwann Cells

Having demonstrated that exposure to high glucose leads to a dose-dependent loss in Schwann cell survival between 2-48 hr in both populations, ISEL combined with simultaneous detection of chromatin condensation with YOYO-1 staining (Tatton et al., 1998) was used to determine whether Schwann cells died via apoptosis following exposure to high glucose media. Figure 10 depicts confocal laser microscopic images of ISEL/YOYO-stained Schwann cells exposed to 40 mM glucose for 24 hr. The upper panel depicts a Schwann cell phagocytosing an apoptotic Schwann cell, observed by differential interference contrast (Figure 10A), with a 600/30 nm bandpass filter (618 nm emission peak) to observe BODIPY-TR fluorescent ISEL (Fig. 10B), or with a 530/30 nm bandpass filter (509 nm emission peak) to observe YOYO-1 denoting chromatin

FIGURE 10. ISEL and YOYO-1 staining of apoptotic Schwann cells. The upper panel shows a confocal laser image of a Schwann cell which has phagocytosed an apoptotic Schwann cell viewed with transmitted light for an interference contrast image (A), with laser excitation to visualize BODIPY-TR-dUTP/ISEL in the 618 nm range (B) and with laser excitation to visualize YOYO-1 fluorescence in the 509 nm range (C). Note that the YOYO-bright chromatin nuclear condensation does not co-localize with the ISEL-bright nuclear regions. The open arrow indicates the nucleus of the phagocytic Schwann cell, the filled arrow indicates the nucleus of the apoptotic Schwann cell. In the lower panel, YOYO reveals chromatin condensation patterns observed in an ISEL positive nucleus (D) and in a blebbed nucleus which was ISEL negative (E). An ISEL positive nucleus from a non-phagocytosed cell is shown (F). Note that ISEL fluorescence remains localized to the nucleus. All scale bars = 10 μm.

84
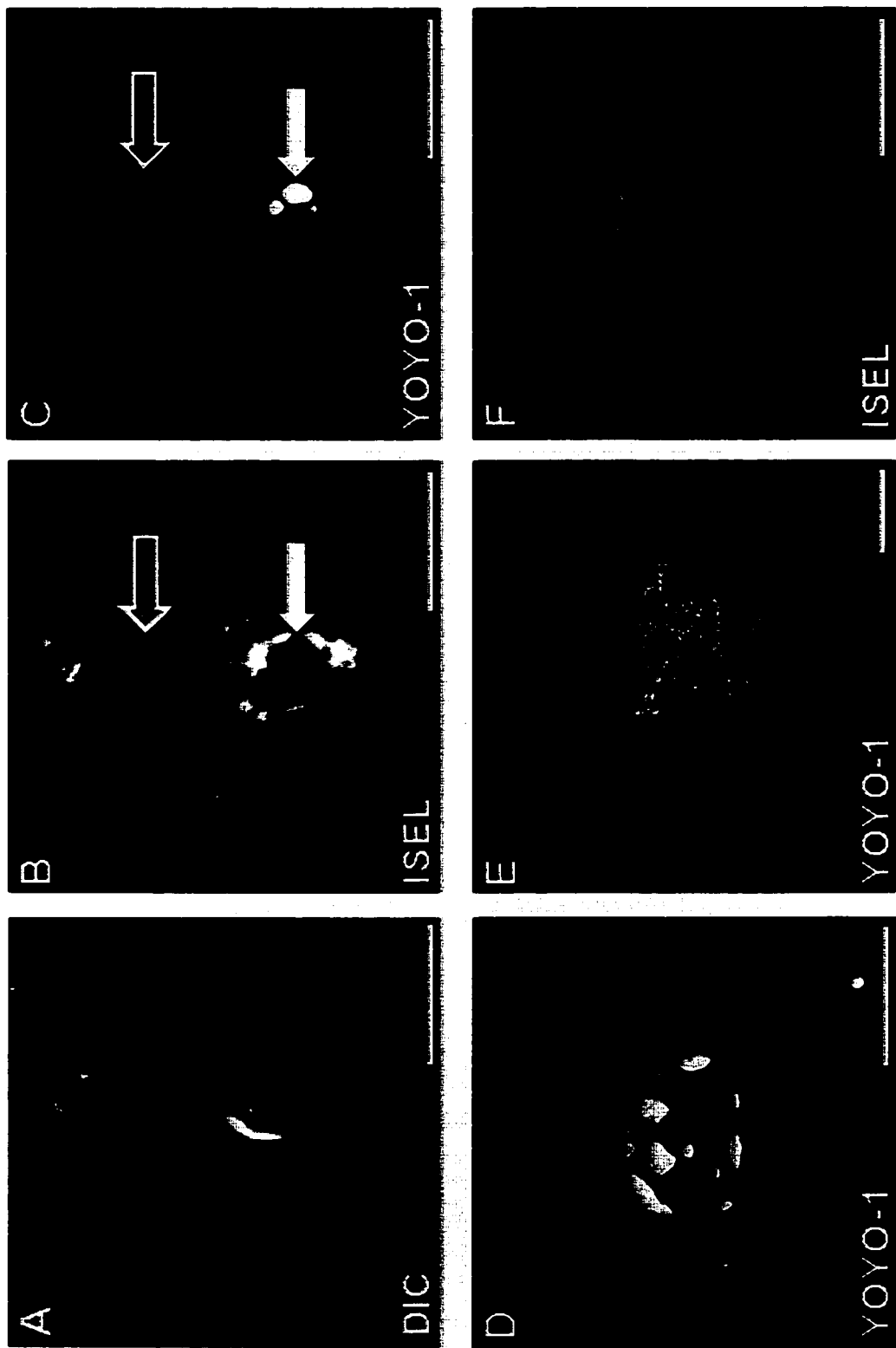
Figure 10.

condensation (Fig. 10C). Following peripheral nerve injury in vivo, resident Schwann cells as well as macrophages recruited to the injury zone are responsible for removal of the cellular debris (Stoll et al., 1989). Schwann cells apparently retain the capacity to phagocytose cell debris in vitro even in the presence of high glucose.

The interference contrast image (Fig. 10A) in the upper left panel clearly shows a small shrunken cell completely engulfed by the larger Schwann cell. Note that the engulfed cell still maintains a well-delineated nucleus and plasma membrane. The phagocytic Schwann cell does not display end-labeling of its nucleus, while the smaller apoptotic Schwann cell is brightly end-labeled throughout the nucleus and cytoplasm (Fig. 10B). The far right panel shows light, filamentous YOYO-staining in the phagocytic Schwann cell nucleus, while the engulfed Schwann cell nucleus shows dramatic chromatin condensation (Fig. 10C). Note that ISEL bright regions of the nucleus do not appear to co-localize with the YOYO-bright regions.

The ISEL staining in the cytoplasm of the apoptotic cell may be due to leakage of low-molecular weight DNA fragments out of the nucleus through nuclear pores, which have been shown in electron microscopy to redistribute in the nuclear membrane of cell undergoing apoptosis (Wyllie et al., 1980). In cells with condensed chromatin arranged along the nuclear membrane, nuclear pores were visible adjacent to areas of loosely arranged chromatin and not clearly present in areas adjacent to condensed chromatin (Wyllie et al., 1980).

Figure 10D shows a YOYO-1 stained Schwann cell nucleus during the

early stages of nuclear degradation where the chromatin has begun to condense and become arranged in small crescent-shaped patches along the inside of the still-intact nuclear membrane. There are also bright condensed chromatin bodies visible within the nuclear matrix. This pattern of chromatin condensation has been reported in the early stages of nuclear degradation in apoptotic cells observed by electron microscopy (Kerr et al., 1972; Wyllie et al., 1980). Figure 10E shows an example of a YOYO stained Schwann cell with nuclear "blebbing" following exposure to 40 mM glucose. Blebbed nuclei were observed at both at 2 hr and 24 hr and have a unique pattern of chromatin organization compared to that observed in normal nuclei, ISEL positive nuclei, and nuclei entering mitosis. There was no evidence of positive end labeling in any blebbed nuclei. Small YOYO-stained bodies that appeared to have been pinched off from the nucleus often accompanied such blebbed nuclei. It was not possible to determine whether Schwann cells with blebbed nuclei would later become ISEL positive. It is possible that the extensive DNA fragmentation (oligonucleosomal) that is detectable by end-labeling (Walker and Sikorska, 1997), may not be a feature of the apoptotic cell death of all Schwann cells. A similar pattern of nuclear blebbing has been previously shown for lymphoblastoid cells undergoing apoptosis following treatment with respiratory chain inhibitors (Wolvetang et al., 1994), in SK-N-MC neuroblastoma cells following treatment with a cholinergic neurotoxin (Rinner et al., 1997), and in acinar epithelial cells and lymphoma cells (Wyllie et al., 1980). Notably, the integrity of the plasma membrane of these cells appeared intact. Very rarely (about 5-6 cells per coverslip at 2 hr) were any

Schwann cells observed which displayed the swollen nuclei and somata indicative of necrotic cell death.

It was determined that all ISEL positive cells also demonstrated the classic chromatin condensation pattern illustrated in Figure 10C. Therefore, counts of ISEL positive nuclei were used to estimate the percentage of apoptotic Schwann cells after exposure to high glucose media. Figure 11 presents the percentage of ISEL positive Schwann cells following exposure to 5.5, 17.5, or 40 mM glucose for 2, 12, and 24 hr. There was no significant increase in the number of ISEL positive cells following 2 hr exposure to 17.5 or 40 mM glucose in either PD2 or PD15 cells (Mann-Whitney U; all p's > 0.3, see Table 5, Appendix B). Both populations of Schwann cells showed a significant dose-dependent increase in the number of ISEL positive cells over 12-24 hr in both 17.5 and 40 mM glucose (all p's < 0.001). Interestingly, about 23% of PD2 cells were ISEL positive at 24 hr, while only 8% of PD15 cells were ISEL positive. Previous counts of intact nuclei demonstrated an approximate 40% decline in surviving PD2 Schwann cells following 24 hr exposure to 40 mM glucose, but only a 20% decrease in surviving PD15 Schwann cells. In both populations, estimates of cell death are approximately 2 fold greater using counts of intact nuclei compared to counts of ISEL positive cells. This may be explained by differences in methodology. The protocol used to obtain intact nuclei effectively tests nuclear fragility and so apoptotic/damaged nuclei will not be counted because, either they are lysed, or they display irregular nuclear membranes. At the same time, this is a cumulative method, since all cells in the well will be sampled. In contrast, ISEL or YOYO

FIGURE 11. Counts of ISEL positive PD2 and PD15 Schwann cell nuclei.

PD2 and PD15 Schwann cells were exposed to base media, 17.5 or 40 mM

glucose and fixed in 4% paraformaldehyde at 2, 12, and 24 hr. Counts of ISEL

positive nuclei increased with glucose concentration and time. A. ISEL positive

nuclei increased from about 8% of PD2 cells counted at 12 hr to over 20% after

24 hr in 40 mM glucose media (red bars). B. ISEL positive nuclei increased from

about 6% of PD15 cells counted at 12 hr to 8% after 24 hr exposure to 40 mm

glucose. Note that in both PD2 and PD15 Schwann cells, high glucose did not

significantly increase the percentage of ISEL positive cells at 2 hr compared to

base media (grey bars).

A. PD2 Schwann Cells

B. PD15 Schwann Cells

5.5 mM
17.5 mM
40 mM

% ISEL +ve Schwann Cells

2 hr   12 hr   24 hr
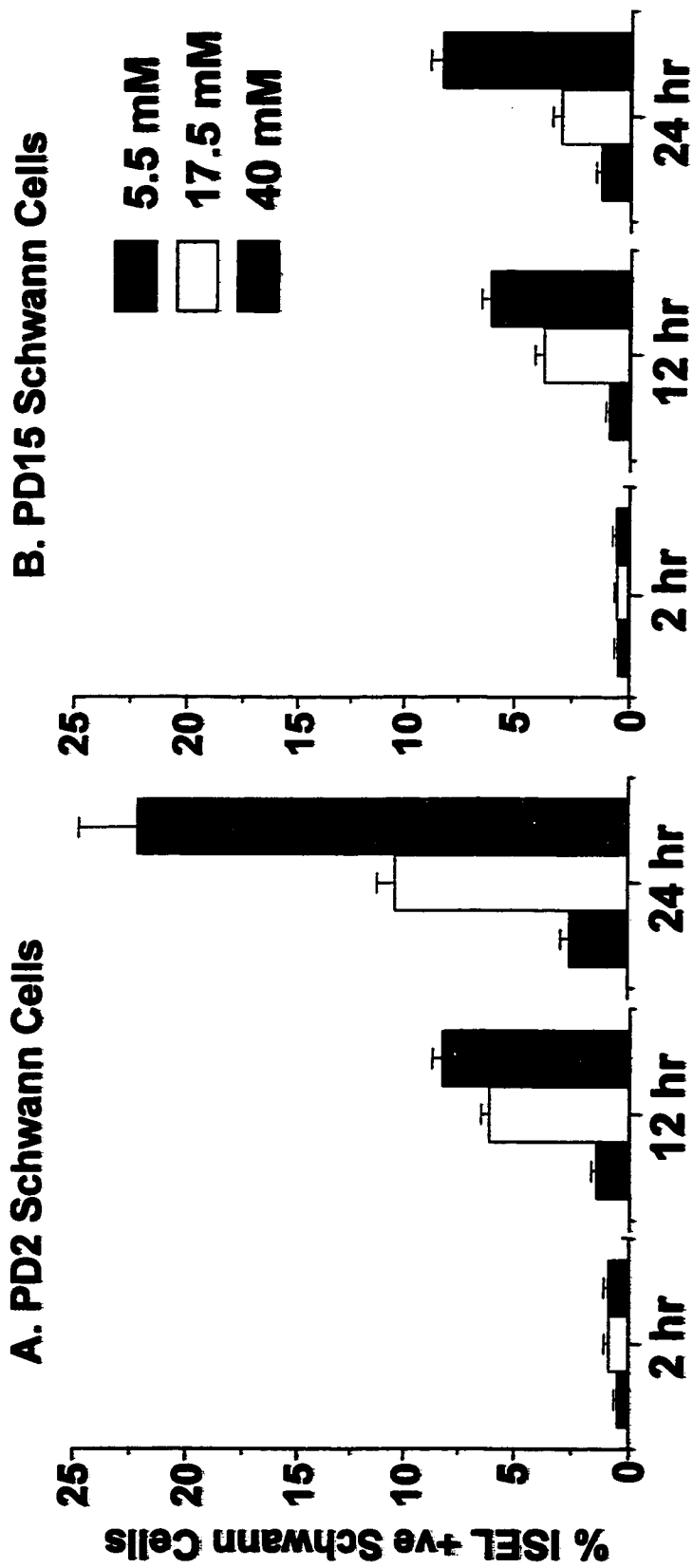
Figure 11.

staining only examines cells which are still attached to the coverslip at a single point in time. Also, it may be that cells with blebbed nuclei are indeed apoptotic, and display high molecular weight DNA fragmentation only, and therefore cannot contribute to the ISEL count. If the Schwann cells which demonstrate chromatin condensation (both blebbed and ISEL nuclei) are apoptotic, it may be possible to improve their survival in high glucose conditions by treatment with agents which have demonstrated a capacity to improve cell survival in other models of apoptosis.

III.d Anti-Apoptotic Drugs Improve Schwann Cell Survival

The ability of IGF-I (1 ng/ml), NAC (10^{-7} M), or DMD (10^{-9} M) to prevent high glucose induced Schwann cell apoptosis was determined. Each of these molecules has been shown to 'rescue' cells from apoptotic cell death induced by trophic withdrawal or toxic injury (D'Mello et al., 1997; Ferrari et al., 1995; Tatton and Chalmers Redman, 1996). Concentrations chosen were based on the most effective dose observed to rescue cells in other in vitro model systems. Counts of intact nuclei were made at 2 hr and 24 hr (n=6 wells) and the mean values expressed as the percentage of cells grown in 5.5 mM glucose for both populations (Figure 12). Mann-Whitney U tests revealed that all three agents (IGF-I, 1 ng/ml; NAC, 10^{-7} M; and DMD, 10^{-8} M) significantly improved cell survival of PD2 cells in 40 mM glucose at 2 hr (all p's < 0.01, see Table 6, Appendix B) and at 24 hr (all p's < 0.01). In PD15 Schwann cells, both DMD and IGF-I significantly prevented the cell death produced by 40 mM glucose at 2 hr

FIGURE 12. IGF-1, NAC and DMD improve Schwann cell survival in 40 mM
glucose. A. Counts of intact nuclei revealed a 20% loss of PD2 cells after 2 hr in
40 mM glucose (red bars). All three agents were able to significantly improve cell
survival at 2 hr. After 24 hr, PD2 Schwann cell survival in high glucose was
maintained at or near control levels by each of the agents. B. Counts of intact
nuclei revealed about a 15% loss of PD15 cells at 2 hr. IGF-1 produced a slight
improvement, while DMD restored counts to or near control values. At 2 hr, NAC
did not significantly prevent high glucose induced apoptosis in PD15 Schwann
cells. All three agents were able to significantly improve PD15 Schwann cell
survival after 24 hr exposure to 40 mM glucose. Counts of treated cells were
normalized to 5.5 mM base media values for each time point for both populations
(+/- SEM).

A. PD2 Schwann Cells

B. PD15 Schwann Cells

Intact Nuclei (% of control)
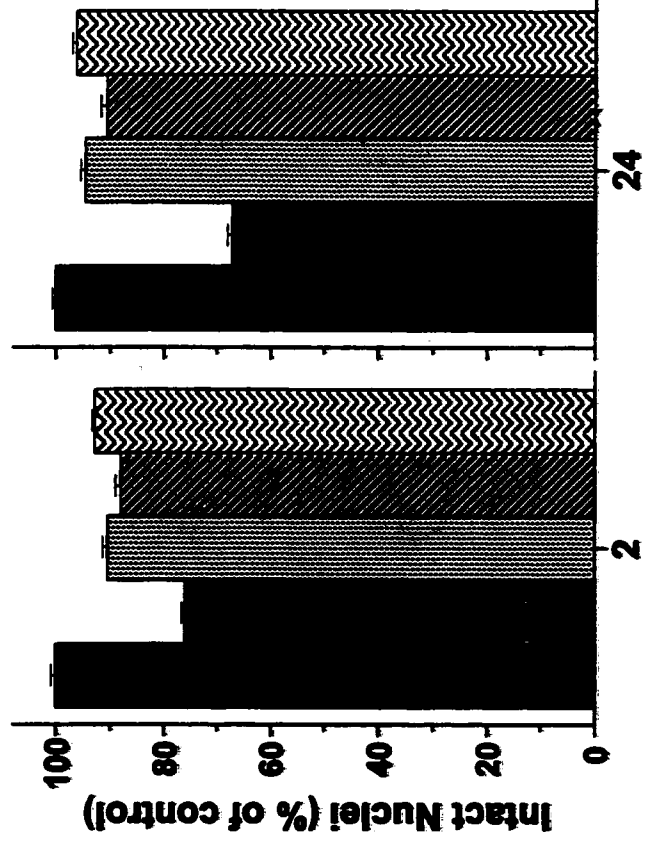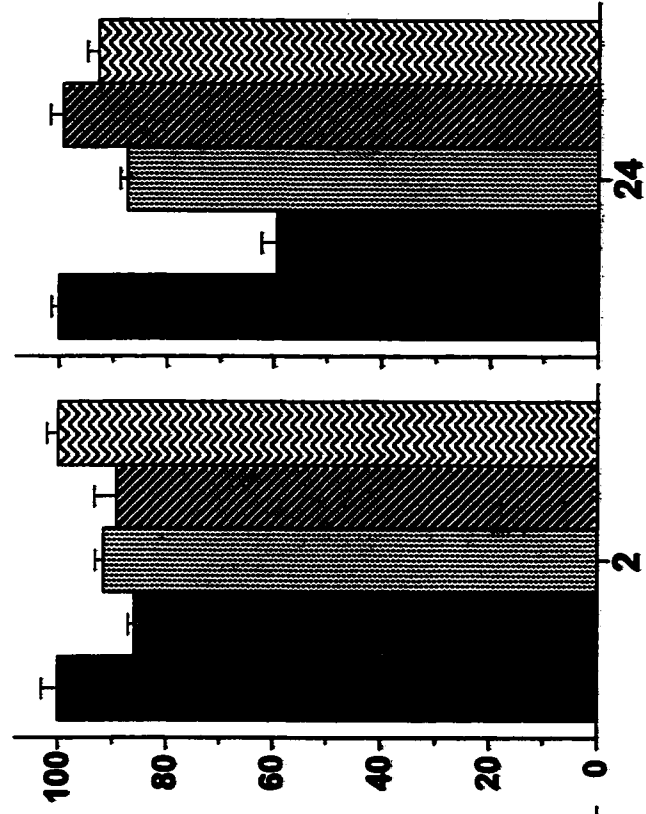
5.5mM
40mM
40mM + IGF-I
40mM + NAC
40mM + DMD

Figure 12.

(p's < 0.05). However NAC only slightly improved survival at 2 hr in PD15 Schwann cells (p > 0.5). This may be a result of only 6 wells being sampled rather than 12, given that NAC was effective at 24 hr. At 24 hr all three agents significantly improved PD15 Schwann cell survival in 40 mM (all p's < 0.01). These data suggest that most of the cell death observed between 0-2 hr was apoptotic given the rescue observed in PD2 and PD15 cells. It also suggests that these agents did not require new protein synthesis to effect rescue.

The first series of studies established 1) that in two populations of Schwann cells ('non-proliferating' cells from PD2 sciatic nerve, and 'proliferating' cells from PD15 nerve), exposure to high glucose causes a dose-dependent reduction in survival, 2) that a significant proportion of PD2 and PD15 Schwann cells display features of nuclear degradative changes characteristic of apoptosis, chromatin condensation and oligonucleosomal DNA fragmentation, and 3) that three different anti-apoptotic agents significantly improved Schwann cell survival in high glucose at 2 hr and to a greater extent at 24 hr.

In an attempt to determine the mechanism of high glucose-induced apoptosis, the production of NO and TNF-α was examined. In addition, the sensitivity of PD2 or PD15 Schwann cells to these agents in high glucose was also tested. Finally, changes in mitochondrial membrane potential ($\Delta\Psi_M$) were examined to determine if a decrease in potential preceded apoptotic cell loss.

Figure 13. Exposure to NO Decreases Schwann Cell Survival. PD15

Schwann cells grown in 24 well plates were treated with 1, 10, or 100 μM of the

NO donor SNAP and harvested 24 hr later for intact nuclear counts. Each bar

represents the percentage of intact nuclei relative to base media (+/- SEM) from

6 replicate wells. NO exposure caused a significant dose-dependent loss of

Schwann cell survival at 24 hr.

Figure 13.
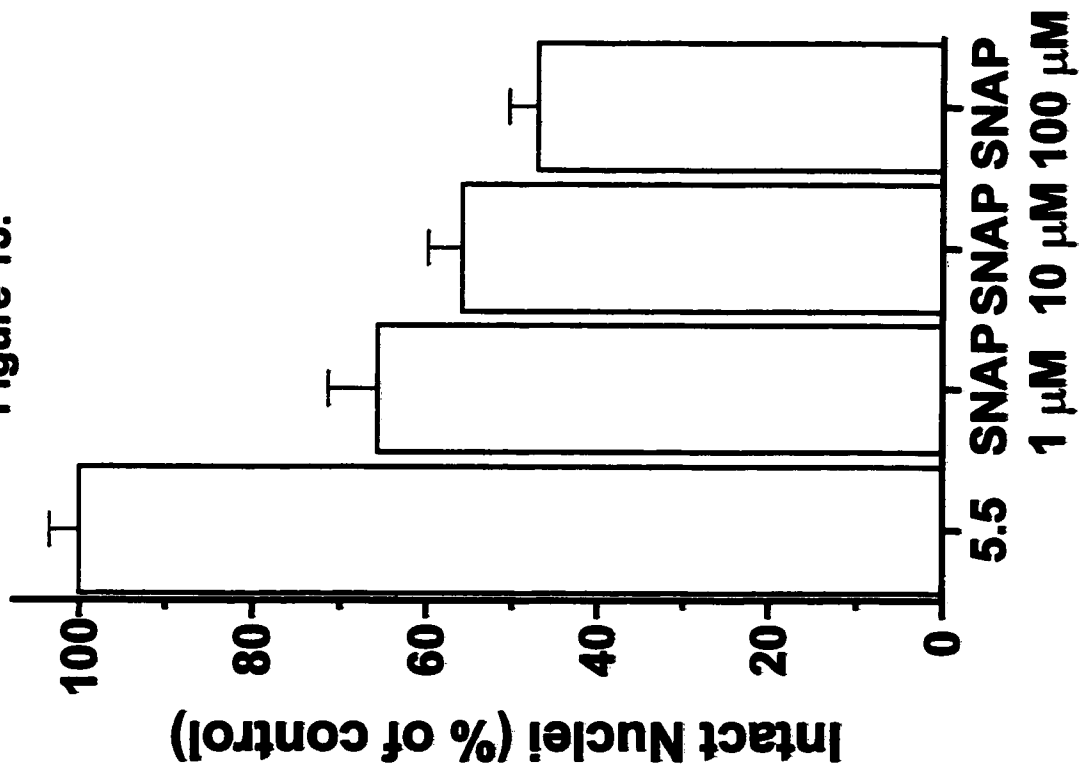
III.e Production of NO in Schwann Cells in High Glucose Media

To determine if increased NO signaling mediates the high glucose induced apoptosis, Schwann cells were first exposed to the NO donor SNAP to determine if increased NO reduced survival. Figure 13 presents the counts of intact nuclei (n = 6 wells) from PD15 Schwann cells exposed to 1, 10, or 100 μM SNAP for 24 hr in base media with 2% FBS. Values are expressed as the percentage of control cells. There was a significant dose-dependent decrease in cell survival over the concentration range tested (Mann-Whitney U; all p's < 0.01, see Table 7, Appendix B) indicating that exogenous NO can be toxic for PD 15 Schwann cells.

The Griess reaction, which measures secreted nitrite (NO_2) was used to determine NO production by Schwann cells in the culture media. Since nitrate (NO_3) is the major degradation product of NO, nitrate was first converted to nitrite by incubation of the media sample with nitrate reductase and NADPH. Nitrite in the media sample was then measured by adding the Griess reagent as described in the Methods. PD2 and PD15 Schwann cells were cultured, as described, in the presence of 5.5 or 40 mM glucose for 24 hr. Cells exposed to 40 mM glucose were also treated with DMD (10^{-9} M), the iNOS inhibitor L-NIL (10^{-4} M) or an inhibitor of the constitutive, Ca^{++}-dependent isoform of NOS (cNOS), S-methyl-thiocitruline (SMTC, 10^{-4} M). As a positive control, Schwann cells in base media were treated with a combination of TNF-α/IFN-γ (100U/100U), which has been shown to increase the production of NO in Schwann cells in vitro (Gold et al., 1996). A standard curve was made using known amounts of $NaNO_2$ in order

Figure 14. NO Production by Schwann Cells in High Glucose Media.

Estimation of NO production in Schwann cells exposed to high glucose by

colourimetric reaction with secreted NO_2 (Griess reaction). Bars represent mean

(+/- SEM) NO_2 (in μM) of 6 wells of PD2 (A) and PD15 (B) Schwann cells grown

in 24 well plates at a density of 100,000 cells per well. Incubation with 100U

TNF-α/IFN-γ served as a positive control for the assay. High glucose exposure

produced a small increase in NO production by PD2 Schwann cells that was

prevented by L-NIL and SMTC. A significant increase in NO production was

seen in PD15 Schwann cells exposed to 40 mM glucose for 24 hr, which was

only partially prevented by DMD and L-NIL.
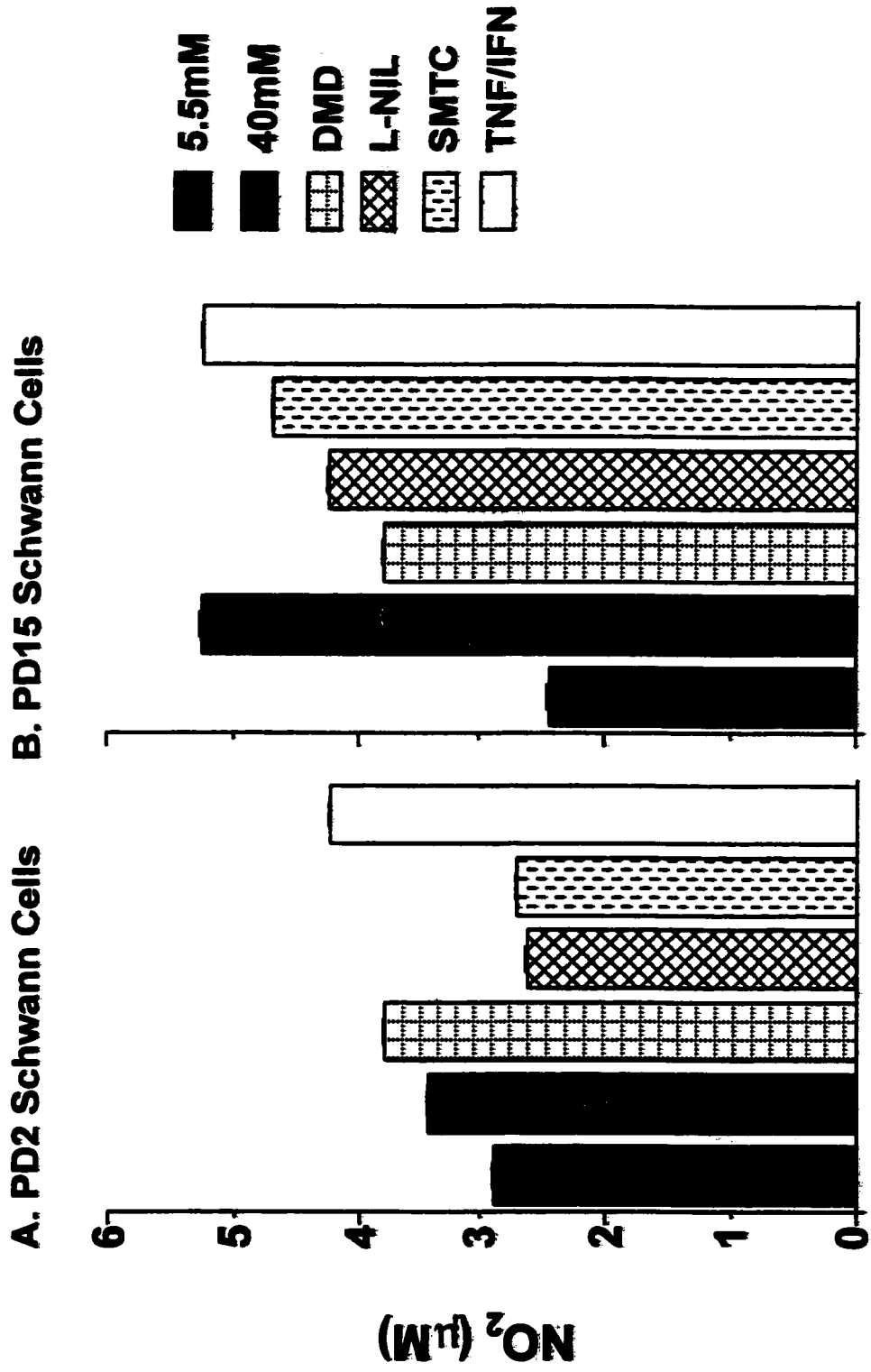
Figure 14.

to estimate the levels of NO production by Schwann cells (see Appendix C).

Figure 14 presents the approximate levels of NO_2 in the media of Schwann cells exposed to high glucose (n = 4-6 wells; 100,000 cells per well). In both PD2 and PD15 cells, 40 mM glucose produced a small but significant increase in detectable NO_2 in the media after 24 hrs (Figure 14A; Mann-Whitney U, p < 0.01, see Table 8, Appendix B). In the PD15 Schwann cells, NO_2 levels were approximately 2 fold greater in 40 mM glucose compared to base media (Figure 14B; p < 0.001). Interestingly, DMD did not completely prevent a glucose-induced increase in NO_2 in PD15 cells or NO_2 in PD2 cells. While L-NIL and SMTC brought NO_2 to baseline levels in the PD2 group (p's < 0.01), they were only partially effective in the PD15 group. In the PD 15 group (p's < 0.01), this may be a reflection of ongoing proliferation providing cells which can continue to produce NO. Although DMD improved cell survival it is not known whether it influences NOS synthesis or activity.

Since both NIL and SMTC were able to effectively inhibit the increase in NO_2 by PD2 cells in high glucose, counts of intact nuclei were done after 24 hrs exposure to NIL and SMTC with 40 mM glucose (Figure 15). Values presented are the average of 6 wells expressed as the percentage of control cells at 24 hr. SMTC did not affect PD2 cell survival (Mann-Whitney U, p > 0.05, see Table 9, Appendix B) while NIL rescued approximately 25% of the PD2 cells (p < 0.01). This would suggest that a certain proportion of PD2 cell death may be attributable to an increase in NO. However, it cannot be determined from this data whether the NO increase was directly toxic or whether the NO increase was

Figure 15. Inhibition of NO Production Only Partially Improves Schwann Cell Survival in High Glucose. PD2 Schwann cells grown in 24 well plates were exposed to 40 mM glucose alone or with the iNOS inhibitor L-NIL or the cNOS inhibitor SMTC for 24 hr and harvested for intact nuclear counts. Each bar represents the percentage of intact nuclei relative to base media (+/- SEM) from 6 replicate wells. L-NIL prevented approximately 25% of the cell death induced by 40 mM glucose, while SMTC had no effect.

Figure 15.
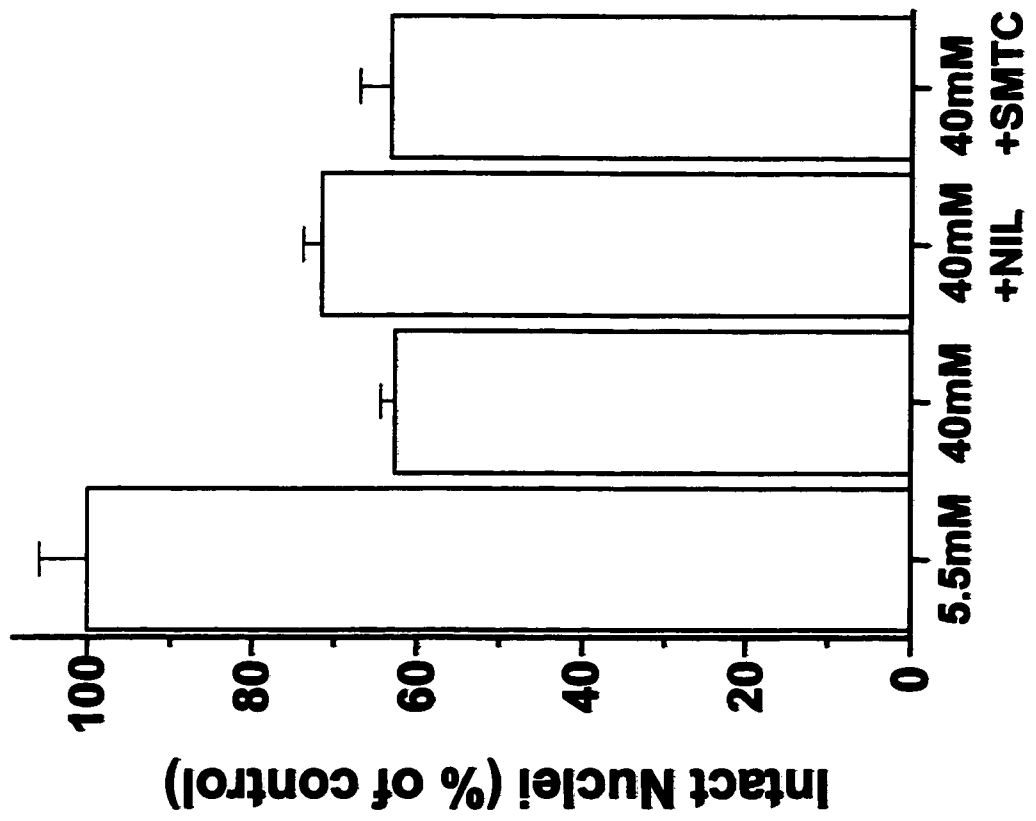
responsible for signaling other changes (e.g reacting with $\bullet O_2^-$ to form $ONOO^-$) in the cell that enhanced vulnerability to increased glucose.

III.f TNF-α Production by Schwann Cells in High Glucose Media

In vivo, in response to nerve injury, Schwann cells upregulate expression of TNF-α as part of the inflammatory signaling pathway involved in the recruitment of macrophages to the injury site (Wagner and Myers, 1996). Others have shown that exposure to TNF-α /IFN-γ produces an increase in NO production by Schwann cells (Gold et al., 1996). PD2 Schwann cells (n = 6 wells, 100,000 cells per well) were treated with TNF-α/IFN-γ (50, 100, 250, 500U) and NO production was measured as previously described. There was about a 4 fold increase in NO levels above baseline (see Figure 14 for baseline value) in cytokine-treated cells in base media (Figure 16; Mann-Whitney U, p's < 0.001, see Table 10, Appendix B). Stimulation of NO_2 release by TNF-α /IFN-γ was prevented in a dose-dependent manner by addition of the iNOS inhibitor L-NIL (Figure 11; p's < 0.001). This indicated that PD2 Schwann cells retained the capacity to up-regulate NO production in response to stimulation by TNF-α /IFN-γ, and that this up-regulation could be prevented by inhibition of iNOS.

Secreted TNF-α in the culture medium was measured by ELISA in order to determine whether high glucose could induce a change in TNF-α production. Figure 17A presents the relative amounts of TNF-α secreted by PD2 Schwann cells (n = 6 wells, 100,000 cells per well) in 5.5 mM, 40 mM glucose or 40 mM glucose plus DMD (10^{-8} M) (see Appendix C for TNF-α standard curve).

Figure 16. TNF-α/IFN-γ Induces Up-regulation of NO Production in Schwann Cells. PD2 Schwann cells grown in 24 well plates (100,000 cells per well) were exposed to a range of TNF-α/IFN-γ concentrations (50, 100, 250, 500 U) for 24 hr or exposed to 250 U plus the iNOS inhibitor L-NIL (10^{-4}, 10^{-6} M). Bars represent the mean NO_2 secreted by the cells from 4 replicate wells. Note here the dose-dependent increase in response to the cytokine and the prevention of the secretion of NO_2 in the presence of L-NIL.
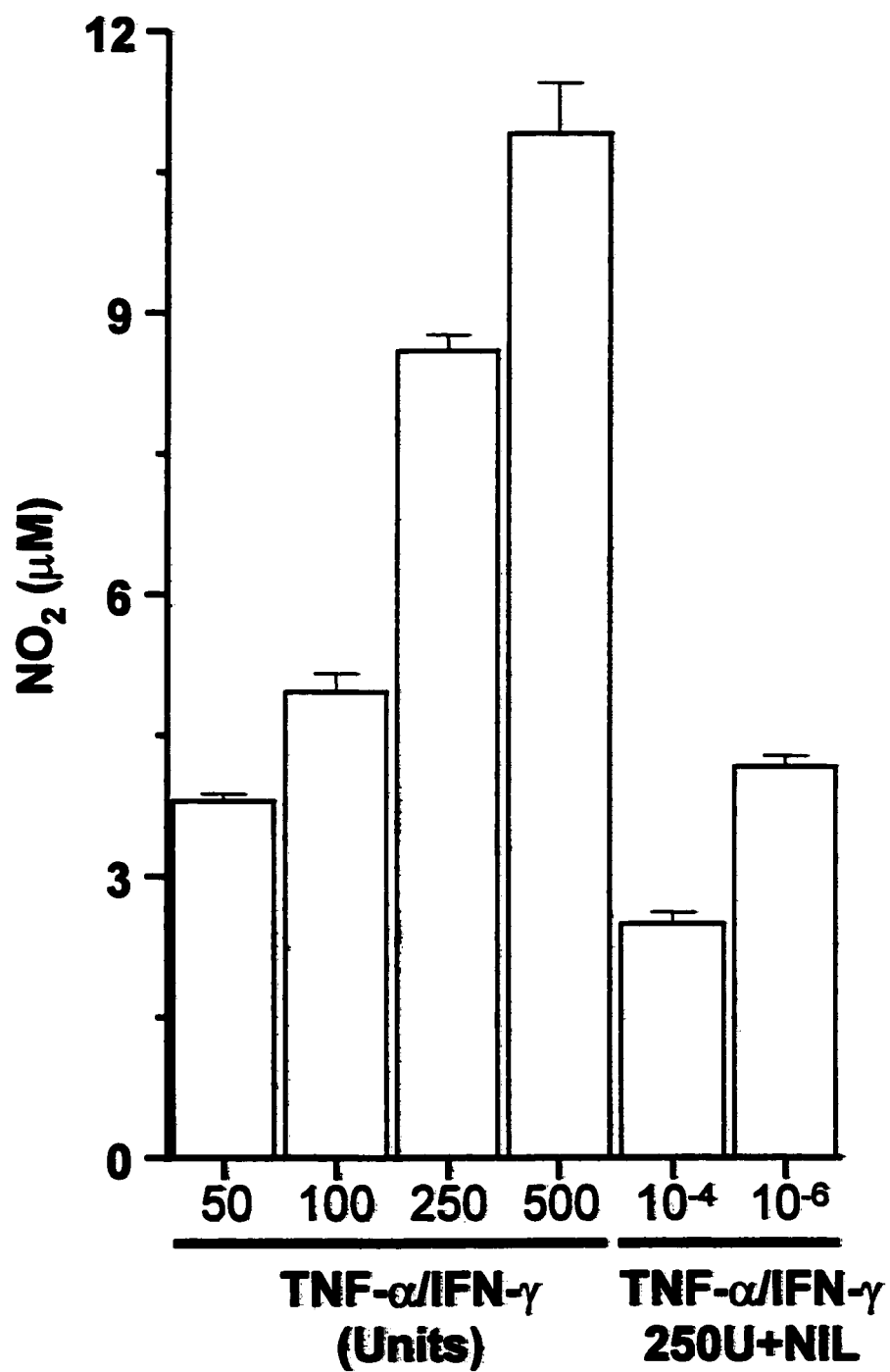
Figure 16.

Figure 17. TNF-α Production by Schwann Cells in High Glucose Media. A.

PD2 Schwann cells were grown in 24 well plates (100,000 cells per well) and

exposed to 40 mM glucose or 40 mM glucose + DMD for 24 hr. The amount of

TNF-α present in the culture medium was assayed using an ELISA kit against

known amounts of TNF-α (see Appendix C for standard curves). High glucose

reduced the amount of TNF-α produced by Schwann cells, whereas treatment

with DMD did not reverse this. B. PD2 Schwann cells were exposed to

increasing concentrations of SNAP in base media or in high glucose and the

amount of TNF-α present in the media assayed. In cells grown in high gluocse,

there was a dose-dependent decrease in TNF-α production following exposure to

SNAP. Each bar represents the mean (+/- SEM) from 6 replicate wells.
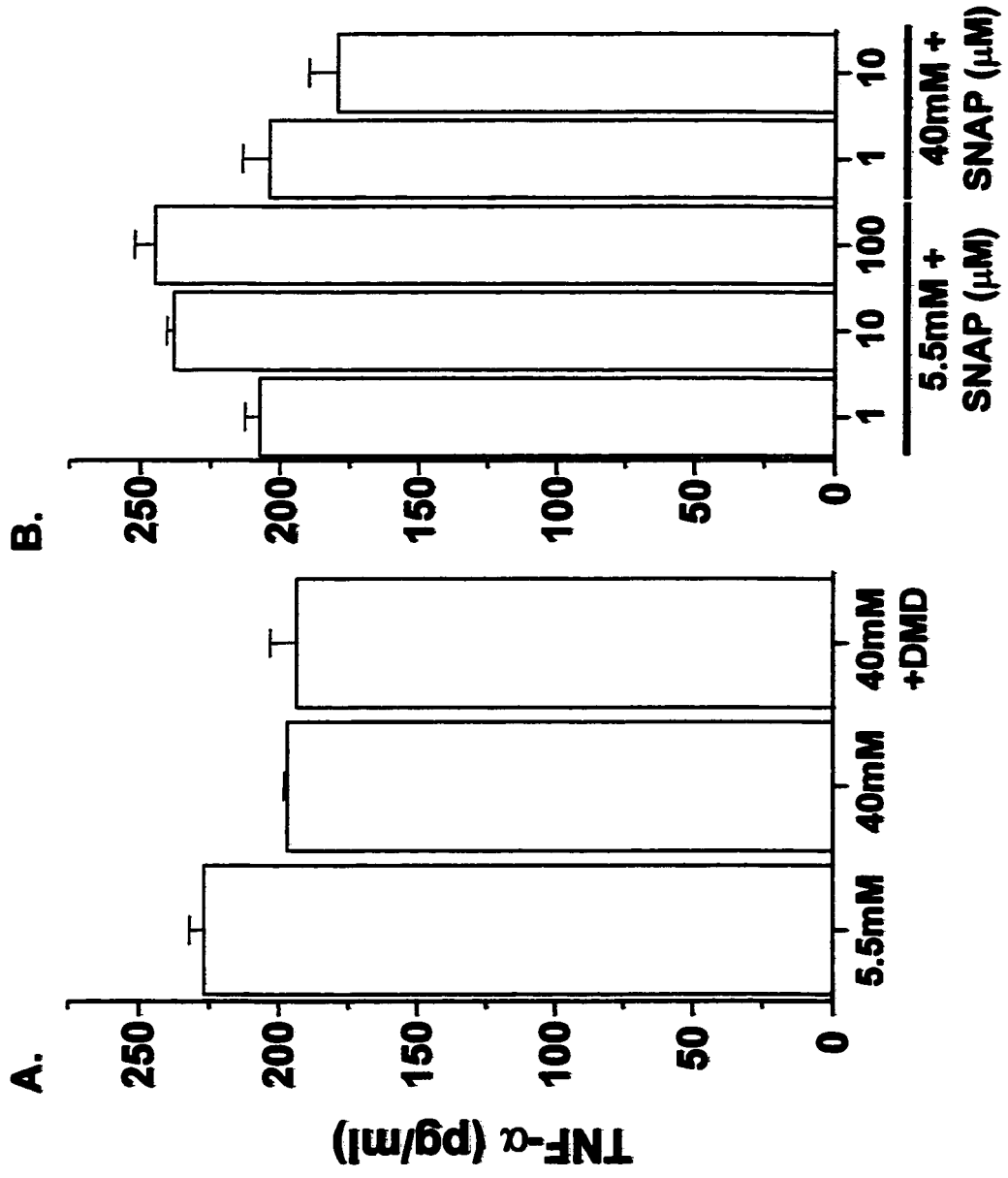
Figure 17.

Surprisingly, there was a significant decrease in the TNF-α production in

Schwann cells exposed to 40 mM glucose for 24 hr (Mann-Whitney U, $p < 0.01$,

see Table 11, Appendix B), which was not prevented by simultaneous exposure

to DMD ($p > 0.05$). PD2 Schwann cells exposed to the NO donor SNAP in 5.5

mM glucose showed a dose-dependent increase in TNF-α production ($n = 6$

wells, 100,000 cells per well). In contrast, Schwann cells exposed to 40 mM

glucose plus SNAP showed a dose-dependent decrease in TNF-α production

(Figure 17B; p's < 0.01). This suggests that the capacity to respond to injury by

an increase in a TNF-α signaling pathway may be compromised by Schwann

cells exposed to high glucose. However, it may be that other local factors

present in the nerve may be necessary for this pathway to be stimulated in

injured Schwann cells.

III.g Changes in Schwann Cell $\Delta\Psi_M$ in High Glucose Media

It has been demonstrated in several different in vitro model systems

(Zamzami et al., 1995; Wadia et al., 1998) that a reduction in $\Delta\Psi_M$ occurs prior to

oligonucleosomal DNA fragmentation with chromatin condensation. The

potentiometric dye CMTMR was utilized to stain Schwann cell mitochondria in

order to determine whether a drop in $\Delta\Psi_M$ was associated with glucose-induced

apoptosis. Further, $\Delta\Psi_M$ was measured at several different time points to

determine whether the drop preceded oligonucleosomal DNA fragmentation as

has been previously reported (e.g., Zamzami et al., 1995).

Figure 18. High Glucose Reduces Schwann Cell $\Delta\Psi_M$. Fluorescence

photomicrograph showing changes in $\Delta\Psi_M$ in PD2 Schwann cells using the

potentiometric dye CMTMR. Cells treated with 5.5, 40 mM, or trophic withdrawal

(M/0) for 6hr were incubated with CMTMR, fixed, and imaged with a confocal

microscope (1400X mag.) at constant power and magnification settings. Note

the reduction in brightness of CMTMR intensity in cells exposed to 40 mM

glucose or in cells deprived of trophic support.
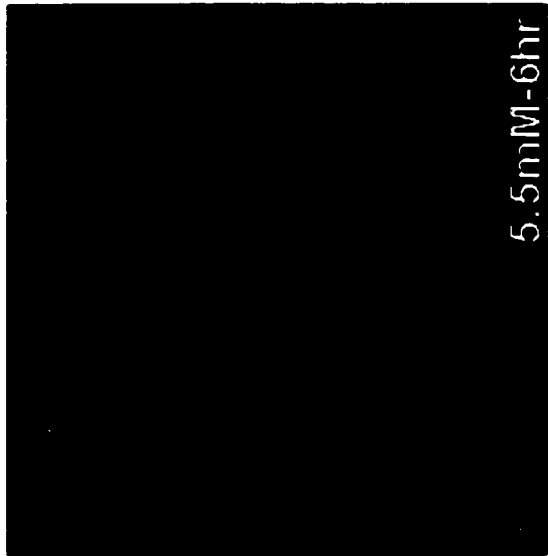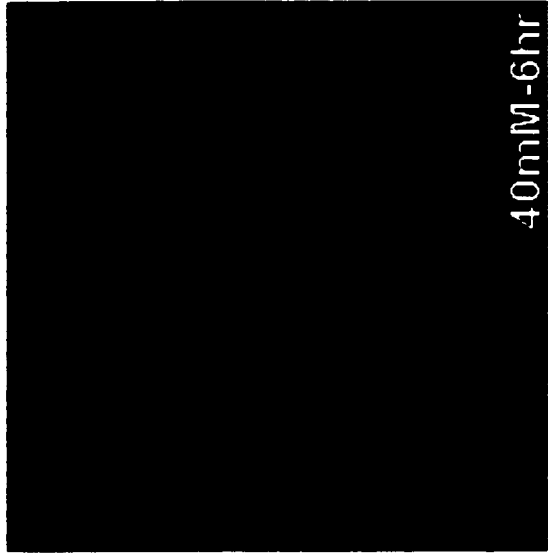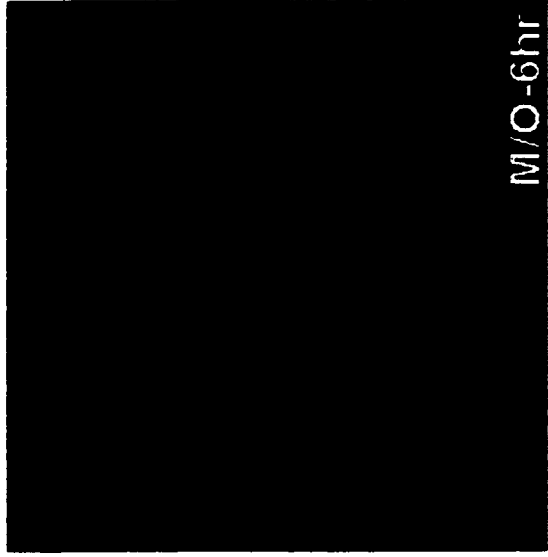
5.5mM-6hr   40mM-6hr   M/O-6hr

Figure 18.

Figure 18 displays representative PD2 Schwann cells stained with the potentiometric dye CMTMR following 6 hr exposure to 5.5 or 40 mM glucose or trophic withdrawal. Trophic withdrawal (serum-free media) was chosen as a positive control for an apoptosis-associated decline in CMTMR. Note the bright fluorescent labeling of mitochondria observed in Schwann cells in 5.5 mM base media (Figure 18A) in contrast to the dramatically reduced CMTMR fluorescence observed in cells in 40 mM glucose (Figure 18B) or serum-free media (Figure 18C).

Figure 19 presents the frequency distributions of high glucose induced changes in $\Delta\Psi_M$ in PD2 Schwann cells. Schwann cells grown on glass coverslips were incubated in 40 mM glucose and stained with 130 nM CMTMR for 15 min prior to paraformaldehyde fixation after 2, 6, or 24 hr exposure to high glucose. Following 2 hr of exposure to 40 mM glucose, there was approximately a 37% drop in the mean of the CMTMR fluorescence intensity distribution, reflecting a dramatic drop in $\Delta\Psi_M$. This is represented by a large shift to the left in the distribution of CMTMR fluorescence intensity. There was a similar decrease in $\Delta\Psi_M$ observed following 6 hr of exposure to 40 mM glucose (a decrease of 41% relative to control cells), accompanied by an equivalent shift to the left in the distribution of CMTMR fluorescence intensity. By 24 hr, the $\Delta\Psi_M$ of cells in 40 mM glucose had dropped to about 50% of that for cells in base media. At each of the time points examined, there was a significant decrease in CMTMR fluorescence intensity (Mann-Whitney U; all p's < 0.001, see Table 12, Appendix B) in PD2 Schwann cells exposed to 40 mM glucose compared to 5.5 mM

Figure 19. Time Course of High Glucose Induced Changes in $\Delta\Psi_M$ in PD2 Schwann Cells. PD2 Schwann cells grown on glass coverslips were exposed to 5.5 or 40 mM glucose, stained with CMTMR and fixed in paraformaldehyde at 2, 6, or 24 hr. Measurements were made from individual mitochondria from a minimum of 30 cells per group. The fluorescence intensity, measured on a scale of 0-255 is indicated along the x-axis of the frequency histograms and the y-axis represents the percentage of mitochondria at each intensity level. Exposure to high glucose produced a large drop in $\Delta\Psi_M$ at 2 hr that persisted at 6 and 24 hr, indicated at each time point by a shift to the left in the distribution of CMTMR fluorescence intensity.
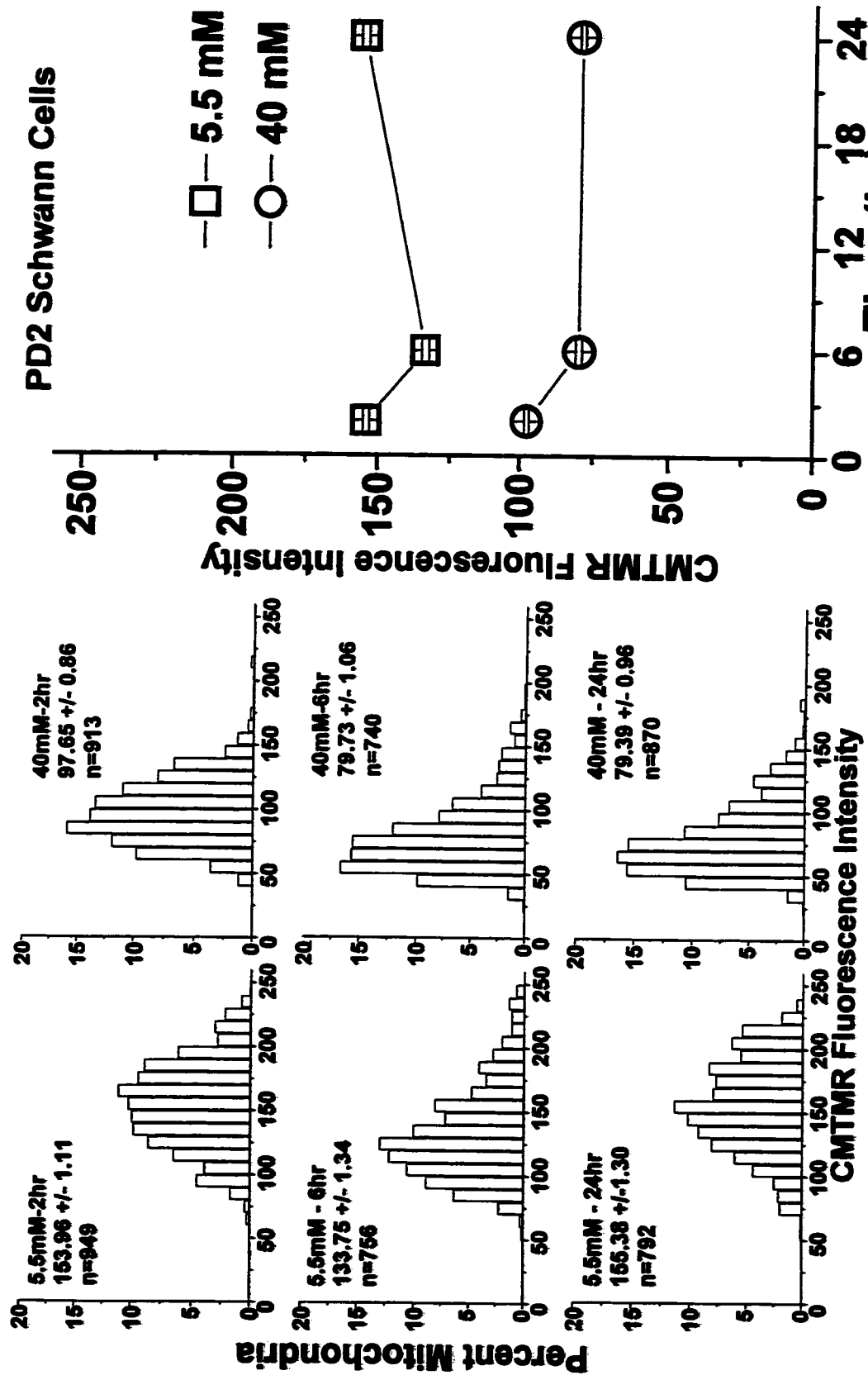
Figure 19.

Figure 20. Time Course of High Glucose Induced Changes in $\Delta\Psi_M$ in PD15 Schwann Cells. PD15 Schwann cells grown on glass coverslips were exposed to 5.5 or 40 mM glucose, stained with CMTMR and fixed in paraformaldehyde at 2, 6, or 24 hr. Measurements were made from individual mitochondria from a minimum of 30 cells per group. The fluorescence intensity, measured on a scale of 0-255 is indicated along the x-axis of the frequency histograms and the y-axis represents the percentage of mitochondria at each intensity level. Exposure to high glucose produced a time-dependent decrease in $\Delta\Psi_M$ from 2-24 hr reflected by a gradually increasing shift to the left of the CMTMR fluorescence intensity distribution.
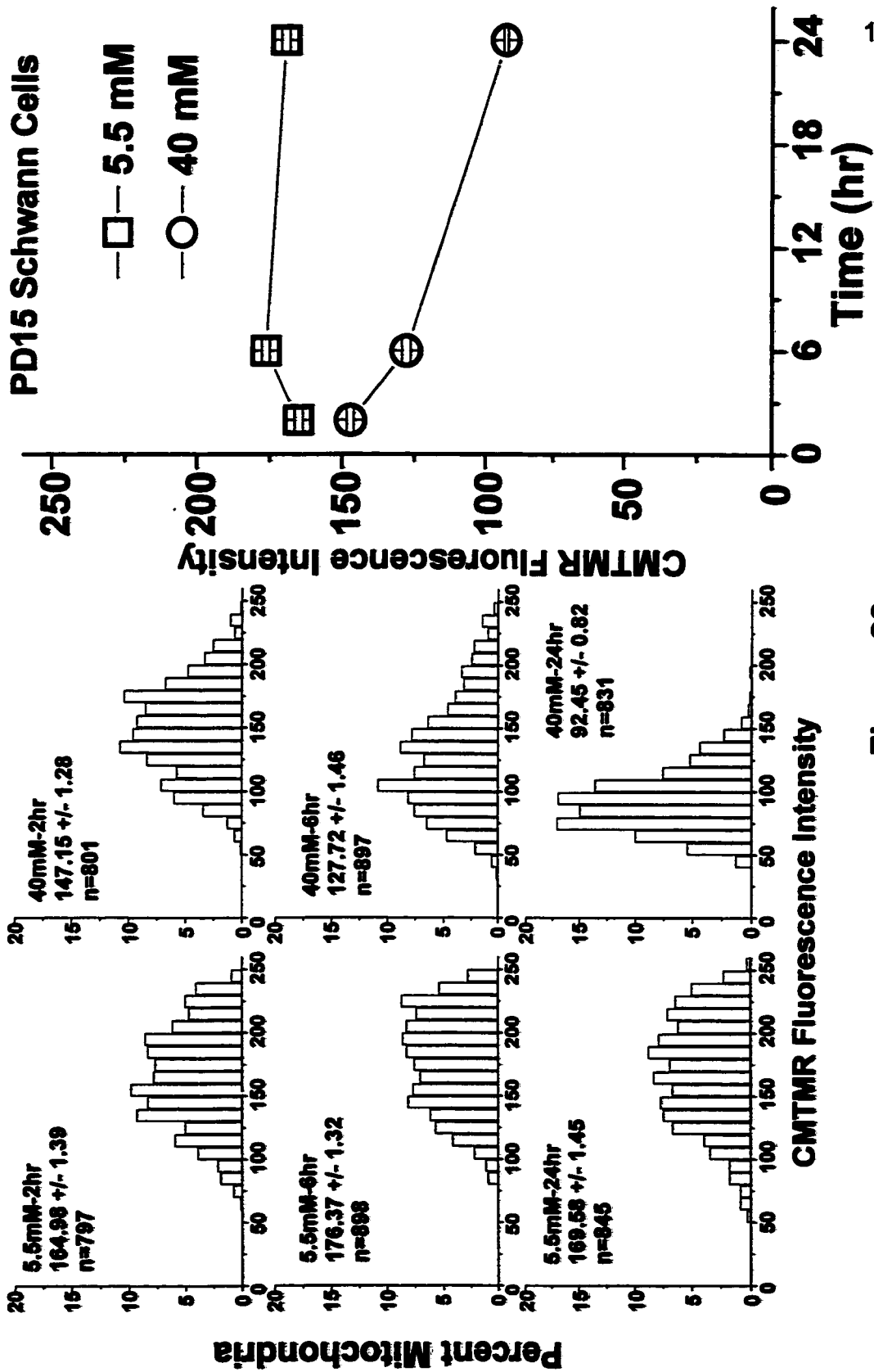
Figure 20.

glucose. At each time point examined between 2-24 hr in 5.5 mM glucose, approximately 30-50% of mitochondria display FIU greater than 150; whereas, in 40 mM glucose, at each time point, at least 95% of mitochondria have fallen below this value.

Figure 20 presents the time course of high glucose induced changes in $\Delta\Psi_M$ in PD15 Schwann cells. After 2 hr in 40 mM glucose, $\Delta\Psi_M$ of PD15 cells had dropped by 11% compared to cells in base media at 2 hr. After 6 hr exposure to high glucose, there was approximately a 28% decrease in $\Delta\Psi_M$ compared to cells in base media, reflected as a significant shift to the left for the CMTMR fluorescence intensity distribution. Following 24 hr of exposure to 40 mM glucose, $\Delta\Psi_M$ dropped by approximately 46% compared to cells exposed to base media (Mann-Whitney U; all p's < 0.001, see Table 12, Appendix B). In PD15 Schwann cells grown in 5.5 mM glucose, between 50-65% of mitochondria display FIU values greater than 150 at each time point. Exposure to 40 mM progressively shifted the percentage down from approximately 55% at 2 hr to greater than 95% of mitochondria below this value by 24 hr.

For both PD2 and PD15 cells, there was a significant drop in $\Delta\Psi_M$ between 2-6 hr. This preceded the appearance of oligonucleosomal DNA fragmentation (see Figure 11), indicating that the second wave of glucose dose-dependent apoptotic death was associated with an increase in mitochondrial membrane permeability (Green and Kroemer, 1998).

Figure 21. DMD Prevents the High Glucose Induced Drop in $\Delta\Psi_M$. PD2

Schwann cells were exposed to 40 mM glucose for 6 hr and stained with

CMTMR. High glucose induced a shift to the left of the CMTMR fluorescence

intensity distribution that was completely prevented by treatment with DMD (10^{-9}

M).

Figure 21.
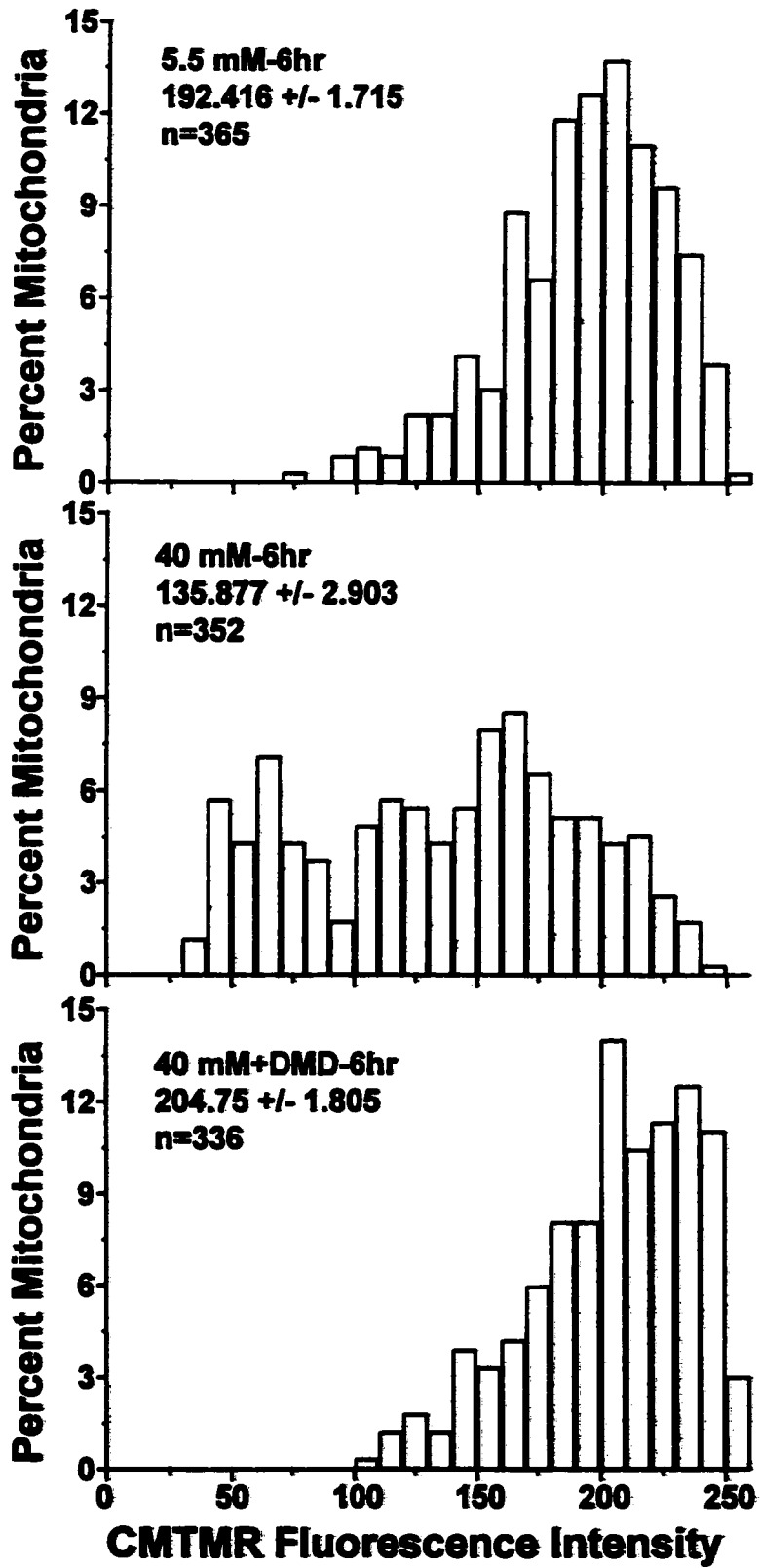
III.h Anti-Apoptotic Molecules Prevent High Glucose Induced Drop in $\Delta\Psi_M$

Since the anti-apoptotic molecules DMD, NAC and IGF-1 were able to

significantly improve Schwann cell survival in high glucose media, it was decided

to examine the effects of these agents on $\Delta\Psi_M$. Figure 21 presents the CMTMR

frequency distributions of PD2 Schwann cells exposed to 5.5 mM, 40 mM, or 40

mM glucose plus DMD (10^{-9} M) for 6 hr. There is about a 30% drop in the mean

of the CMTMR fluorescence distribution of cells exposed to 40 mM glucose

compared to cells in 5.5 mM glucose at 6 hr. Simultaneous treatment with DMD

of Schwann cells, exposed to 40 mM glucose for 6 hr, completely prevented the

leftward shift of the CMTMR fluorescence intensity distribution (Mann-Whitney U;

all p's < 0.001, see Table 13, Appendix B). This data indicates that DMD

rescued Schwann cells by maintaining the $\Delta\Psi_M$ near control levels. It was not

determined whether DMD also provoked new protein synthesis as has been

shown for the rescue of apoptotic PC12 cells (Wadia et al., 1998).

Similarly, the effects of NAC (10^{-7} M) on $\Delta\Psi_M$ were examined in PD2 cells

in high glucose. Figure 22 presents the time course of NAC-induced recovery of

$\Delta\Psi_M$ in PD2 Schwann cells exposed to 40 mM glucose for 2, 6, 12, and 24 hr.

There was a time dependent recovery of CMTMR fluorescence intensity in

Schwann cells treated with NAC (10^{-7} M). By 2 hr, a small increase (Mann-

Whitney U; p < 0.001) in the mean CMTMR fluorescence intensity, represented

by a small shift to the right of the distribution occurred in the NAC-treated cells.

By 6 hr, almost one third of the high glucose-induced drop in $\Delta\Psi_M$ is recovered by

NAC (Mann-Whitney U; p < 0.001). Between 12-24 hr, NAC had shifted the

Figure 22. NAC Prevents the High Glucose Induced Drop in $\Delta\Psi_M$. PD2

Schwann cells were exposed to 40 mM glucose for 2, 6, 12, or 24 hr with or

without treatment with NAC (10^{-7} M) and stained with CMTMR. High glucose

induced a large shift to the left of the CMTMR fluorescence intensity distribution

at each time point. There was a time-dependent improvement in $\Delta\Psi_M$ in

Schwann cells treated with NAC; between 2-24 hr following exposure, the

fluorescence intensity distribution was gradually shifted back to the right,

approaching control levels by 24 hr.
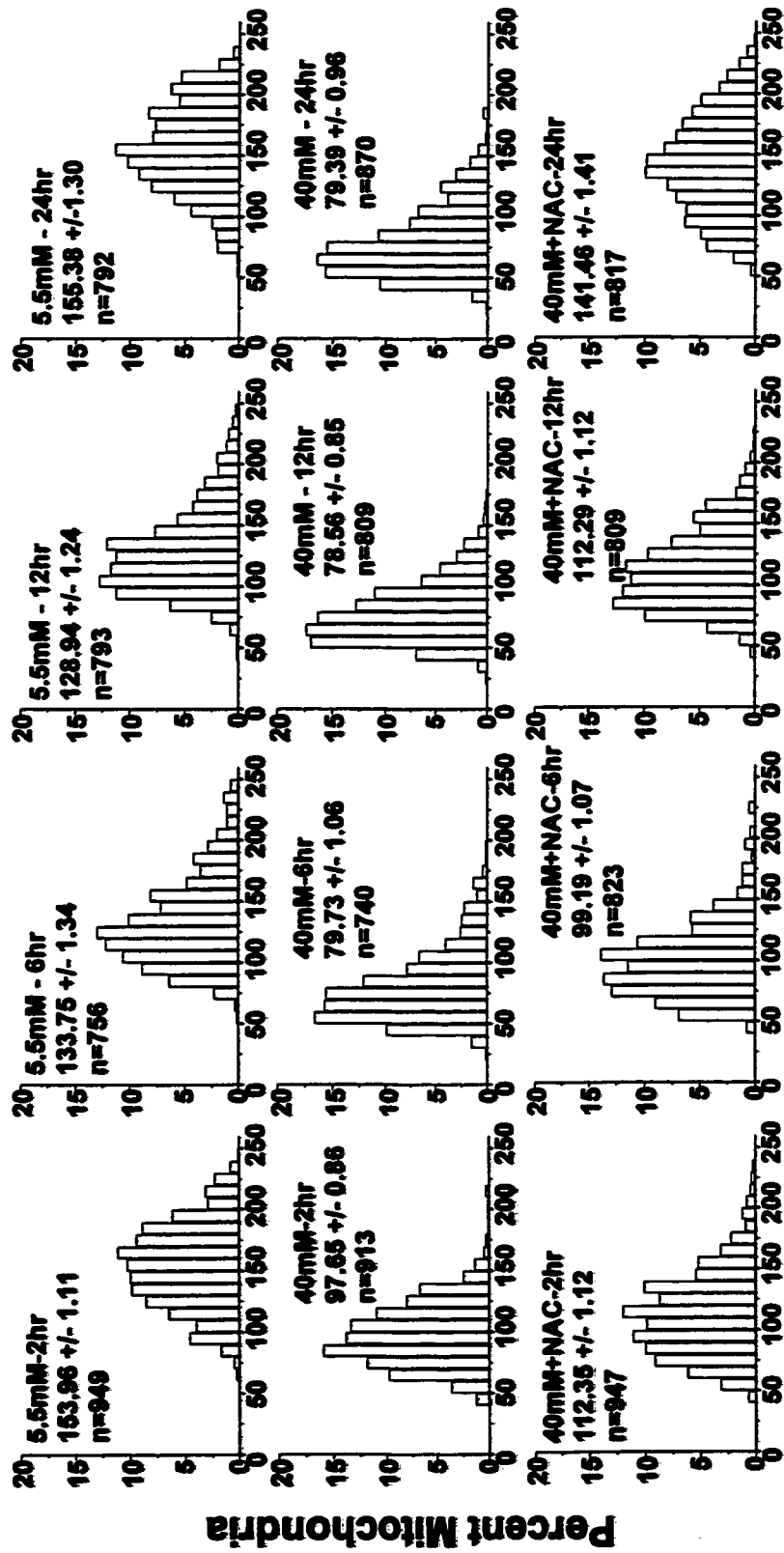
Figure 22.

CMTMR distribution to within 10% of that found for control cells in 5.5 mM glucose. These data indicate that NAC was able to rescue cells by its ability to maintain the $\Delta\Psi_M$ near control levels in the presence of high glucose. Administration of NAC gradually shifted the percentage of mitochondria above 150 FIU from approximately 20% at 2 hr to about 45% by 24 hr (see Figure 22).

Figure 23 presents the effects of IGF-I (1 ng/ml) on $\Delta\Psi_M$ in PD2 Schwann cells after 2 and 6 hr exposure to 40 mM glucose. For cells treated with IGF-I in 40 mM glucose, there was a time dependent recovery of the high glucose induced drop in CMTMR fluorescence intensity at 2 and 6 hr (Mann-Whitney U, p's < 0.001, see Table 13, Appendix B). Approximately 50-75% of the high glucose induced drop in $\Delta\Psi_M$ was prevented by IGF-I between 2-6hr respectively. Similarly, treatment with IGF-I in high glucose media maintained approximately 50-60% of mitochondria above 150 FIU over the 2-6 hr time period.

III.i Inhibition of NO Production and $\Delta\Psi_M$.

Given that excess NO can have deleterious effects on mitochondrial function (Bolanos et al., 1994; Bolanos et al., 1995), the effects of L-NIL (10^{-4} M) treatment on $\Delta\Psi_M$ was examined in 40 mM glucose-treated PD2 Schwann cells. At 2 hr following exposure to 40 mM glucose, L-NIL did not have any effect on $\Delta\Psi_M$ (p > 0.05, see Figure 24). Similarly at 6 hr following exposure, there was only a small, but statistically significant, increase in mean CMTMR fluorescence intensity; however, the distibution was not shifted back to the right, illustrating the importance of distribution analysis rather than simply relying on changes in the

Figure 23. IGF-I Prevents the High Glucose Induced Drop in $\Delta\Psi_M$. PD2 Schwann cells were exposed to 40 mM glucose for 2 or 6 hr in the presence of IGF-I (1 ng/ml) and stained with CMTMR. Treatment with IGF-I produced a time-dependent recovery of $\Delta\Psi_M$ shown as a shift to the right of the CMTMR fluorescence intensity distribution compared to cells exposed to 40 mM glucose alone.
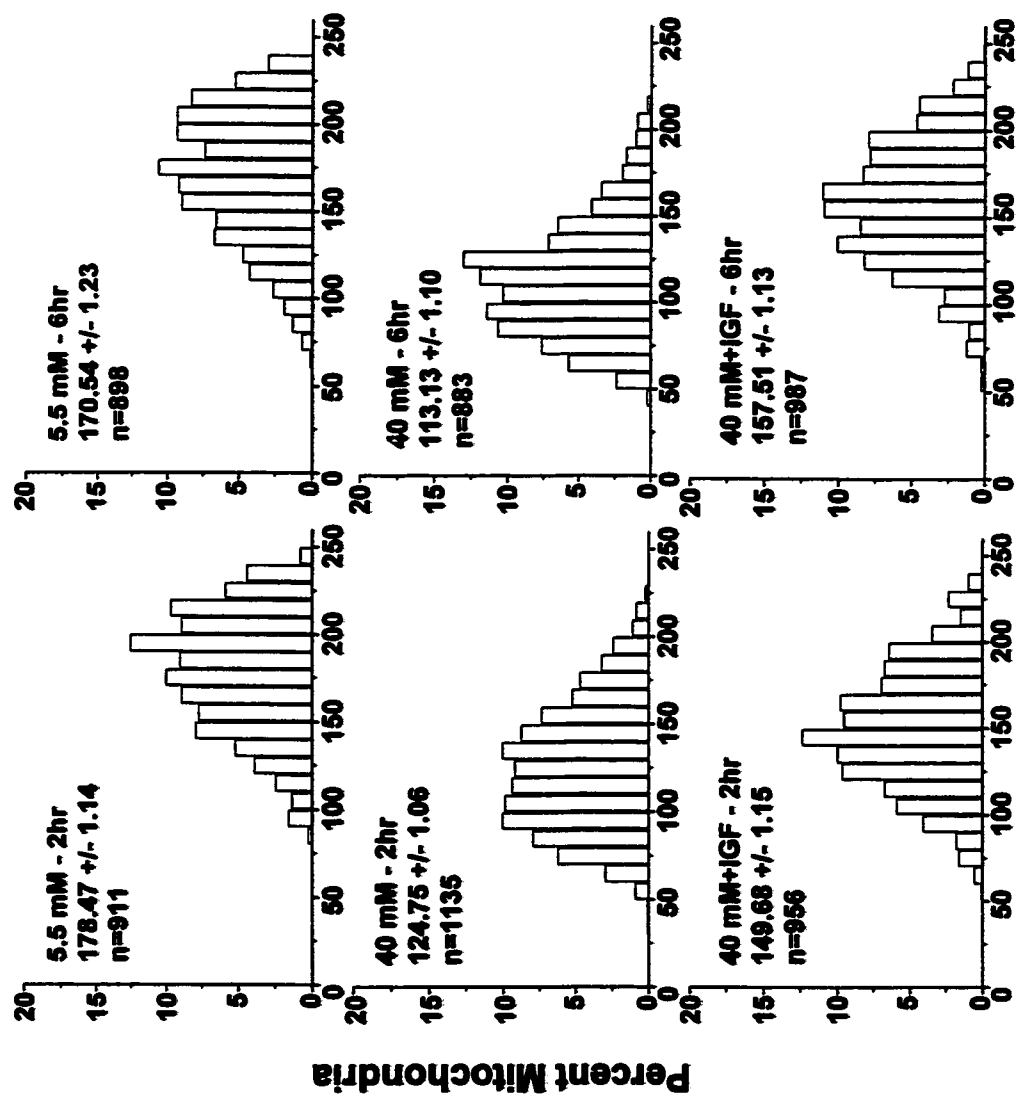
Figure 23.

Figure 24. Inhibition of iNOS Produces a Time-Dependent Recovery of ΔΨ$_M$ in PD2 Schwann Cells. PD2 Schwann exposed to 40 mM glucose were treated with the selective iNOS inhibitor L-NIL (10^{-4} M) for 2, 6, or 12 hr and stained with CMTMR. L-NIL did not prevent the high glucose induced drop in ΔΨ$_M$ in PD2 Schwann cells at 2 or 6 hr; however, by 12 hr the CMTMR intensity distribution was shifted back toward the right compared to 40 mM glucose alone.

PD2 Schwann Cells

5.5mM-2hr
153.98 +/- 1.11
n=949

5.5mM - 6hr
133.75 +/- 1.34
n=756

5.5mM - 12hr
128.94 +/- 1.24
n=793

40mM-2hr
97.65 +/- 0.86
n=913

40mM-6hr
79.73 +/- 1.06
n=740

40mM - 12hr
78.56 +/- 0.85
n=809

40mM+NIL-2hr
99.58 +/- 0.98
n=977

40mM+NIL-6hr
86.51 +/- 0.91
n=779

40mM+NIL-12hr
110.64 +/- 1.29
n=794

Percent Mitochondria
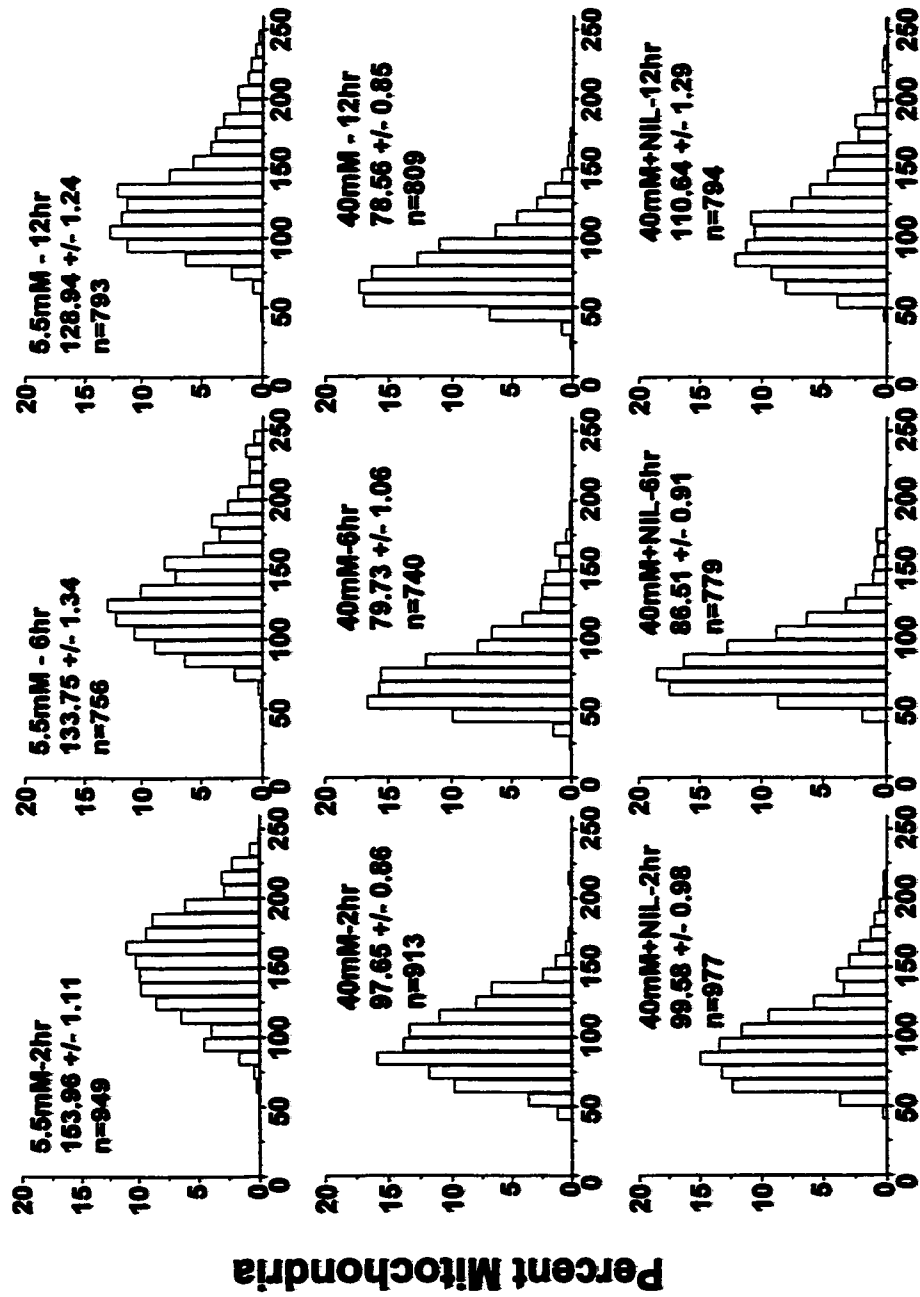
CMTMR Fluorescence Intensity

Figure 24.

sample mean. The absence of a significant change would be expected given that L-NIL inhibits inducible NOS, which requires about 16-18 hr to achieve full activity after induction (Gardiner et al., 1995). However, by 12 hr, L-NIL treatment had a significant effect on the $\Delta\Psi_M$ of PD2 cells in 40 mM glucose (Mann-Whitney U, p < 0.001, see Table 14, Appendix B), as shown by a rightward shift in the CMTMR fluorescence intensity distribution. This would suggest that the presence of NO may exacerbate the effects of high glucose and inhibition of NO production could potentially ameliorate some of its effects. However, given the earlier findings presented in Figure 15, inhibition of iNOS only slightly increased cell survival at 24 hr. This suggests that NO is more likely to be a contributor to the effector phase of glucose-induced apoptosis in Schwann cells as a signaling intermediary, but it is not essential for committing cells to the apoptotic process.

Figure 25 presents the effects of NO inhibition by L-NIL on the high glucose induced changes in $\Delta\Psi_M$ in PD15 Schwann cells at 2 and 24hr. After 2 hr exposure to 40 mM glucose there was approximately a 15% drop in mean CMTMR fluorescence intensity. The CMTMR distribution of mitochondria in PD15 cells treated with L-NIL maintained their $\Delta\Psi_M$ (Mann-Whitney U, p < 0.001) nearer control values. However, after 24 hr exposure to 40 mM glucose, L-NIL treatment only slightly influenced the drop in $\Delta\Psi_M$ (p < 0.01) in PD15 Schwann cells. This suggests either that significant iNOS stimulation does not occur in PD15 Schwann cells in high glucose to influence mitochondrial membrane permeability (Figure 14), or that cNOS may contribute more NO under high

Figure 25. High Glucose Induced Drop in $\Delta\Psi_M$ in PD15 Schwann Cells is Not Significantly Improved by Inhibition of iNOS. PD15 Schwann cells were exposed to 40 mM glucose for 2 or 24 hr and treated with the selective iNOS inhibitor L-NIL (10^{-4} M) and stained with CMTMR. The mean CMTMR fluorescence intensity in PD15 Schwann cells in high glucose was slightly increased by treatment with L-NIL at each time point, however this was not reflected by a shift in the distribution of CMTMR fluorescence intensity at either time point.

128
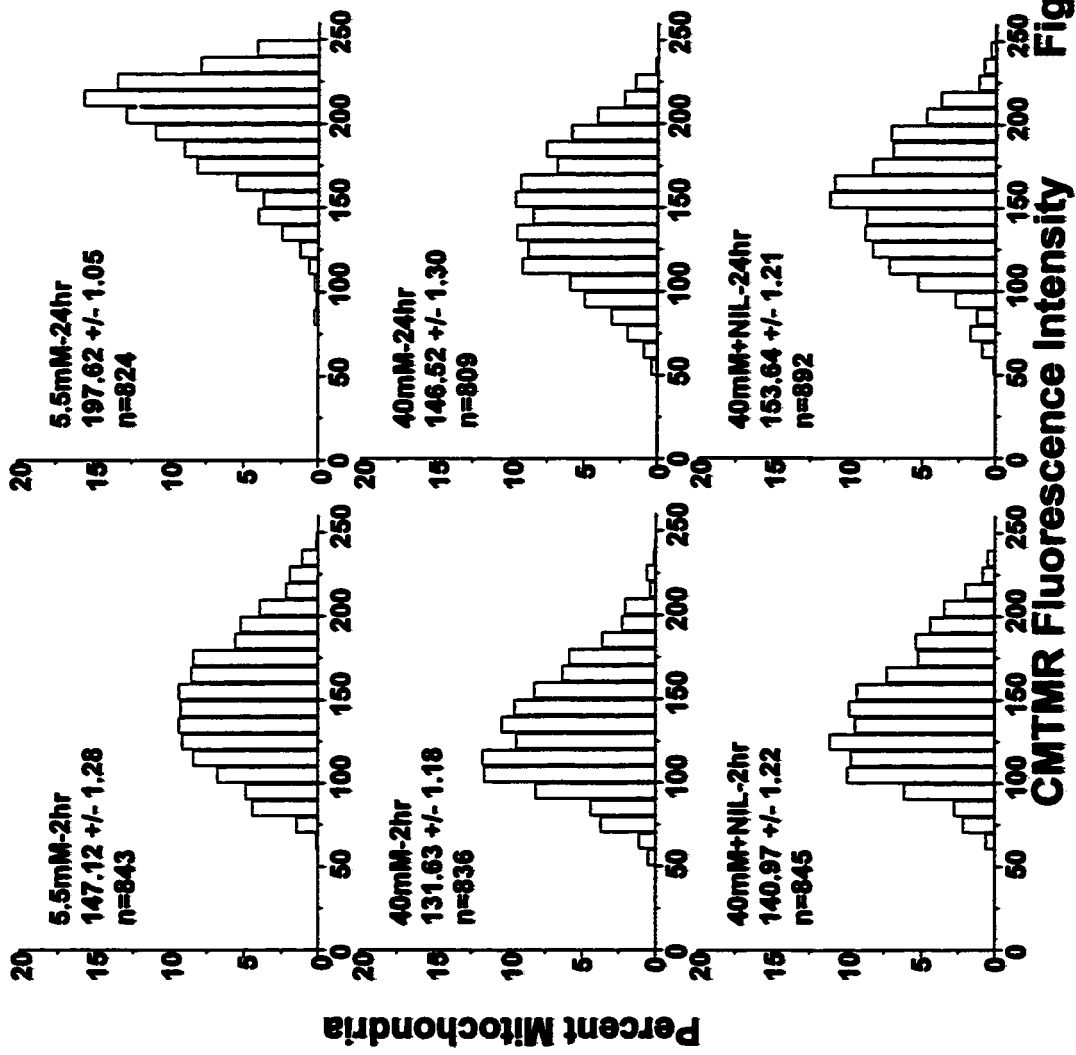
Figure 25.

glucose conditions in PD15 cells. Whether this would impact on $\Delta\Psi_M$ would require using a cNOS inhibitor like SMTC in combination with CMTMR.

III.j Involvement of the Mitochondrial PTP in High Glucose Induced Schwann Cell Apoptosis

Hexokinase is the initial enzyme in the glycolytic pathway and has been recently co-localized with the proteins that form the mitochondrial PTP. It has been suggested that the frequency of hexokinase (HK) binding at the contact sites between the inner and outer mitochondrial membrane in preparations of isolated mitochondria may correlate with sites of closed PTPs (Beutner et al., 1997). It was reasoned that the HK immunofluorescence intensity together with the corresponding CMTMR intensity might provide a measure of mitochondrial permeability transition. Therefore, there should be a positive linear relationship between CMTMR intensity and the intensity of HK immunofluorescence.

Dual-channel laser confocal images were obtained using a tunable filter system that permits the fine adjustment of the strength of the beam passing through the appropriate excitation filter before hitting the specimen. This system has several advantages: 1) it permits the collection of images with multiple fluorochromes within the same optical plane and allows the precise co-localization of proteins within the cell, and 2) it permits the virtual elimination of any bleed-through of signal between channels which may arise with certain fluorochromes that have wide emission spectra.

The Leica confocal microscope used is equipped with an argon/krypton laser with three independent laser lines (488 nm, 568 nm, and 647 nm). For visualization of CMTMR and Cy5 labeled HK (see Materials and Methods), the 568 and 647 laser lines are used, coupled with the 600/30 nm bandpass and 665 nm longpass emission filter sets respectively. To eliminate the potential bleed-through of signal from the CMTMR detector channel into the Cy5 detector channel, the laser intensity is attenuated by the tunable filter system to a level that produces no signal in the Cy5 channel from excitation of the CMTMR channel. For the image pairs obtained here, the strength of the excitation in the CMTMR channel (the 568 nm laser line) was attenuated to 35% of maximum in order to eliminate signal bleed-through into the Cy5 channel (the 647 nm laser line). This ensured that the corresponding fluorescence intensity measurements obtained for CMTMR and HK were not contaminated by signal from the alternate channel. This adjustment only impacts the strength of the excitation; and given that at all times, the filter attenuation and photodetector voltage levels were maintained at constant settings, valid relative comparisons of fluorescence intensity can be made.

Figure 26 presents representative images of the distribution of CMTMR fluorescence and HK immunofluorescence within mitochondria of PD2 Schwann cells exposed to 5.5 and 40 mM glucose for 6 hr. In each of the panels in Figure 26, CMTMR is represented in red, HK in green, and the co-localization of CMTMR and HK as orange-yellow. Series A (Figure 26A1, -A2), depicts bright mitochondrial CMTMR fluorescence and bright HK immunofluorescence

Figure 26. HK-I Co-localizes With Mitochondria With Respect to $\Delta\Psi_M$.

Fluorescence photomicrograph of the co-localization of HK-I immunoreactivity

with CMTMR in mitochondria of PD2 Schwann cells maintained in base medium

(series A), 40 mM glucose (series B), or ATR (1 mM, series C). Confocal images

taken with the same optical plane of CMTMR fluorescence shown in red (A1, B1,

C1) and HK-I immunofluorescence shown in green (A2, B2, C2). A3, B3, and C3

represent the combined colour image of A1+A2, B1+B2, and C1+C2 respectively.

In the combined images CMTMR is seen as red and HK-I as green fluorescence,

whereas the co-localization is seen as yellow/orange. Note the reduction in

fluorescence intensity of both CMTMR and HK in mitochondria following

exposure to high glucose or ATR. Note that the extremely low-level HK

immunofluorescence in the 2 cells visible in the corner of image pairs A1/A2 and

B1/B2 is masked in the re-coloured images (see page 65 in Materials and

Methods). However, the original confocal images do contain both HK and

CMTMR signals obtained on separate channels (see page 65 for details).

Therefore measurements of CMTMR and HK intensity (see Figure 27) were

made from the original black and white images.

CMTMR
($\Delta\Psi_M$)
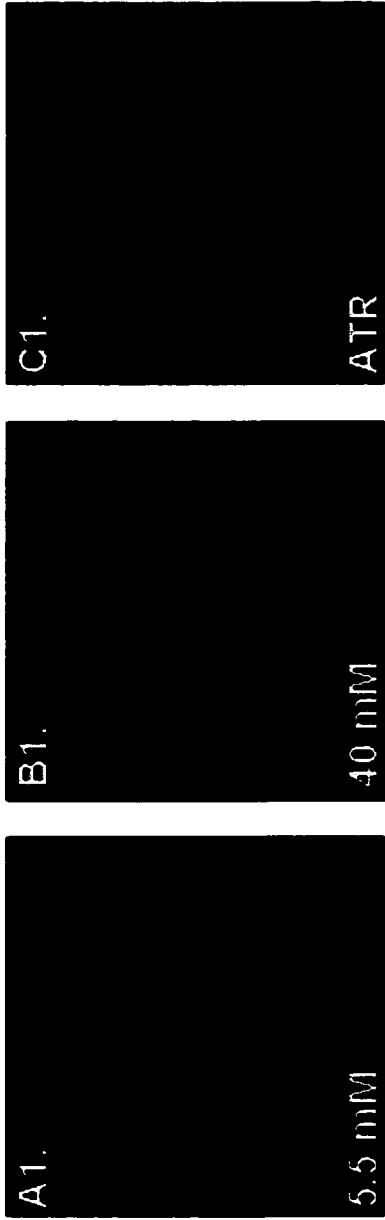
HK-I
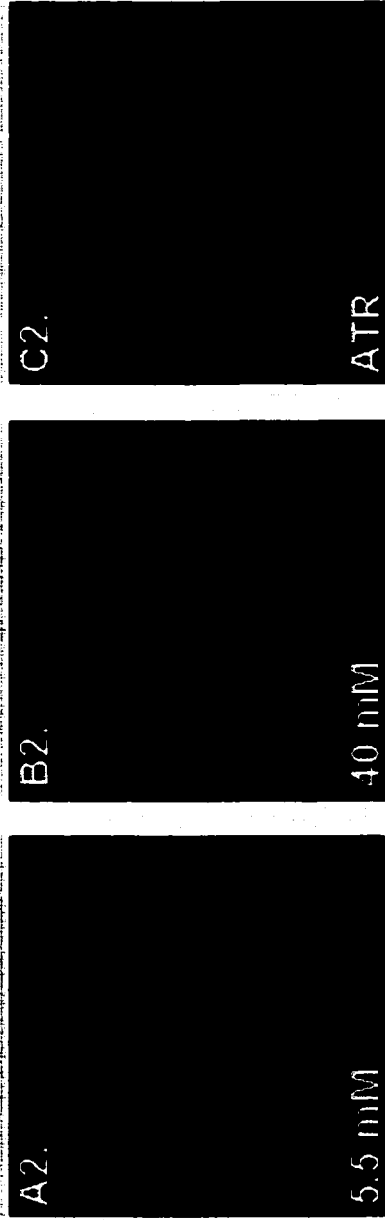
Combined
Image
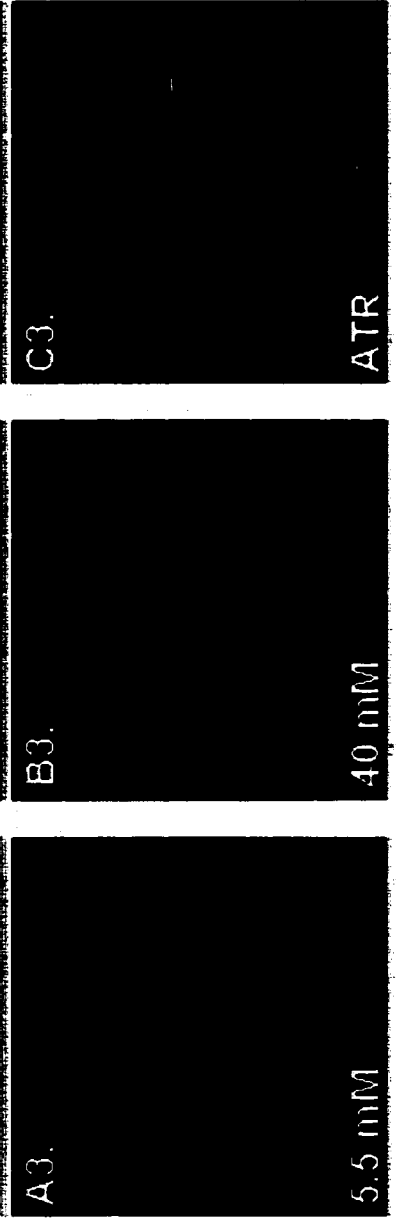
Figure 26.

respectively. In the combined image (Figure 26A3), the majority of HK immunoreactivity is associated with bright CMTMR fluorescence resulting in bright yellow-orange color throughout the mitochondrial volume. However, there are some portions of the mitochondria with bright CMTMR fluorescence but lower-intensity HK immunoreactivity resulting in red-orange mitochondria in the combined image. This would indicate decreased HK binding in these regions.

In PD2 Schwann cells exposed to 40 mM glucose for 6 hr, there is a reduction in CMTMR fluorescence intensity (Figure 21B1) along with a reduced level of HK immunofluorescence (Figure 26B2). In the combined image depicted in Figure 26B3, there is considerably less bright yellow-orange fluorescence compared to 26A3. This indicates that the reduced $\Delta\Psi_M$ (indicated by lower CMTMR intensity) is accompanied by a decrease in mitochondrial HK immunofluorescence, and thus possibly a decrease in binding of HK to the PTP.

PD2 Schwann cells were also exposed to the PTP-opening agent atractyloside (ATR, 1 mM) in base media for 6 hr (Figure 26C1). ATR produced a reduction in CMTMR fluorescence intensity and mitochondrial HK immunofluorescence (Figure 26C1, -C2 respectively) similar to that observed with 40 mM glucose. In the combined image (Figure 26C3), there is a clear reduction in mitochondrial yellow-orange fluorescence suggesting a decrease in co-localization of HK with the PTP.

Figure 27 presents the CMTMR fluorescence and HK immunofluorescence intensity distributions for PD2 Schwann cells exposed to 5.5 or 40 mM glucose or ATR (1 mM) in base media for 6 hr. Note the prominent

Figure 27. Quantification of High Glucose or ATR Induced Changes in $\Delta\Psi_M$ and Mitochondrial Bound HK. PD2 Schwann cells were exposed to 5.5 or 40 mM glucose, or the PTP opening agent ATR for 6 hr and stained with CMTMR. Fixed cells were then immunoreacted with antibodies against HK-I. CMTMR and HK-I immunofluorescence were measured on alternate image pairs from corresponding individual mitochondria and plotted as frequency distributions. Note the dramatic shift to the left of CMTMR fluorescence intensity following treatment with either high glucose or ATR; and a similar shift to the left of HK-I immunofluorescence intensity.
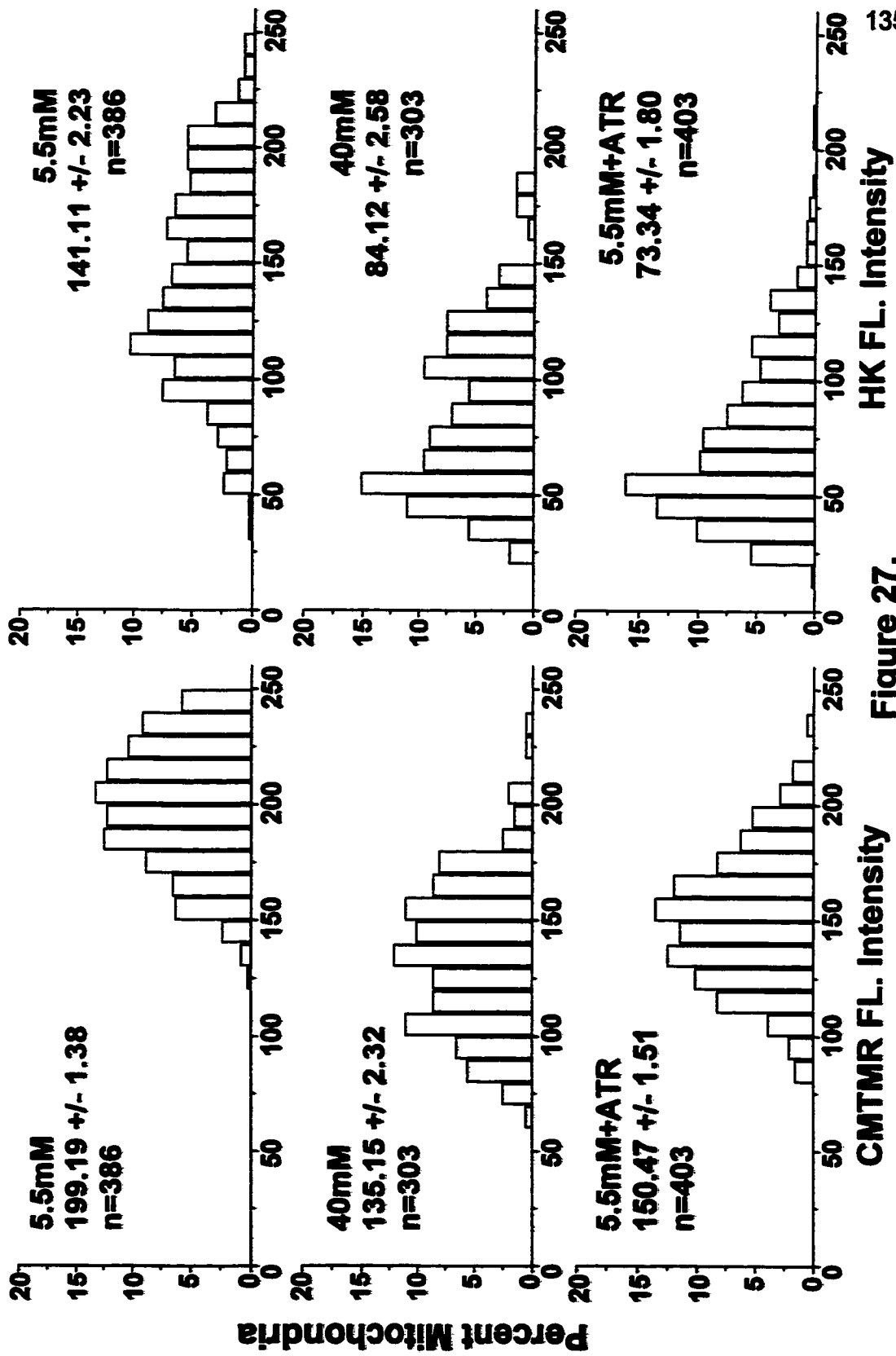
Figure 27.

shift to the left of the CMTMR fluorescence intensity distribution in Schwann cells exposed to 40 mM glucose or ATR. There was a reduction in $\Delta\Psi_M$ of approximately 30 and 25% in cells exposed to 40 mM or ATR/base media respectively compared to control cells in base media (Mann-Whitney U, $p <$ 0.001, see Table 15, Appendix B). Similarly, there was also a large shift to the left of the mitochondrial HK immunofluorescence intensity distribution in cells exposed to 40 mM glucose or ATR/base media. Mean HK immunofluorescence was reduced by approximately 40 and 48% in Schwann cells exposed to 40 mM glucose or ATR respectively ($p < 0.001$).

To determine the relationship between $\Delta\Psi_M$ and HK localization to mitochondria, fluorescence intensity measured from identical points within mitochondria were obtained for CMTMR and HK. Figure 28 presents the regression lines obtained for CMTMR fluorescence intensity plotted against HK immunofluorescence intensity. There is a linear relationship between $\Delta\Psi_M$ and HK immunofluorescence in PD2 Schwann cells exposed to 5.5 mM glucose for 6 hr (Figure 28A). After 6 hr exposure to 40 mM glucose, there was a reduction in the slope of the regression line from 0.81 to 0.50 ($p < 0.05$, see Table 16, Appendix B), indicating that exposure to high glucose alters the relationship between $\Delta\Psi_M$ and HK localization to mitochondria. Overall, there is a downward trend in HK intensity, which indicates a decline in its mitochondrial localization. Accompanying this decline, is a leftward shift in CMTMR fluorescence indicating a decline in $\Delta\Psi_M$. The decline in mitochondrial HK fluorescence may be due either to a release of HK from its PTP binding site, or it may be due to a change

Figure 28. High Glucose or ATR Alters the Relationship Between $\Delta\Psi_M$ and Mitochondrial Bound HK. Regression analysis of the corresponding CMTMR and HK fluorescence intensity measurements obtained from individual mitochondria following exposure to 5.5 or 40 mM glucose or ATR. In base media, there is a strong linear relationship between $\Delta\Psi_M$ and mitochondrial bound HK. As seen in Figure 27, the intensity of both CMTMR and HK fluorescence is decreased following exposure to high glucose or ATR. However, note also the reduction in the slope of the regression lines from 0.81 to 0.50 and 0.35 in high glucose and ATR respectively indicating that as $\Delta\Psi_M$ drops there is an associated drop in mitochondrial HK.

5.5 mM/ATR1- 6 hr
Y=20.61+0.35X
r=0.29
n=403

40 mM-6 hr
Y=16.2+0.50X
r=0.45
n=303

5.5 mM-6 hr
Y= -20.51+0.81X
r=0.50
n=386

HK FL. Intensity

250   200   150   100   50   0

0 50 100 150 200 250   0 50 100 150 200 250   0 50 100 150 200 250

CMTMR Fluorescence Intensity
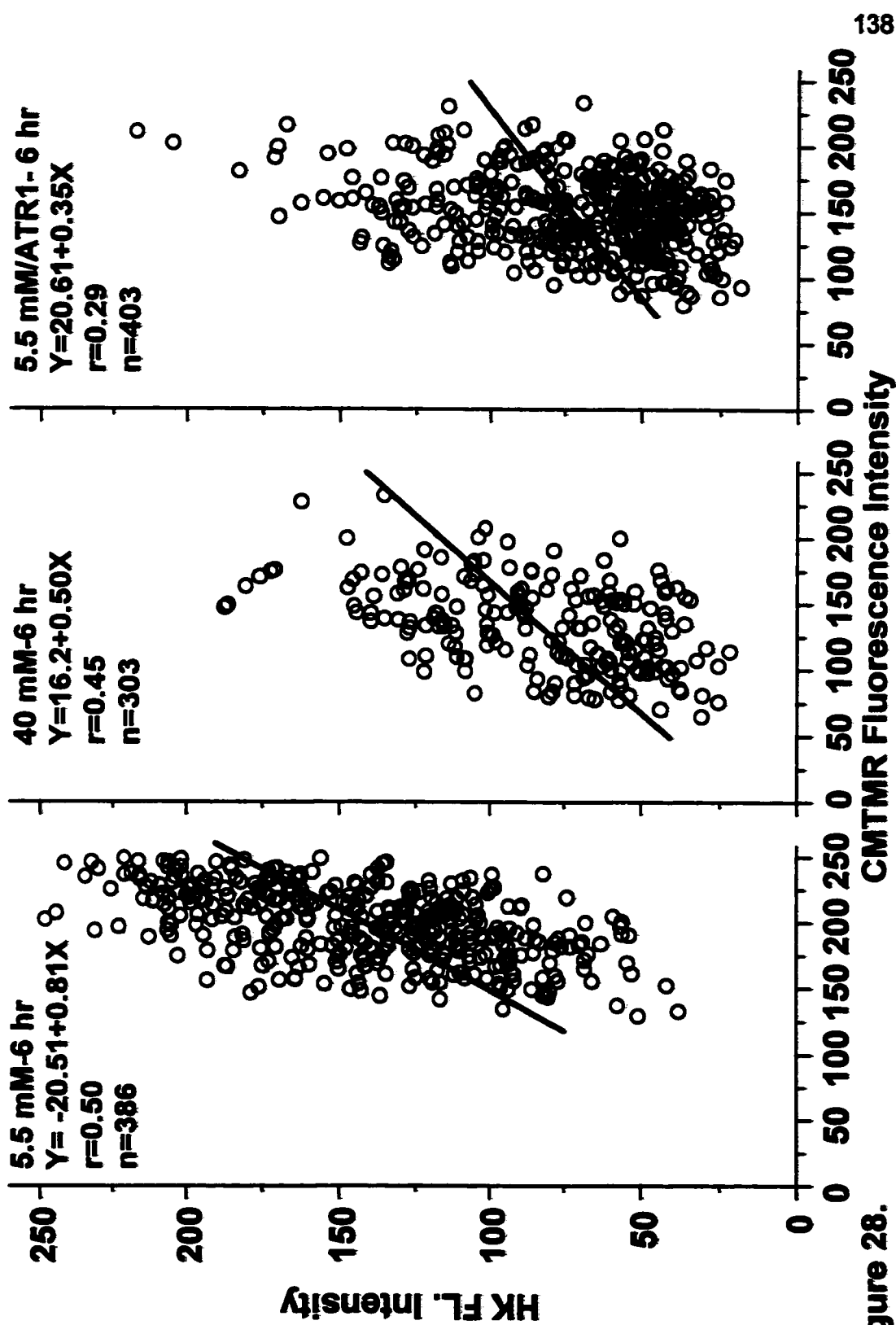
Figure 28.

in HK conformation (or PTP conformation) which masks the antigenic site of the protein. In cells exposed to ATR/base media for 6 hr, there was a further reduction in the slope of the regression line from 0.81 to 0.35, indicating that opening the mitochondrial PTP does alter the relationship between $\Delta\Psi_M$ and HK localization. Similarly there is a leftward shift in CMTMR intensity compared to base media values and a downward shift towards lower mitochondrial HK immunofluorescence as was observed with 40 mM glucose exposure. The fact that exposure to high glucose produces a similar disruption of the relationship between $\Delta\Psi_M$ and the mitochondrial localization of HK, as does an agent that opens the PTP, suggests that the PTP may be involved in high glucose induced Schwann cell apoptosis.

To determine the impact of modifying PTP conformation on Schwann cell survival, counts of intact nuclei were performed on PD15 Schwann cells (n = 6 wells) exposed to high glucose in the presence of the PTP-closing agent CsA $(10^{-7}$ M), or exposed to the PTP-opening agent ATR in base media for 24 hr. Exposure to 40 mM glucose for 24 hr induced a large drop in cell survival of approximately 42% (Figure 29; Mann-Whitney U, p < 0.001, see Table 17, Appendix B), while exposure to ATR produced about a 50% decline in Schwann cell survival at 24 hr compared to control cells. Treatment of cells exposed to high glucose with CsA prevented approximately one half of the cell death observed (p < 0.001). This would suggest that opening of the PTP underlies high glucose-induced Schwann cell apoptosis. The fact that treatment with CsA did not prevent the cell loss induced by ATR likely reflects the different mechanism of

Figure 29. CsA Improves Schwann Cell Survival in High Glucose. PD15

Schwann cells grown in 24 well plates were treated with 5.5 or 40 mM glucose,

or 40 mM glucose + the PTP closing agent CsA for 24 hr. Other cells were

exposed to ATR in base media or ATR + CsA. Cells were harvested for intact

nuclear counts. Each bar represents the percentage of intact nuclei relative to

base media (+/- SEM) from 6 replicate wells. Treatment with CsA prevented

approximately one half of the high glucose induced cell death, but did not

significantly improve survival following exposure to ATR. This could reflect a

different site of action at the PTP for each agent.
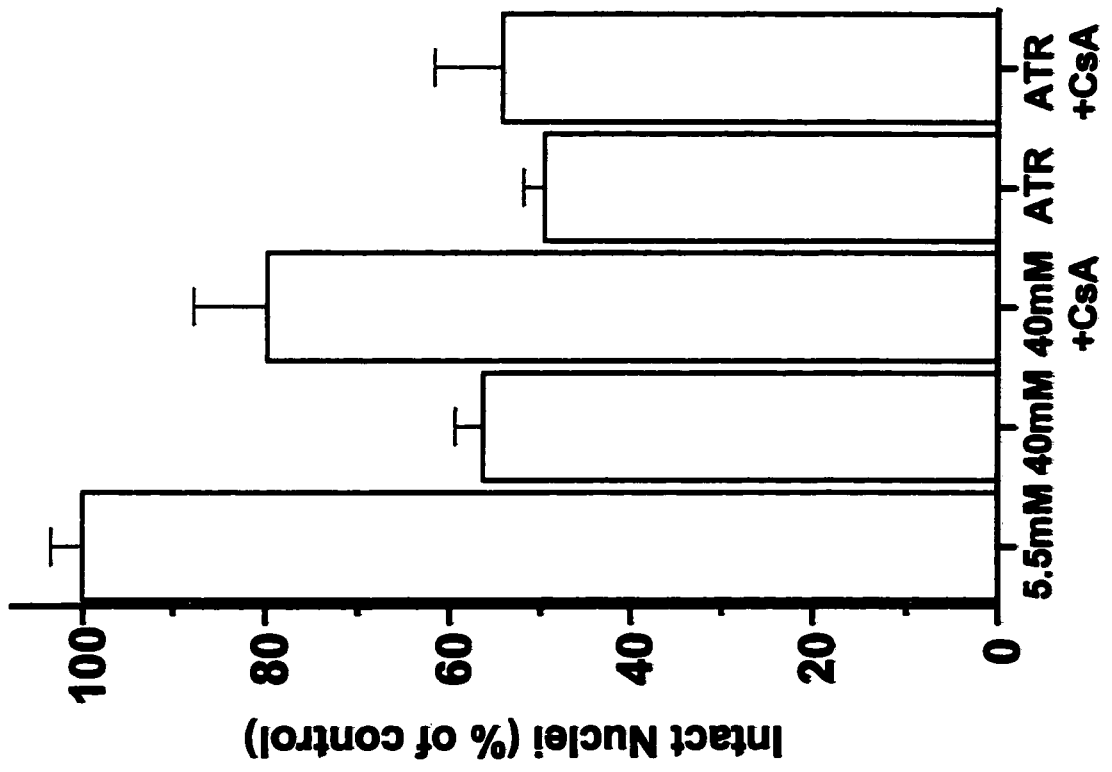
Figure 29.

action that each agent has at the ANT. While the specific interaction between between ATR and the ANT that induces opening of the pore is not known, it is believed that CsA maintains pore closure by preventing binding of cyclophilin D to the ANT (Petronilli et al., 1994).

To determine if the improved survival observed with CsA was due to maintenance of $\Delta\Psi_M$, Schwann cells exposed to high glucose were stained with the potentiometric dye CMTMR to estimate $\Delta\Psi_M$. Figure 30 presents the time course of CsA induced recovery of $\Delta\Psi_M$ in PD2 Schwann cells. Treatment with the PTP-closing agent CsA (10^{-7} M) produced a time dependent recovery of $\Delta\Psi_M$ between 2-12 hr following exposure to 40 mM glucose (Figure 30). At 2 hr, there was about two-thirds recovery of $\Delta\Psi_M$ toward control values by CsA (Mann-Whitney U, p < 0.001, see Table 18, Appendix B), represented by a shift to the right of the CMTMR fluorescence intensity distribution. By 6 hr, CsA had reclaimed approximately 85% of the high glucose induced drop in $\Delta\Psi_M$ (p < 0.001), seen as a rightward shift in the intensity distribution. By 12 hr, CsA completely prevented the high glucose induced drop in $\Delta\Psi_M$ (p < 0.001).

As with PD2 Schwann cells, treatment with the PTP closing agent CsA significantly improved $\Delta\Psi_M$ of PD15 Schwann cells exposed to 40 mM glucose. Two hr following exposure to 40 mM glucose there was an approximate 10% drop in $\Delta\Psi_M$ (Mann-Whitney U, p < 0.01) with a small shift to the left of the CMTMR fluorescence intensity distribution (Figure 31). Treatment with CsA completely prevented this drop and produced an increase in $\Delta\Psi_M$ above control levels (p < 0.001, see Table 18, Appendix B). By 6 hr, approximately two thirds

Figure 30. CsA Prevents the High Glucose Induced Drop in $\Delta\Psi_M$ in PD2 Schwann Cells. PD2 Schwann cells were exposed to 5.5 or 40 mM glucose, or 40 mM glucose + CsA for 2, 6, or 12 hr and stained with CMTMR. Measurements were made from individual mitochondria from a minimum of 30 cells per group. At each time point, treatment with CsA significantly shifted the CMTMR fluorescence intensity distribution back to the right compared to 40 mM glucose alone.

Figure 30.

5.5 mM - 12hr
146.12 +/- 1.28
n=822

40 mM - 12hr
82.08 +/- 0.98
n=960

40 mM+CsA - 12hr
144.21 +/- 1.30
n=883

5.5 mM - 6hr
170.54 +/- 1.23
n=914

40 mM - 6hr
113.13 +/- 1.10
n=883

40 mM+CsA - 6hr
162.76 +/- 1.12
n=960

5.5 mM - 2hr
178.47 +/- 1.14
n=911

40 mM - 2hr
124.75 +/- 1.06
n=1135

40 mM+CsA - 2hr
162.40 +/- 1.25
n=931

Percent Mitochondria
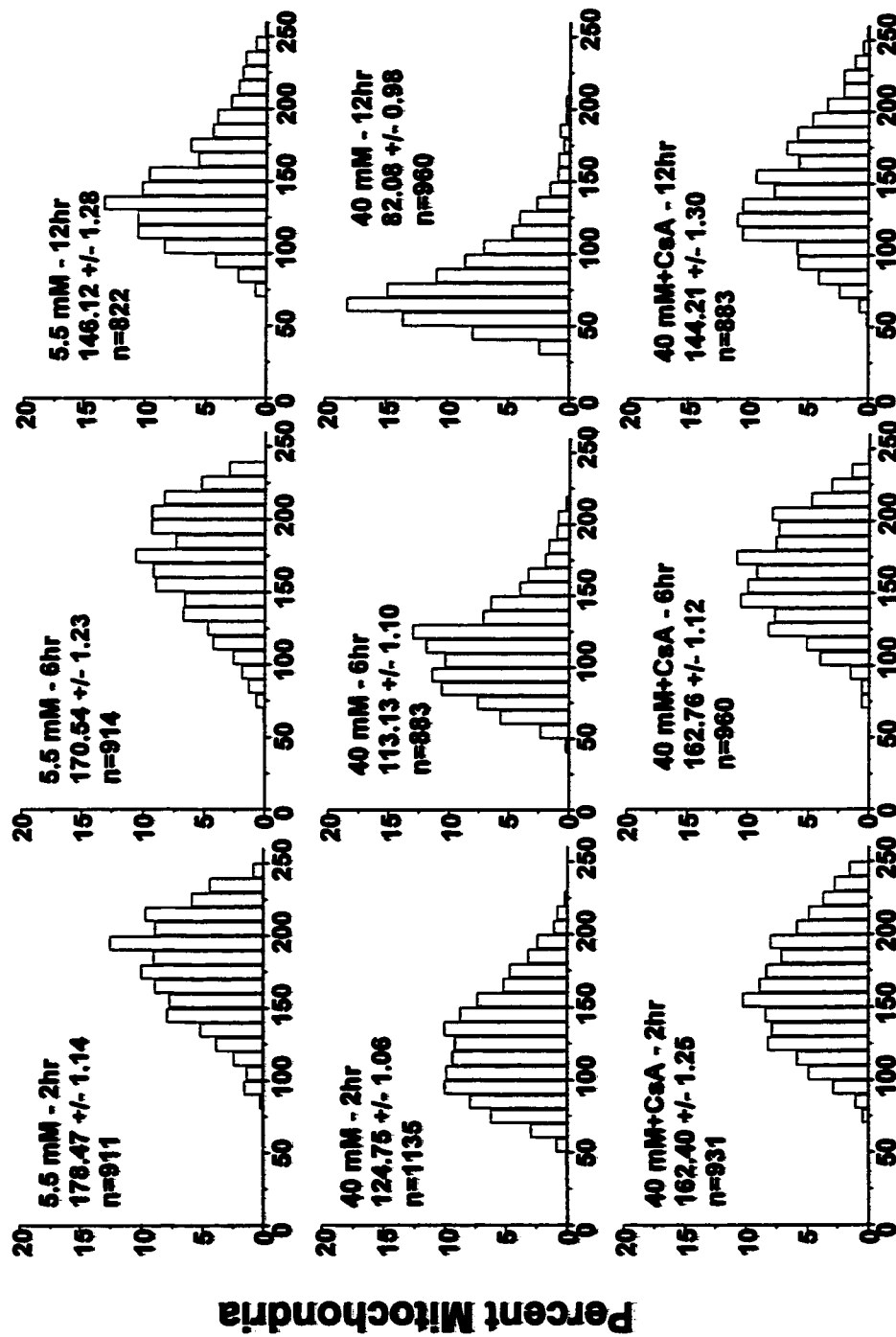
CMTMR Fluorescence Intensity

Figure 31. CsA Prevents the High Glucose Induced Drop in $\Delta\Psi_M$ in PD15 Schwann Cells. PD15 Schwann cells were exposed to 5.5 or 40 mM glucose, or 40 mM glucose + CsA for 2, 6, or 24 hr and stained with CMTMR. Measurements were made from individual mitochondria from a minimum of 30 cells per group. At each time point, treatment with CsA significantly shifted the CMTMR fluorescence intensity distribution back to the right compared to 40 mM glucose alone; at 2 and 24 hr CMTMR fluorescence was maintained at higher levels than in Schwann cells grown in base media.

Percent Mitochondria

CMTMR Fluorescence Intensity

Figure 31.

5.5mM-2hr
164.98 +/- 1.39
n=797

5.5mM-6hr
176.37 +/- 1.32
n=898

5.5mM-24hr
169.58 +/- 1.45
n=845

40mM-2hr
147.15 +/- 1.28
n=801

40mM-6hr
127.72 +/- 1.46
n=897

40mM-24hr
92.45 +/- 0.82
n=831

40mM+CsA-2hr
188.10 +/- 1.35
n=701

40mM+CsA-6hr
161.13 +/- 1.44
n=831

40mM+CsA-24hr
175.53 +/- 1.19
n=813
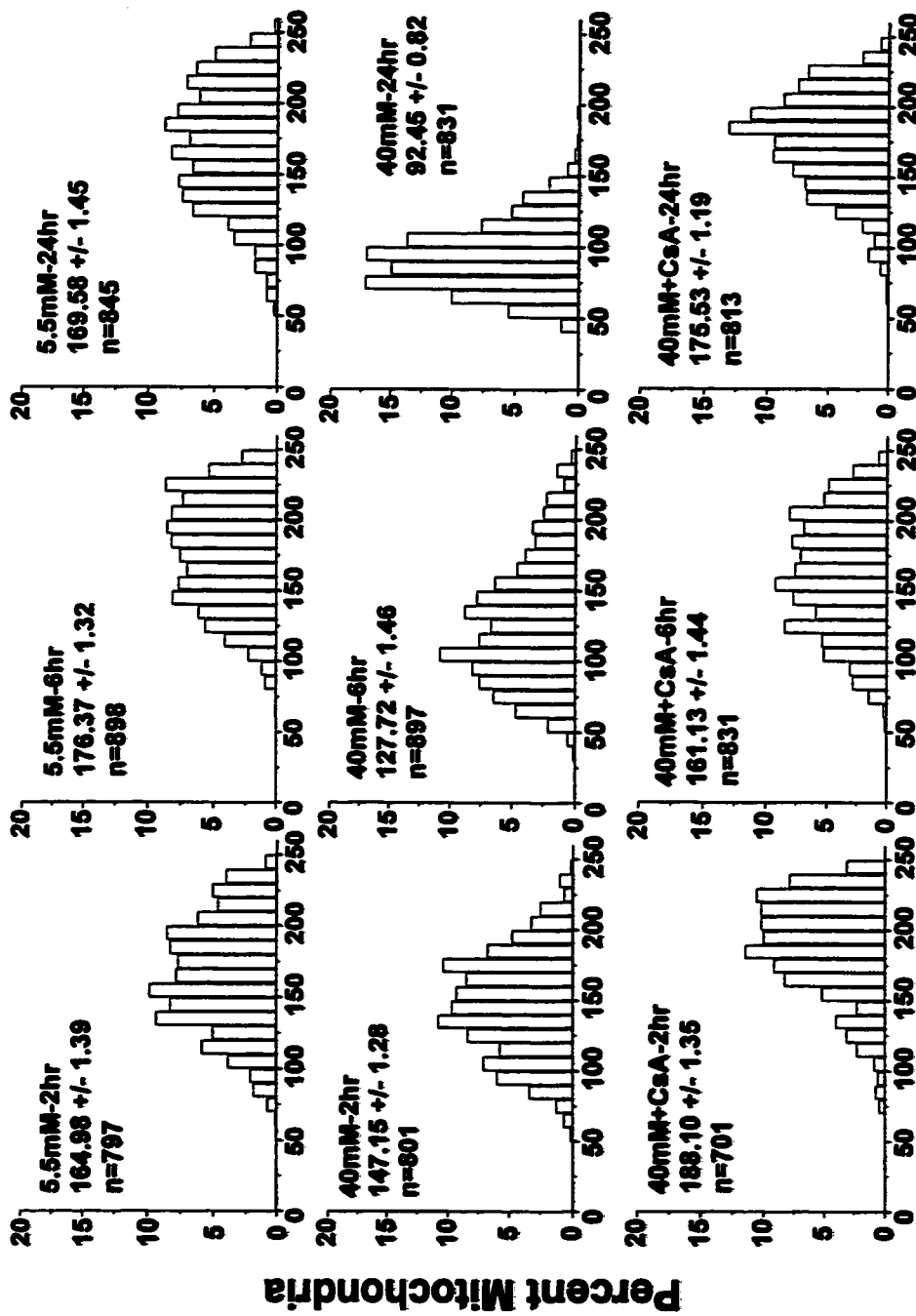
of the high glucose induced 30% drop in $\Delta\Psi_M$ was recovered by treatment with

CsA (p < 0.01). At 24 hr, treatment with CsA completely prevented the 50% drop

in $\Delta\Psi_M$ produced by 40 mM glucose (p < 0.001), and shifted the CMTMR

fluorescence intensity distribution back to the right. Since it was not possible to

determine by these methods whether HK physically left the PTP site on the

mitochondrion or whether conformational changes masked the HK antigenic site,

subcellular fractionation studies were performed in an attempt to address this

question.

III.k Western Blot Analysis of the Sub-cellular Localization of HK and Bax

Western blots were performed on enriched mitochondrial, cytoplasmic,

and nuclear sub-cellular fractions using antibodies raised against HK-I and Bax

to confirm the reduction of mitochondrial bound HK seen with confocal imaging.

Enriched sub-cellular fractions from PD2 Schwann cells were obtained using a

variation of the method described by Kluck et al. (1997). Figure 32 presents the

time course of changes in HK protein levels in each of the enriched cellular

fractions. The strong bands present in the nuclear fraction are likely the result of

contaminating mitochondria either in unbroken cells that were pelleted during the

initial low-speed nuclear isolation, or from mitochondria that were also pelleted

during this initial low-speed spin, rather than from HK present in the nucleus.

This is confirmed by the absence of HK immunofluorescence in the confocal

images presented here (see Figure 26) and reported previously by others (Lynch

et al., 1991). The presence of double bands in the mitochondrial fraction (and in

Figure 32. Time Course of Changes in Sub-cellular Localization of HK.

PD2 Schwann cells grown in 100 mm culture dishes (approximately 2,500,000

cells per dish) were exposed to 5.5 or 40 mM glucose for 2, 6, or 24 hr and

harvested. Cell lysates were made in a Dounce homogenizer and enriched

nuclear, mitochondrial, and cytoplasmic fractions obtained by differential

centrifugation. A. Autoradiographs showing bands corresponding to HK-I in

each cellular fraction. Note decrease in total HK following exposure to high

glucose. B. Optical density values measured from bands in A. Note the

reduction in HK-I levels in the mitochondrial fraction at 2 hr following exposure to

high glucose.
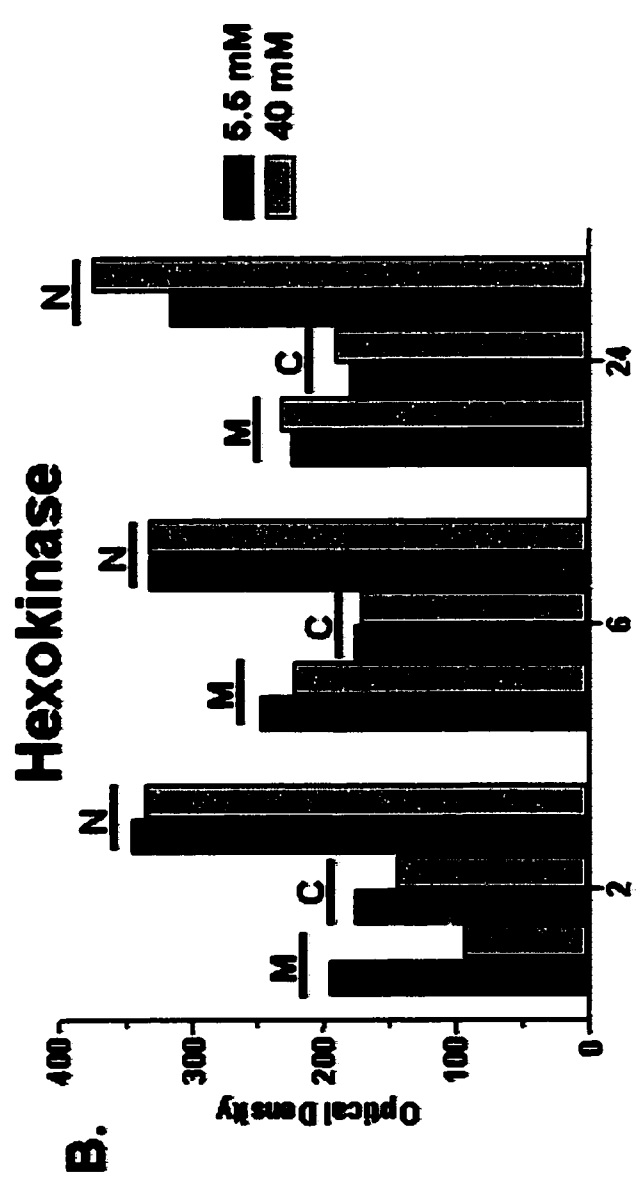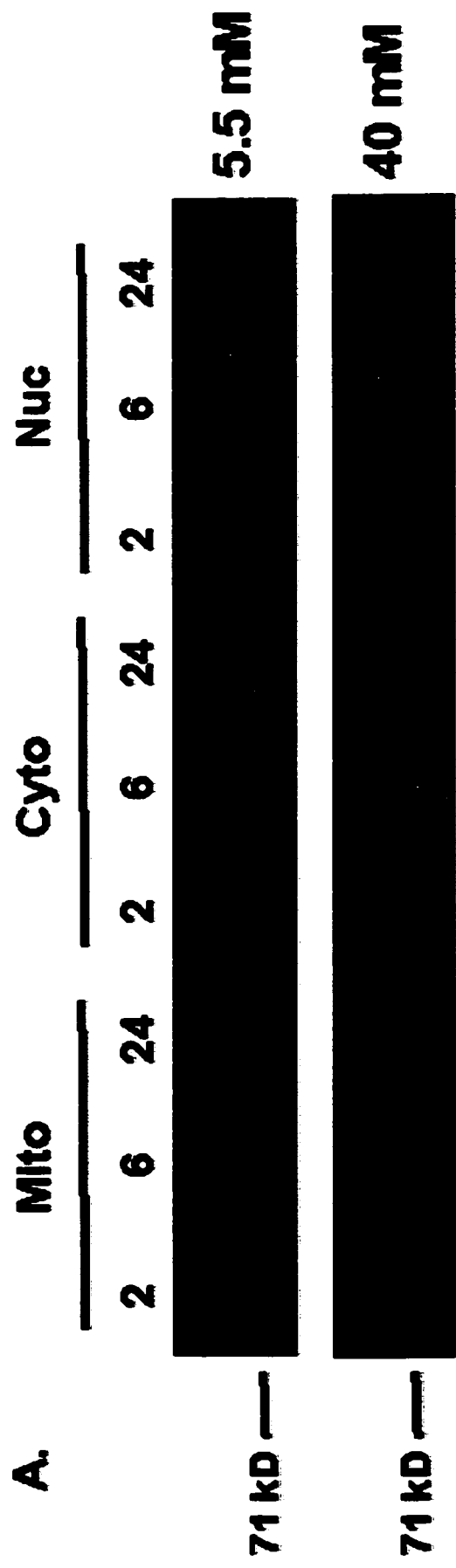
Figure 32.

the nuclear fraction that is likely mitochondrial in origin) can be accounted for by a number of things. It is possible that there is a specific post-translational modification involving a site-specific cleavage of HK during the insertion into mitochondria resulting in a lower band at approximately 71 kD rather than the expected size of approximately 100kD. Alternatively, the antibody, a monoclonal antibody raised against a peptide region located between residues 191-209 of HK-I may recognize an epitope common to another isoform of HK unique to Schwann (glial) cells. However, it is not likely to be the HK-II isoform, which shares a mitochondrial insertion domain (Sui and Wilson, 1997). Expression of the HK-II isoform is restricted to insulin-sensitive cells (McCabe, 1994; Wilson, 1997; Wilson, 1998) and would not likely be present in Schwann cells that do not require insulin for the transport of glucose. A third alternative is that a specific degradation occurred during the isolation of the mitochondrial fraction, that is also present in the mitochondrial contamination seen in the nuclear fraction.

There appears to be a drop in total HK protein levels at 2 and 6 hr in Schwann cells exposed to 40 mM glucose. Additionally, in the cytoplasmic fraction of cells exposed to 40 mM glucose, there is a progressive increase in the amount of HK protein between 2-24 hr (see Figure 32).

The pro-apoptotic protein Bax has recently been demonstrated to shift from the cytosol to the mitochondria of cells entering apoptosis (Hsu et al., 1997; Wolter et al., 1997). Additionally it has also been shown that an interaction between Bax and the ANT is required for opening of the PTP (Marzo et al., 1998; Narita et al., 1998). Western blots of enriched sub-cellular fractions were

Figure 33. Time Course of Changes in Sub-cellular Localization of Bax.

PD2 Schwann cells grown in 100 mm culture dishes (approximately 2,500,000

cells per dish) were exposed to 5.5 or 40 mM glucose for 2, 6, or 24 hr and

harvested. Cell lysates were made in a Dounce homogenizer and enriched

nuclear, mitochondrial, and cytoplasmic fractions obtained by differential

centrifugation. A. Autoradiograph of western blot showing bands corresponding

to Bax in each cellular fraction. Note the prominent band appearing in the

mitochondrial fraction following 24 hr exposure to high glucose. B. Optical

density values were obtained for each band in A. C. Autoradiograph of replicate

western blot performed on enriched sub-cellular fractions of PD2 Schwann cells

following 24 hr exposure to 5.5 or 40 mM glucose. Note here the increased Bax

levels in mitochondrial fraction in high glucose.
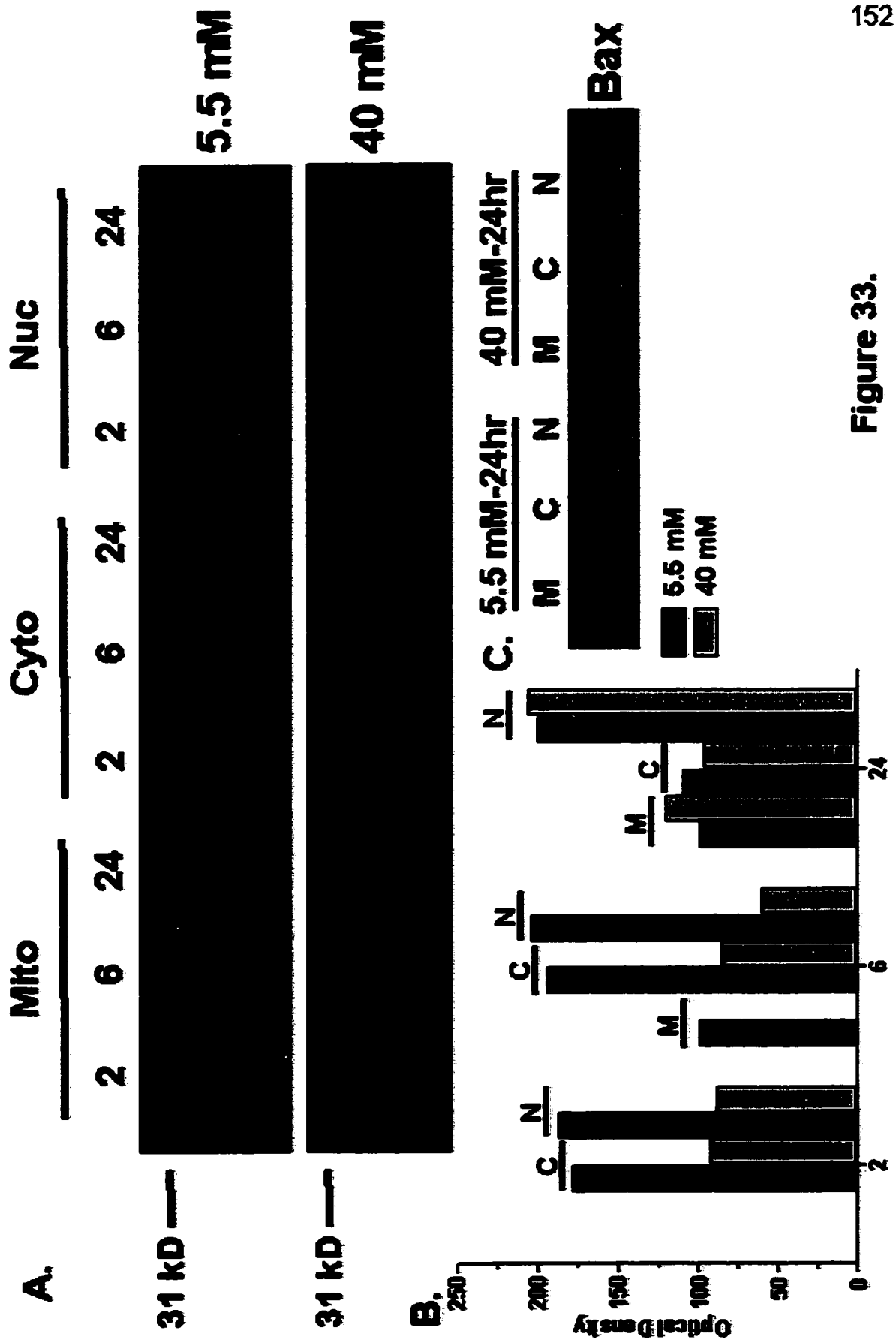
Figure 33.

performed to determine if high glucose induced opening of the PTP in Schwann cells was associated with translocation of Bax to the mitochondria (Figure 33). In addition to the bands seen at the expected weight of approximately 22 kD, an upper band running at a higher molecular weight is present in the mitochondrial (and nuclear) fractions. Because there were no other bands present on the blot, it is unlikely that this is due to non-specific binding. It could, however be due to a covalent association between Bax and a second, smaller protein causing it to migrate at a higher molecular weight than expected.

There is a clear increase in the amount of Bax protein in the mitochondrial fraction of PD2 Schwann cells after 24 hr exposure to 40 mM glucose. Additionally, there is a decrease in the amount of Bax protein in the cytoplasmic fraction by 24 hr in cells exposed to 40 mM glucose, suggesting a translocation of Bax from the cytosol to the mitochondria. There was also an increase in the amount of Bax protein in the nuclear fraction in cells exposed to 40 mM glucose during the 2-24 hr period. This may be due to mitochondrial contamination in the nuclear fraction; however it has recently been reported that Bax binds to the promyelocytic protein, PML, in the nucleus of cells undergoing apoptotic cell death (Quignon et al., 1998). Interestingly, the level of Bax appears to increase over time in 40 mM glucose, suggesting that this band may not be due to mitochondrial contamination but actual translocation to the nucleus. These studies offer some preliminary insights into the relationship between HK and the PTP during high glucose-induced apoptosis in Schwann cells. Because of the large number of Schwann cells required to obtain adequate protein for a single

lane (approximately 5 million cells per lane), it was not feasible to attempt further fractionations with primary Schwann cells.

IV. Discussion

The primary goal of this study was to isolate the effects of high glucose on Schwann cells by removing the potential influence of the peripheral axon and other cell types present in the nerve (e.g., fibroblasts, endothelial cells) that may also be affected by hyperglycemia. Therefore, an in vitro model was established using primary Schwann cells isolated from rat sciatic nerve. Schwann cells are a crucial element in the successful regeneration of the injured peripheral nerve, and part of that process involves the de-differentiation of mature Schwann cells into precursor-like cells capable of proliferation. Two distinct populations of Schwann cells were established from PD2 and PD15 rat sciatic nerve that displayed different antigenic, morphological, and proliferative properties. Further, Schwann cells from PD15 nerve proliferated without the need for growth supplementation whereas PD2 Schwann cells required additional support.

It was found that exposure to high glucose elicited a dose-dependent decrease in survival in both populations of Schwann cells. By using two independent in situ markers of apoptosis, this death was determined to be primarily apoptotic. Additionally, it was found that high glucose led to an impairment of mitochondrial function, specifically a drop in mitochondrial membrane potential, $\Delta\Psi_M$, and opening of the mitochondrial permeability transition pore, which has been shown to be a central event in many forms of apoptosis (Marchetti et al., 1996). Finally, it was shown that two proteins associated with the permeability transition pore, hexokinase and Bax, were re-distributed between the cytoplasmic and mitochondrial compartments in Schwann cells undergoing apoptosis. These findings introduce the possibility

that the observed functional and morphological changes in human DPN (e.g., abnormal nerve conduction, segmental demyelination) may be due to hyperglycemia induced Schwann cell death.

IV.a Development of a Novel Schwann Cell Isolation Method

The method of isolating primary Schwann cells described here resulted in the establishment of two populations of Schwann cells, a 'non-proliferating' population and a 'proliferating' population. Other methods in the literature, all essentially derived from a protocol by Brockes (1979), generally use 2-5 day old, and occasionally adult sciatic nerve to provide Schwann cells. Combined with immune panning methods or complement mediated lysis, a relatively pure population of Schwann cells can be obtained. Having tried the established methods, I found that I could obtain both better yields and purer populations by using the methods described earlier (see section II.a - Methods).

Schwann cells isolated from PD2 rat sciatic nerve divide very slowly unless supplemented with bovine pituitary extract and cholera toxin. The counts of intact nuclei of Schwann cells cultured in base media (5.5 mM glucose) containing 2% FBS over the duration of the experiment (0-48 hr), did not show any significant change, indicating a quiescent population. Conversely, Schwann cells isolated from later post-natal rats (PD 15) proliferated in vitro without the need for supplementation by bovine pituitary extract or cholera toxin. Counts of intact nuclei from this proliferating population of Schwann cells maintained in base media with 2% FBS over the duration of the experiment revealed a 1.2 fold

increase in the number of cells after 48 hr.

Ki67 immunoreactivity supported these findings, indicating that approximately 40% of PD2 Schwann cells remained in the G_0 phase over 24 hr. The proportion of PD15 cells in G_0 dropped from 30% to approximately 15% over 24 hr, indicating that cells were leaving G_0 and entering the cell cycle, since there was no significant amount of cell death in 2% FBS base media. The staining pattern of this nuclear antigen is routinely used to stage cancerous tissue, and provides a reliable estimate of the proportion of cells in various stages of the cell cycle (Braun et al., 1988).

The basis for the difference in proliferation between PD2 and PD15 Schwann cells is unclear. In vivo, Schwann cells increase in number over days E14-E20 (Jessen and Mirsky, 1991). Differentiation into myelin forming Schwann cells usually begins immediately following birth and coincides with a sharp reduction in Schwann cell proliferation (Stewart et al., 1993), possibly due to the presence of signals that inhibit proliferation (Jessen and Mirsky, 1991). The onset of myelination and the suppression of proliferation are initiated at or about the time in which the nerves are harvested from PD2 animals, and therefore, the putative inhibitory signals (Jessen and Mirsky, 1991) would still be present in the nerve fragments. This could account for the reduced proliferation seen in PD2 Schwann cells compared to PD15 cells. It has been shown that axolemmal fragments are mitogenic to Schwann cells if they are allowed to adhere to the Schwann cell surface for a period of at least 6 hr, with maximum effect seen following incubation of 24 hr or more (Sobue and Pleasure, 1985). The

proliferative capacity of the PD15 cells may reflect the presence of such mitogens in the older nerve and not in the younger nerve, or that the younger, less differentiated PD2 cells may not be able to respond to these mitogens.

The region of nerve contained within each fragment that is seeded onto the tissue culture flask in the present study might be considered analogous to the region immediately distal to a site of injury such as a crush or transection. The differences in proliferation between PD2 and PD15 Schwann cells may therefore represent a difference in response to injury in vivo between younger and older nerves and the ability to upregulate cytokines and/or growth factors by the more differentiated, older cells. Interestingly, it has been shown that conditioned medium from both primary (from PD3 rats) and immortalized Schwann cells contain an unidentified growth factor that can enhance the proliferation of primary Schwann cells (Porter et al., 1987). The growth enhancing properties of this autocrine growth factor were potentiated by the addition of laminin to the cultures (Porter et al., 1987), which is normally secreted by Schwann cells and forms a major component of the extracellular matrix (Bunge et al., 1986). In this model, poly-L-lysine was used as a growth substrate, which may not promote, and may possibly inhibit the actions of endogenous mitogens in the nerve fragment.

Komiyama and Suzuki (1992) compared the proliferation rates of Schwann cells in nerves that were sectioned at PD3, PD10, PD30, and PD60. They found that ^{3}H-thymidine uptake following nerve section was significantly less in Schwann cells from PD3 mice compared to that from PD10 mice. Further, it has been shown that the majority of Schwann cell proliferation was in myelin-

forming Schwann cells and that there was virtually no Schwann cell proliferation in younger nerves that had not been completely myelinated (Salzer and Bunge, 1980). It was suggested that the capacity of Schwann cells to proliferate during Wallerian degeneration depended upon differentiation into myelin-forming Schwann cells (Komiyama and Suzuki, 1992; Salzer and Bunge, 1980). PD15 cells do express MBP, but whether they share similar characteristics with myelinating Schwann cells in vivo remains to be determined. In the model system described here, the axon associated signaling molecules which stimulate myelin protein production in Schwann cells are presumably withdrawn during the removal of the axonal fragments at the fifth day in vitro, so the signal inducing the expression of MBP in the PD15 Schwann cells is unknown. However it has been shown that the induction of expression of myelin proteins such as P_0 in early post-natal (PD2-5) Schwann cells can occur in chemically defined (serum-free) medium containing cholera toxin or forskolin, agents that raise intracellular levels of cAMP (Morgan et al., 1991).

IV.b Dose-Dependent Apoptotic Death of Schwann Cells in High Glucose Media

Using counts of intact nuclei as a measure of cell survival, it was shown that high glucose is toxic to pure populations of PD2 and PD15 Schwann cells. This glucose induced cell death was dose-dependent at concentrations between 17.5 mM and 50 mM. In PD2 Schwann cells, between 0-2 hr following washing, the amount of cell death observed ranged between 13-26% for cells exposed to

17.5-50 mM glucose, whereas in PD15 Schwann cells, the amount of death observed during the same time period ranged between 7-18%. Over the remaining 2-48 hr, the amount of cell loss in PD2 Schwann cells ranged from 29-50%, whereas the amount of PD15 Schwann cell death ranged between 10-26%. There may be a difference in susceptibility between PD2 and PD15 Schwann cells, or there may be a difference in the ability of PD2 and PD15 cells to respond to injury. Alternately, the proliferative capacity of the PD15 cells may be masking the toxic effects of high glucose. Or, Schwann cells in G_0 may be the most vulnerable to high glucose.

IV.c DNA Fragmentation, Chromatin Condensation and Apoptotic Morphology of Schwann Cells

Apoptotic DNA fragmentation appears to involve two stages that are characterized by fragment sizes that are related to higher order structures of chromatin. The early, high molecular weight stage of DNA fragmentation results in 50 kbp loop and 300-400 kbp supra-loop elements that can be detected only by pulsed-field electrophoresis (Beere et al., 1995; Filipski et al., 1990; Khodarev et al., 1998). The later stage of fragmentation involves the degradation of DNA into smaller fragments with the eventual production of 180 bp oligonucleosomal fragments, detectable by constant field electrophoresis or ISEL. It is now clear that not all cells degrade their DNA to oligonucleosomal fragments (Saura et al., 1997). While high molecular weight fragmentation may be essential for apoptosis to occur, oligonucleosomal fragmentation is not (Cohen et al., 1992;

Hara et al., 1996; Oberhammer et al., 1993a; Oberhammer et al., 1993b; Schulz et al., 1998; Walker and Sikorska, 1997). Therefore, those apoptotic cells with chromatin condensation accompanying DNA fragmentation limited to loop and supra-loop elements will be ISEL negative. Whether these early changes in chromatin condensation can be visualized with confocal microscopy and nucleic acid specific dyes remains to be established. The morphological changes which attend later chromatin condensation and internucleosomal fragmentation of DNA by activated endonucleases are generally considered to be characteristic features of late stage apoptosis (Zamzami et al., 1996). DNA fragmentation can be detected by ISEL, while nucleic acid specific stains such as YOYO-1, propidium iodide, and Hoescht 33258 can demonstrate condensation of the chromatin particularly when combined with confocal microscopy which provides high resolution imaging of nuclear substructure. Fluorescent-tagged dUTP has allowed ISEL and YOYO-staining to simultaneously detect oligonucleosomal DNA fragmentation and chromatin condensation in the same nucleus (Tatton et al., 1998).

It has been suggested that ISEL may also mark necrotic cells (Charriaut-Marlangue and Ben-Ari, 1995; Collins et al., 1992; Dong et al., 1997; Fukuda et al., 1993; Portera Cailliau et al., 1997), leading to an overestimation of apoptotic death or a misidentification of the mode of death. Under specific conditions that depend in part upon pH, concentration of divalent cations and buffer composition, TdT can be made to label single strand or double-stranded DNA (Grosse and Manns, 1993). Therefore it is necessary to use an independent marker of

apoptosis in conjunction with ISEL. This would include visualization of chromatin condensation with fluorescent dyes, detecting DNA "ladders" on gel electrophoresis, or the spectrofluorometric quantification of small fragmented DNA that has been purified from intact genomic DNA. In the present study, condensation of chromatin was visualized by YOYO-1. YOYO-1 binds to DNA in a sequence-specific manner, recognizing regions of DNA that contain the four-base sequence C-T-A-G. In a non-apoptotic cell, these regions would be homogeneously distributed throughout the nucleus resulting in the typical staining pattern observed in Figure 10C. However in an apoptotic cell, as the chromatin is reorganized and begins to condense, these regions are no longer randomly distributed throughout the nucleus, and are likely to be more available to the dye. This may be due to the collapse of the chromatin and nuclear matrix protein network, or margination of histones (Wadia et al., 1998) to provide greater access of the dye to DNA, the end result being a brighter signal.

While ISEL remains a useful marker of apoptosis when lower molecular weight DNA fragmentation occurs, internucleosomal double-stranded DNA digestion by endonucleases may not occur in all apoptotic cells. Both PD2 and PD15 Schwann cells were ISEL positive following 12 hrs exposure to high glucose media. However, two distinct patterns of nuclear chromatin condensation and nuclear morphology were observed. One group of Schwann cells displayed ISEL positive, shrunken nuclei with a chromatin condensation pattern considered typical of apoptosis. However, a subset of cells displayed a patchy, irregular pattern of chromatin condensation throughout the nucleus

combined with nuclear blebbing. These nuclei were generally the same size as normal Schwann cell nuclei, but were not ISEL positive. This pattern did not appear to resemble the condensation pattern observed in Schwann cell nuclei entering mitosis. In those Schwann cells with blebbed nuclei, observed both in PD2 and PD15 cells, the blebs appeared to eventually separate from the nucleus and form discrete nuclear bodies containing condensed chromatin (see Figure 10E). This pattern of chromatin condensation and nuclear re-modeling appears similar to that observed in the developmentally regulated apoptotic death of embryonic Schwann cells precursors isolated in vitro (Jessen et al., 1994). These authors observed discrete patches of chromatin enclosed in conspicuous nuclear protrusions into the cytoplasm, suggesting that this pattern of nuclear blebbing may be a feature of apoptosis in some Schwann cells.

In those Schwann cells which were ISEL positive, the pattern of chromatin condensation resembled that described by Wyllie and his colleagues using electron microscopy to observe changes in nuclear morphology (Wyllie et al., 1980) in cells in the early stages of the degradative phase of apoptotic death. In the Schwann cell, bright, condensed bodies of chromatin appeared along the inner surface of the nuclear membrane, as well as in the nuclear matrix (see Figure 10C, D). In these cells, the nuclear membrane appeared intact and no blebbing was observed. In general, these nuclei were smaller, with a rounded or oval shape compared to normal, non-apoptotic nuclei.

Counts of ISEL positive nuclei indicated that after 2hr exposure to high glucose (17.5 or 40 mM) there was not a significant increase in the percentage of

ISEL positive cells in either population. In contrast, counts of intact nuclei at the same period revealed an approximate 13-26% and 7-18% cell loss for PD2 and PD15 Schwann cells respectively. It is possible that an initial wave of necrotic cell death occurred following exposure to high glucose in the 2% FBS media, and therefore, the cells would not necessarily demonstrate ISEL positive nuclei. However, approximately 60% of cell death at 2 hr was prevented in PD2 cells and 40% in PD15 cells was prevented by treatment with anti-apoptotic agents such as NAC, DMD, or IGF-I (see Figure 12 and below). This would argue that a significant portion of the initial wave of Schwann cell death occurred via apoptosis. It is possible that these cells underwent rapid, high molecular weight DNA fragmentation but not the low molecular weight, internucleosomal fragmentation that can be detected by ISEL (Walker and Sikorska, 1997; Saura et al., 1997; Schulz et al., 1998). It is also possible that internucleosomal DNA fragmentation detectable by ISEL does not occur until later in the apoptotic process (i.e., by 12 hr). The time course of nuclear changes during the final degradative phase of apoptosis varies greatly between cell types, and thus has been difficult to reconstruct (Wyllie et al., 1980).

IV.d Anti-Apoptotic Agents Prevent Schwann Cell Apoptosis in High Glucose Media

Schwann cell survival was significantly improved by the addition of IGF-I, NAC, and DMD to the high glucose media. These molecules have been shown to rescue neurons both in vitro and in vivo following insults that induce apoptosis.

IGF-I prevents the apoptotic death of differentiated oligodendrocytes, pro-

oligodendrocytes, and type-I astrocytes during trophic withdrawal (S. Shankar,

personal communication) and neuronal cells (D'Mello et al., 1997). In addition,

IGF-I has been recently shown to prevent the high glucose induced apoptotic

death of cultured neuroblastoma cells (Gandhi et al., 1995; Cheng and Feldman,

1998). In neuroblastoma cells exposed to hyperosmotic concentrations of

mannitol, Bcl-2 levels were reduced approximately 4-fold (Singleton et al., 1996).

Treatment with IGF-I prevented this decrease via activation of the IGF-I receptor,

and prevented activation of caspase-3 (Singleton et al., 1996), suggesting that

IGF-I prevents the release of cytochrome c from mitochondria, which has been

shown to activate caspase-3 (Kluck et al., 1997).

NAC has been shown to prevent the apoptotic death of trophically

withdrawn, neuronally differentiated PC12 cells (Ferrari et al., 1995; Tatton et al.,

1997). Additionally, it has been shown that administration of NAC reduces the

decline in MNCV, and attenuates the increased myelin wrinkling and myelinated

fiber loss in STZ treated rats (Sagara et al., 1996). DMD, the active metabolite of

(-)-deprenyl, can prevent the apoptotic death of neuronal cells and

oligodendrocytes (Mytilineou et al., 1997; Tatton and Chalmers-Redman, 1996);

S. Shankar, personal communication). In the present study the co-administration

of IGF-I, NAC, or DMD simultaneously with 40 mM glucose reduced the amount

of Schwann cell death at 2 and 24 hr.

IV.e Mechanism of High Glucose Induced Apoptosis

The mechanism by which high glucose can induce the apoptotic death of cultured Schwann cells is unclear. The induction of Schwann cell apoptosis by high glucose is likely the direct result of the metabolism of D-glucose rather than the effects of hyperosmolarity. Use of similar concentrations of D-mannitol, L-glucose and sucrose (33 mM) in endothelial cells and smooth muscle cells in vitro (Graier et al., 1995), could not replicate the toxic actions of high D-glucose nor its effects on cell proliferation. Hyperosmotic conditions, induced by exposure to 300 mM of mannitol or 150 mM of glucose, or iso-osmotic high glucose conditions following exposure to 20 mM of glucose, were found to induce DNA fragmentation in neuroblastoma cells (Cheng and Feldman, 1998; Singleton et al., 1996). Schwann cells may share a capacity for volume regulation with central glia (Ballanyi and Grafe, 1988; Strange and Morrison, 1992) and thus may not be osmotically perturbed by 20-50 mM glucose media. Interestingly, studies on immortalized Schwann cells suggest that increased polyol formation could be used as a means of responding to hyperosmotic stress (Mizisin et al., 1996).

Tissues such as peripheral nerve, kidney, retina and lens, which have insulin-independent glucose uptake, tend to be sites of diabetic complications. It is believed that the major source of energy for the normal working peripheral nerve is glucose (Greene and Winegrad, 1979). It has been suggested that glucose reaches nerve axons via the Schwann cell, where uptake is facilitated by the glucose transporters GLUT1 and GLUT3 (Magnani et al., 1996). GLUT5 is

overexpressed by Schwann cells in the peripheral nerve of hyperglycemic streptozotocin-injected rats, and has been suggested as a possible trigger for diabetic neuropathy (Asada et al., 1998).

Glucose is primarily oxidized via the glycolytic pathway, but it can also be metabolized via the polyol pathway which is driven by the enzymes, aldose reductase and sorbitol dehydrogenase. Under normoglycemic conditions (3-6 mM) aldose reductase is relatively inactive. With uncontrolled hyperglycemia ($\geq$ 25 mM), aldose reductase can convert as much as one third of available glucose in the lens to sorbitol (Williamson et al., 1993), a sugar alcohol that is metabolized relatively slowly in cells. Sorbitol dehydrogenase converts sorbitol to fructose in a reaction which increases the cytosolic NADH + H^+/NAD ratio which in turn inhibits glycolysis by preventing the oxidation of glyceraldehyde-3-phosphate by GAPDH (Williamson et al., 1993). Interestingly, activity of aldose reductase did not increase in JS1 Schwann cells exposed to high glucose (Mizisin et al., 1996).

Since aldose reductase generates NADP+ in converting glucose to sorbitol, the NADPH + H^+/$NADP^+$ ratio is decreased and the supply of NADPH to such pathways as the glutathione redox cycle may be reduced (Asahina et al., 1995; Kashiwagi et al., 1994). This would in turn increase activity of the pentose phosphate pathway. Unfortunately, there does not appear to be any direct evidence as yet that cytosolic NADPH is decreased in diabetic tissue. However, the NADH + H^+/NAD^+ ratio does appear to be increased in diabetes and has been referred to as "hyperglycemic pseudohypoxia" (Williamson et al., 1993).

Free radicals (specifically $\bullet O_2-$) may be generated under conditions of increased NADH $+H^+/NAD^+$ through a mechanism involving the over-utilization of Complex II of the mitochondrial respiratory chain. The excess cytosolic NADH generated in glycolosis is re-oxidized to NAD^+ in the mitochondrial respiratory chain via the glycerol-3-P shuttle (Williamson et al., 1993). Excessive transfer of electrons through this complex, bypassing Complex I, has been shown to result in a 4-fold increase in the generation of $\bullet O_2-$ (Cortopassi and Wang, 1995). Alternatively, an overproduction of $\bullet O_2-$ may result from lowered cytosolic pH, which is observed during increased glycolytic activity (see Siesjo, 1988).

The involvement of oxidative radical formation is also inferred from the observation that the addition of exogenous SOD to endothelial cells treated with high glucose prevented their apoptotic death (Du et al., 1998). There is some evidence from experimental diabetic neuropathy that exogenous antioxidants may ameliorate early neurovascular dysfunction (Cameron et al., 1993).

In trophically withdrawn PC12 cells, the increase in intracellular oxidative radical levels occurs after the fall in $\Delta\Psi_M$ (Wadia et al., 1998) suggesting that in neuronal-type cells, oxidative radical formation occurs downstream, and perhaps only secondarily to, critical signaling events within the cell such as mitochondrial permeability transition. It is not known in Schwann cells exposed to high glucose, whether there is an increase in the production of oxidative radicals and if the increase precedes or follows changes in mitochondrial function. CMTMR (see below) could be combined with the fluorescent dye dyhydroethidium (DHE) which fluoresces only upon oxidation by $\bullet O_2-$ in mitochondria to construct a time

course of changes in $\Delta\Psi_M$ with respect to the production of oxidative radicals by mitochondria. This would help to determine whether the overproduction of oxidative radicals is a causitive signal or merely a consequence of mitochoondrial failure.

Another possible mechanism for high-glucose induced apoptosis in Schwann cells could involve the ligation of the Fas receptor. This receptor belongs to the TNF-α receptor family and when bound, by endogenous Fas ligand or by a ligating antibody, activates a specific signaling pathway leading to the apoptotic death of the cell. This apoptotic cascade involves the activation of specific interleukin-converting enzyme- (ICE) like proteases associated with the Fas receptor complex, and also caspase 3, prior to mitochondrial changes such as a drop in $\Delta\Psi_M$ (Enari et al., 1996). Activation of the Fas ligand apoptotic pathway is not inhibited by Bcl-2 (Memon et al., 1995; but see also Adachi et al., 1997) unlike other apoptotic processes that are more closely tied to early mitochondrial signaling events (Susin et al., 1996). Interestingly, there are several recent reports demonstrating that serum from diabetic patients with peripheral neuropathy can induce the apoptotic cell death of cultured adrenergic neuroblastoma cells, and that this cell death is mediated by the Fas pathway (Pittenger et al., 1997). Serum from diabetic patients also blocked immunocytochemical detection of Fas protein on the surface of cultured neuroblastoma cells. This would suggest that a circulating ligand or antibody may be present which could contribute to the development of peripheral neuropathy by activating apoptotic processes in certain populations of Schwann

cells. However, in the absence of any evidence concerning the expression of Fas or Fas receptor on or by Schwann cells, the involvement of this pathway in the present system cannot be determined.

IV.f NO Production by Schwann Cells Exposed to High Glucose

It is not known whether Schwann cells up-regulate the production of NO in response to high glucose either in vivo or in vitro. Others have shown that cultured Schwann cells increase NO production when exposed to a combination of TNF-α/IFN-γ (Gold et al., 1996), indicating the capacity to up-regulate NO synthesis in response to stimulation. Schwann cells were first exposed to increasing concentrations of the NO donor SNAP in order to determine if increased NO production reduced Schwann cell survival. There was a significant dose-dependent decrease in PD15 Schwann cell survival following 24 hr exposure to 1, 10, or 100 μM SNAP. This would suggest that if there is a local increase in NO production in the peripheral nerve of diabetic patients either by endothelial cells or by Schwann cells themselves, Schwann cells could potentially be damaged by this route.

In order to determine whether Schwann cells could upregulate NO in response to high glucose levels, the Griess reagent was used to determine the amount of secreted nitrite (NO_2) into the culture medium. In biological systems, NO_2 is readily oxidized to nitrate (NO_3). Therefore prior to determination of NO_2 levels in the culture medium, the existing NO_3 was reduced to NO_2 in the presence of nitrate reductase, NADPH and FAD. This provides a much more

accurate estimate of total NO production by the cells. A small increase from approximately 3.0 to 3.5 μM in NO_2 was observed in PD2 Schwann cells after 24 hr exposure to 40 mM. In PD15 Schwann cells, NO_2 release was increased approximately 2 fold (from 2.5 to 5 μM) (see Figure 14). It has been suggested that NO exerts direct signaling effects at concentrations below 10 μM. Indirect toxic effects, which depend on the formation of reactive intermediates (i.e. peroxynitrites), would result from exposure to concentrations of NO between 10-20 μM (Wink et al., 1996). It is not likely that the increase in NO_2 release to approximately 3.5 μM in PD2 Schwann cells in 40 mM glucose significantly contributed to the cell death observed. It is possible that the production of approximately 5 μM NO seen in PD15 Schwann cells, may mediate part of the high glucose induced cell death seen in this population given the decrease in survival seen with a similar concentration of SNAP.

An interaction between NO and GAPDH has been proposed as possibly being involved in apoptotic cell death. NO has been shown by several groups to inhibit the enzymatic activity of GAPDH (Itoga et al., 1997; Sirover, 1997). NO has also been shown to induce the nuclear translocation of GAPDH in fibroblasts and PC12 cells (Tatton, et al., personal communication). It was suggested that NO stimulates the binding of NAD^+ to GAPDH (Nomura et al., 1996). This interaction between NAD^+ and GAPDH may initiate the translocation of GAPDH to the nucleus. The small amount of NO produced by Schwann cells in high glucose may promote the interaction between NAD^+ and GAPDH, thereby initiating apoptosis.

NO has been shown to induce apoptosis in several systems. Isolated mitochondria from cultured thymocytes exposed to several different NO donors display swelling (detected by spectrophotometry) typical of mitochondria undergoing permeability transition, a reduction in $\Delta\Psi_M$, and induced nuclear DNA fragmentation (Hortelano et al., 1997). These changes were all prevented by CsA, suggesting that NO-induced apoptosis involves the PTP. Human neuroblastoma cells treated with a NO donor display increased caspase-3 activity concomitant with release of cytochrome c from the mitochondria into the cytosol (Uehara et al., 1999). In addition to disruptions of mitochondrial function via the PTP, NO may directly modify mitochondrial respiration at several sites in the respiratory chain. NO exposure can disrupt Complexes II, III, and IV of the respiratory chain (Bolanos et al., 1994) and activity of succinate dehydrogenase (Mitrovic et al., 1994). This occurs likely as a result of its conversion to $ONOO^-$ in the presence of $\bullet O_2^-$ (Bolanos et al., 1995).

Given the effects of NO on mitochondrial function, the relationship between NO inhibition and $\Delta\Psi_M$ in Schwann cells was examined. In PD2 Schwann cells, inhibition of NO production significantly prevented the high glucose induced drop in $\Delta\Psi_M$ by 12 hr, but not before; while L-NIL only slightly prevented the fall in $\Delta\Psi_M$ in PD15 Schwann cells even at 24 hr. This was unexpected given that PD15 Schwann cells showed a somewhat larger increase in NO production. One explanation may be that increased activity of cNOS contributed more to increased NO production than iNOS in the PD15 cells. Therefore any significant contribution NO might make to $\Delta\Psi_M$ in PD15 cells would

be more likely to be blocked by SMTC or other inhibitors of cNOS. These data are intriguing in that one may speculate as to whether NO regulation differs between myelinating and non-myelinating (or proliferating and non-proliferating) Schwann cells depending on the developmental age of the cell or during their response to (hyperglycemic) injury.

IV.g Production of TNF-α in Schwann Cells Exposed to High Glucose

Schwann cells upregulate expression of TNF-α and IL-6 in response to sciatic nerve crush (Wagner and Myers, 1996; Bolin et al., 1995); each of which may induce activation of Schwann cell iNOS through an autocrine mechanism. Bolin and co-workers showed that stimulation of Schwann cells with TNF-α, LPS, IL-1, IL-6, or with trophic withdrawal induced up-regulation of the IL-6 receptor (Bolin et al., 1995). In addition, STZ-treated diabetic rats show an increased production of TNF-α in response to treatment with LPS compared to non-diabetic rats (Tanaka et al., 1992). In order to determine whether isolated Schwann cells in vitro increased NO production via increased TNF, PD2 cells were exposed to a combination of TNF-α/IFN-γ and NO production measured via the Griess reagent assay. There was a significant dose-dependent increase in the amount of NO_2 detected following exposure to 50, 100, 250, or 500 U TNF-α/IFN-γ for 24 hr, which was inhibited dose-dependently by treatment with the iNOS inhibitor L-NIL (see Figure 16). This confirms the finding of Gold et al. (1996) who demonstrated increased NO_2 release by Schwann cells following exposure to 100 U TNF-α/IFN-γ.

Using a rat TNF-α ELISA kit, it was then determined whether Schwann cells exposed to high glucose increased production of TNF-α. There was a small but significant decrease in the amount of total TNF-α released by PD2 Schwann cells exposed to 40 mM glucose for 24 hr. The amount of TNF-α detected, however, was not normalized to total protein, nor was it corrected for cell number. However, this assay measures the total amount of protein secreted into the culture medium during the particular time period, and assuming that free TNF-α remains stable during the 24 hr period examined here the observed decrease is likely valid. The implications of reduced TNF-α levels in the peripheral nerve of diabetics are not clear. Part of the Schwann cell response to injury is the up-regulation and secretion of TNF-α along with IL-1 for macrophage recruitment to the injury zone (Wagner and Myers, 1996). The attenuation of this response would result in reduced macrophage involvement and somewhat compromised Wallerian degeneration and subsequent regeneration. Interestingly, Wallerian degeneration has been reported to be decreased in DPN (Kamijo et al., 1996).

IV.h Reduction in $\Delta\Psi_M$ in Schwann Cells Exposed to High Glucose

Given the close association between glucose metabolism and mitochondrial function, it is reasonable to expect that mitochondrial function may be perturbed in a disease characterized by abnormal carbohydrate metabolism. This is particularly true in insulin-independent cells like Schwann cells in which a large amount of glucose can be transported during periods of hyperglycemia.

High glucose induced a significant decline in $\Delta\Psi_M$ within 2-6 hrs of exposure to high glucose (see Figures 19 & 20). Consistent with estimates of cell death obtained by counts of intact nuclei and ISEL positive Schwann cells, the reduction in $\Delta\Psi_M$ was considerably larger in PD2 Schwann cells, decreasing by approximately 35% by 2 hr exposure to high glucose, compared to a drop of approximately 11% in PD15 Schwann cells during the same period of time. By 24 hr following exposure to high glucose, however, both populations showed an approximate 46-48% decrease in CMTMR fluorescence intensity. A recent report has noted that freshly isolated dorsal root ganglion neurons from STZ treated rats showed a marked reduction in baseline $\Delta\Psi_M$ compared to normal rats, and a potentiated decrease, and delayed recovery, of $\Delta\Psi_M$ in response to glutamate challenge (Srinivasan and Wiley, 1997). The reduction in $\Delta\Psi_M$ invoked by high glucose in cultured neuroblastoma cells and primary DRG neurons was prevented by treatment with IGF-I (Russell et al., 1998).

In this study, DMD, NAC and IGF-1 were all able to prevent the drop in CMTMR fluorescence intensity, returning $\Delta\Psi_M$ to near-control levels. (-)-Deprenyl, the parent molecule of DMD has been shown to reduce the apoptotic death of neuronal and non-neuronal cells (Paterson et al., 1998; Tatton et al., 1994; Wadia et al., 1998; Wu et al., 1995; S. Shankar, personal communication). In PD2 or PD15 Schwann cells, the addition of DMD, NAC, or IGF-I to high glucose media prevented the shift to the left of the distribution of CMTMR intensity. It has been postulated that (-)deprenyl and its metabolite DMD reduce apoptosis by the induction of protective genes such as sod 1 & 2, bcl-2 and bcl-

X_L (Li et al., 1997; and see Tatton and Chalmers-Redman, 1996 for review). It has also been shown in the PC12 cell system that the administration of NAC is protective for trophically withdrawn PC12 cells, and induces similar gene changes as DMD (Tatton et al., 1997). DMD improved cell survival in both Schwann cell populations after 2 hr exposure to 40 mM glucose. Wadia et al. (1998) reported that (-)-deprenyl significantly prevented the drop in $\Delta\Psi_M$ at 3 hr following serum and NGF withdrawal. The maintenance of $\Delta\Psi_M$ in PC12 cells by (-)-deprenyl seen at 3 hr coupled with the improvement of Schwann cell survival seen at 2 hr suggests that this agent may directly affect mitochondrial function independently of its ability to influence 'anti-apoptotic' protein synthesis (Tatton, 1994).

The mechanism of high glucose induced disruption of $\Delta\Psi_M$ could be due to a number of factors. High glucose conditions may lead to the development of pseudohypoxic conditions within the cell. Pseudohypoxia can be created within cells that have increased NADH/NAD$^+$ ratios (Williamson et al., 1993) under conditions of increased glycolysis as has been reported in the endoneurium of diabetic rats (Williamson et al., 1993). The NADH/NAD$^+$ ratio is coupled to glycolysis and can be influenced by a number of separate pathways. The increased oxidation of sorbitol to fructose, which is coupled to the reduction of NAD$^+$ to NADH in cells with up-regulated aldose reductase activity, can increase the intracellular ratio of NADH/NAD$^+$. This pathway has been implicated in Schwann cell dysfunction in diabetic nerve due to the localization of aldose reductase in Schwann cells. However, evidence for this mechanism is somewhat

controversial. Aldose reductase activity in JS1 Schwann cells exposed to high glucose was no different from cells exposed to normal glucose, and the levels of sorbitol were the same (Mizisin et al., 1996).

Alternatively, excess cytosolic NADH in high glucose conditions can be re-oxidized to NAD^+ via the glycerol 3-phosphate shuttle which transfers reducing equivalents to the respiratory chain via Complex II. The capacity of cells to oxidize excess NADH by this shuttle or by lactate deydrogenase which converts pyruvate to lactate, is limited and may not be able to sufficiently oxidize all of the NADH resulting in an increased $NADH/NAD^+$ ratio. Consequently, as a result of an increased $NADH/NAD^+$ ratio, leading to pseudohypoxia, increased free-radical production may occur, specifically $\bullet O_2^-$. Increased $\bullet O_2^-$ production has been reported in cultured endothelial cells in hypoxic conditions (Ratych et al., 1987). This radical can react with NO to form $ONOO^-$, or be metabolized further to form H_2O_2 or hydroxyl radical. Additionally, the increased activity of the glycerol 3-phosphate shuttle during oxidation of NADH to NAD^+ in mitochondria can favor the production of $\bullet O_2^-$ at the Complex II site in the respiratory chain.

Enhanced production of oxidative radicals are associated with reduction of $\Delta\Psi_M$ and opening of the PTP. However, some controversy exists concerning the causative role that they play versus indirect signaling functions. Exogenous H_2O_2 has been shown to reduce $\Delta\Psi_M$ and cell survival in cultured PC12 cells (Chalmers-Redman et al., personal communication). But, in serum- and NGF-withdrawn PC12 cells, the increase in intracellular peroxide levels measured by DCF fluorescence was preceded by a drop in $\Delta\Psi_M$ (Wadia et al., 1998). The

generation of reactive oxygen species has been demonstrated as a secondary event following induction of mitochondrial permeability transition in other in vitro models as well (Marchetti et al., 1996). It has not yet been determined if there is an increase in intracellular free-radical levels in Schwann cells exposed to high glucose and whether this increase would precede or follow the observed reduction in $\Delta\Psi_M$.

The use of CMTMR and similar lipophilic dyes that sequester in mitochondria with respect to $\Delta\Psi_M$ has been criticized recently due to potential artifacts (Green and Reed, 1998). This is based in part on the recent observation that the dye rhodamine 123 (Rh123) can potentially indicate mitochondrial hyperpolarization (i.e. an increase in $\Delta\Psi_M$). In a comparison of four $\Delta\Psi_M$-dependent fluorochromes and two $\Delta\Psi_M$-independent dyes that provide a measure of mitochondrial mass, Metivier and colleagues (Metivier et al., 1998) observed that following ligation of the FAS receptor, $\Delta\Psi_M$ appeared to increase when measured with Rh123 compared to a significant decrease observed with $DiOC_6$, CMXRos, and TMRM. The difference was not due to changes in mitochondrial volume as MitoTracker Green (MTG) or nonyl acridine orange (NAO) which stain mitochondria independent of $\Delta\Psi_M$ did not change following induction of apoptosis. It was also observed that there was no correlation between Rh123 concentration and its fluorescence (Metivier et al., 1998), suggesting that Rh123 may interact with mitochondria due to non-specific lipid interactions. No such artifacts have been reported for CMXRos, which showed significant reductions in fluorescence following FAS ligation or treatment with the

protonophore CCCP, which dissipates $\Delta\Psi_M$; and the absence of concentration-dependent autoquenching (Metivier et al., 1998). The aldehyde fixable dye CMXRos incorporates into mitochondria linearly with respect to $\Delta\Psi_M$ (Macho et al., 1996; Poot et al., 1996; Poot et al., 1997) and is essentially identical in structure to the dye employed here (CMTMR) except that it emits at a slightly longer wavelength.

IV.i The Mitochondrial PTP and High Glucose Induced Apoptosis

The association between $\Delta\Psi_M$ and the PTP is well established, and it has been found that opening of the PTP causes a near-simultaneous collapse of $\Delta\Psi_M$ (Zamzami et al., 1996). Given the role of hexokinase in glucose metabolism this protein may provide a link, via the PTP, between high glucose induced disruption of $\Delta\Psi_M$ and the apoptotic death of Schwann cells.

Hexokinase drives the initial step in the metabolism of glucose, phosphorylating glucose to glucose-6-phosphate. Current evidence from studies of isolated mitochondria suggests that hexokinase binding to mitochondria and the activity of this enzyme are dependent upon the maintenance of $\Delta\Psi_M$ (see Gerbitz et al., 1996). The activity of HK-I has been shown to increase 5- to 10-fold upon binding to mitochondria (Weiler et al., 1985). Its putative involvement in apoptotic cell death arises from the recent identification of the binding sites for HK on mitochondria: the ANT, VDAC, and peripheral benzodiazepine receptor. These proteins have been identified as components of the mitochondrial PTP (Zoratti and Szabo, 1995). The function of the PTP under normal conditions is

not yet completely understood. It is believed to be a dynamic structure that participates in the maintenance of ionic homeostasis (Gunter and Pfeiffer, 1990) between the mitochondrial matrix and the intermembrane space, opening and closing in response to changes in intracellular or matrix Ca^{++} concentrations. It has also been shown to be the site of $\Delta\Psi_M$ -dependent protein transport into the mitochondrion (Nicolay et al., 1990; Pfanner et al., 1990).

The mechanism of high glucose induced reduction of $\Delta\Psi_M$ in cultured Schwann cells appears to involve the regulation of the mitochondrial PTP (see below). In Schwann cells exposed to normal and high glucose, regression analysis suggested that HK-I immunofluorescence varied linearly with $\Delta\Psi_M$ (see Figure 28). Populations of mitochondria within individual cells that display bright CMTMR fluorescence also show bright HK-I immunoreactivity. However, in Schwann cells exposed to 40 mM glucose for 6 hr, in which $\Delta\Psi_M$ is lowered, there is a marked reduction in mitochondrial HK-I immunofluorescence, and a change in the relationship between $\Delta\Psi_M$ and HK binding. The addition of atractyloside, a ligand of the ANT which opens the PTP (Marchetti et al., 1996) to cells grown in normal glucose elicited a similar shift to the left in CMTMR intensity. The relationship between $\Delta\Psi_M$ and HK binding to mitochondria was similarly altered by atractyloside (see Figure 28). This suggests that 1) a similar mechanism mediates the high glucose and atractyloside induced dissipation of $\Delta\Psi_M$, and 2) that localization of HK to mitochondria with respect to $\Delta\Psi_M$ may provide evidence concerning the state of individual PTP's.

The binding and activity of HK-I to mitochondria and specifically, PTP

sites, in isolated mitochondria, is related to the frequency of contact sites between the inner and outer mitochondrial membrane (Wicker et al., 1993). In mitochondria without contact sites, the frequency of binding of HK-I was not different from that of spontaneous binding to isolated outer mitochondrial membrane. If the contact sites between the inner and outer mitochondrial membrane represent the PTP in a closed conformation (Beutner et al., 1996), then HK binding to mitochondria could be used to estimate contact site frequency, and thus PTP closure.

It follows that co-localization of HK-I immunoreactivity with both $\Delta\Psi_M$ - dependent and -independent mitochondrial markers (CMTMR and anti-biotin antibody respectively), determined by high resolution confocal imaging, may provide a measurable estimate of PTP formation in mitochondria, or more importantly sub-populations of mitochondria, in whole cells. In this regard, it is possible that subtle changes in CMTMR or immunofluorescence levels in small populations of mitochondria within a single cell may be overlooked using whole-cell fluorescence or isolated and pooled mitochondria. It would therefore be extremely beneficial to combine the dual labeling techniques employed here with deconvolution image analysis to visualize the distribution of HK on the surface of mitochondria in high power images with relation to immunoreactivity of other members of the PTP complex such as Bax or the ANT.

The data presented here represent the first demonstration of differential binding of HK-I to mitochondria with respect to $\Delta\Psi_M$ in intact cells. Further, the demonstration that this binding shift was in response to treatment with high

glucose suggests a possible regulatory role of HK in PTP formation. This is consistent with recent in vitro evidence in artificial PTP complexes made up of HK, the VDAC, and the ANT (Beutner et al., 1996). ATP-loaded vesicles constructed with HK-VDAC-ANT complexes exposed to ATR or Ca^{++} released ATP indicating functional complexes that resembled the PTP. CsA and the non-immunosuppressive CsA derivative N-methyl-Val-4-cyclosporin inhibited the ATP release. Further, the addition of physiological concentrations of glucose (5 mM) to the preparation prevented spontaneous ATP release suggesting that regulation of the PTP may be related to HK activity.

In most tissues, HK activity is regulated by a feedback inhibition mechanism whereby its reaction product, glucose-6-phosphate, solubilizes HK from its binding site on mitochondria (Sui and Wilson, 1997; Kabir and Wilson, 1994), subsequently inhibiting HK activity. The consequences of this are small under normal conditions, serving as one of the regulatory sites for glycolosis. However, under hyperglycemic conditions, the excessive phosphorylation of glucose may lead to an accumulation of glucose-6-phosphate, and a large increase in the amount of soluble HK. This may be especially true for cells that do not require insulin for glucose uptake, such as Schwann cells.

The absence of HK from artificial PTP complexes in vitro resulted in the release of ATP (Beutner et al., 1996) that had been loaded into vesicles as a marker of PTP opening, suggesting that bound HK may facilitate the closure of the PTP. The glucose analogue, 3-O-methyl-glucose, which is phosphorylated by HK but not further metabolized by cells, caused the apoptotic death of

cultured endothelial cells (Du et al., 1998) and reduced the amount of mitochondrial-bound HK in smooth muscle cells (Lynch et al., 1996). Assuming that phosphorylated 3-O-methyl-glucose similarly inhibits and solubilizes HK as does glucose-6-phosphate, this finding suggests that excessive release of HK from its PTP binding sites may alter the conformation of the PTP favoring the open state. Further, incubation of primary astrocytes with 2-deoxyglucose which leads to an increase in intracellular glucose-6-phosphate, also reduced the binding of HK to mitochondria (Lynch et al., 1991). Similarly, a reduction in HK binding to the PTP may be responsible for the apoptotic death of cultured Schwann cells exposed to high glucose.

If high glucose induced Schwann cell apoptosis and reduction in $\Delta\Psi_M$ involves the PTP, then an agent that prevents PTP opening should improve Schwann cell survival and maintain $\Delta\Psi_M$ in high glucose. The addition of CsA, has been shown to facilitate the closure of the PTP (Bernardi, 1996; Zamzami et al., 1996). This may occur via binding to mitochondrial cyclophilin (Petronilli et al., 1994) and thus preventing the reduction in $\Delta\Psi_M$ induced by high glucose (see Figures 30 & 31). In both PD2 and PD15 Schwann cells, CsA maintained $\Delta\Psi_M$ at or near control levels at all time points examined between 2-24 hr. Additionally, in PD15 Schwann cells exposed to 40 mM glucose for 24 hr, the addition of CsA prevented approximately 50% of the cell death (see Figure 29).

The capacity of CsA to inhibit PTP-dependent dissipation of $\Delta\Psi_M$, and thus apoptosis is well documented. Zamzami et al. showed that CsA and a non-immunosuppressive analogue dose-dependently inhibited mitochondrial

permeability transition and the collapse of $\Delta\Psi_M$ in splenocytes of dexamethasone treated mice (Zamzami et al., 1996). CsA has been shown to reduce the ability of mitochondrially-released factors (e.g. AIF) to induce DNA fragmentation in isolated nuclei (Petit et al., 1998), and the large amplitude swelling indicative of permeability transition in mitochondria treated with NO donors (Hortelano et al., 1997). The protective effects of CsA coupled with the $\Delta\Psi_M$ -dependent regulation of HK binding to mitochondria in high glucose or atractyloside suggested that high glucose induced apoptosis of Schwann cells is mediated in part by a disruption in the regulation of the PTP.

IV.j Sub-Cellular Localization of Apoptosis-Related Proteins Bax and HK

Western blots of enriched sub-cellular fractions were probed with an antibody raised against HK in order to confirm the reduction in HK binding to mitochondria seen with confocal imaging. In addition, movement of the pro-apoptotic protein Bax was examined to determine if high glucose induced apoptosis was accompanied by movement of Bax between different cellular compartments. Overall, a time-dependent reduction in total HK protein levels between 2-24 hr in PD2 Schwann cells exposed to 40 mM glucose. There was a particular reduction in the amount of HK present in the mitochondrial fraction, and a progressive increase between 2-24 hr in cytoplasmic HK in cells exposed to 40 mM glucose. This was accompanied by an up-regulation of Bax protein levels in the mitochondrial fraction of Schwann cells exposed to high glucose for 24 hr.

The reduction in HK protein in the mitochondrially-enriched fraction of

Schwann cells supports the metabolic regulation of HK localization suggested by Lynch et al. (Lynch et al., 1991; Lynch et al., 1996). These authors demonstrated that a specific increase in intracellular glucose-6-phosphate reduced the amount of HK that was bound to mitochondria, and that incubation with 3-O-methyl-glucose also reduced mitochondrial HK. This particular glucose analogue is phosphorylated by HK but not further metabolized by the cell (Du et al., 1998). Therefore, it is possible that there was a similar reduction in mitochondrial bound HK in the endothelial cells causing a conformational change in the PTP favoring the open state.

The impact of localization of HK to the PTP on mitochondrial function and survival has recently been demonstrated in intact cells. The anti-cancer agents lonidamine, clotrimazole and bifonazole, each of which prevent binding of HK to mitochondria, have been shown to reduce $\Delta\Psi_M$ (Pulselli et al., 1996) and cell viability (Penso and Beitner, 1998) in tumor cells. Thus, in Schwann cells exposed to high glucose, excess phosphorylation of glucose by hexokinase may lead to an accumulation of glucose-6-phosphate within the cell resulting in a feedback inhibition and release of HK from its binding site at the mitochondrial PTP. This release is followed by a conformational change in the PTP favoring the open state, resulting in a collapse of $\Delta\Psi_M$ and induction of apoptosis.

The re-distribution of Bax from the cytosol to the mitochondria during the early stages of apoptotic cell death has been shown in a number of systems as demonstrated by confocal imaging of GFP-fusion proteins of Bax, Bcl-2, and Bcl-X_L (Wolter et al., 1997) or western blot analysis of sub-cellular fractions (Hsu et

al., 1997). Thymocytes treated with dexamethasone or γ-irradiation, or HL-60 cells treated with staurosporine each showed a significant increase in the amount of Bax localized in mitochondria within 2 hr of insult, with a concomitant reduction in the amount of Bax in the cytosolic fraction (Hsu et al., 1997). It is interesting to note that levels of the anti-apoptotic protein Bcl-X_L was also seen to increase in the mitochondrial fraction along with Bax. GFP-Bax was shown to have a diffuse distribution throughout the cytosol, whereas GFP-Bcl-2 and GFP-Bcl-X_L had a punctate co-localization with mitochondria visualized with a variant of CMTMR (Wolter et al., 1997). Following induction of apoptotic cell death with staurosporine, the GFP-Bax fusion protein re-distributed from the cytosol to mitochondria within 30 min, preceding chromatin condensation and other morphological signs of apoptosis. However, these authors neglected to relate the re-distribution of Bax to the mitochondria with CMXRos fluorescence intensity, which also varies with respect to $\Delta\Psi_M$. This would have allowed them to reconstruct the time course of critical mitochondrial changes early on in the apoptotic cascade with regards to the Bax induced collapse of $\Delta\Psi_M$.

The targeting of Bax to the mitochondria appears to depend upon the presence of an apoptotic trigger that signals its re-distribution. The transmembrane insertion domain of Bax, which anchors the protein to mitochondria, is located at the COOH terminus (Zamzami et al., 1998). Goping et al. (1998) identified a region at the NH$_2$-terminal of Bax that actively inhibits the transmembrane anchor region, thereby preventing insertion into mitochondria. Upon induction of apoptosis, the inhibitory function of the NH$_2$-terminal domain is

suppressed. The antagonistic interaction between the NH_2- and COOH-terminal regions of Bax is specific. The NH_2-terminal domain was unable to prevent mitochondrial insertion of a mutant Bax protein in which the native transmembrane insertion domain had been replaced by the insertion domain of Bcl-2 (Goping et al., 1998).

Paradoxically, in a cell-free system of apoptosis in which an apoptosis-inducing cytosolic extract was added to isolated mitochondria containing full-length Bax or mutant Bax lacking the NH_2-terminal inhibitory domain, addition of the extract did not induce insertion of the truncated Bax but did induce insertion of full-length Bax (Goping et al., 1998). This suggests that a specific interaction between certain components present in the apoptosis-inducing extract and the NH_2-terminal domain is required for the activation of the mitochondrial insertion domain of Bax. The lower bands observed in the cytosolic fraction of Schwann cells (see Figure 33) may correspond to a truncated isoform of Bax that will not be targeted to the mitochondria.

The question of the nature of Bax-induced mitochondrial alterations has suggested a specific interaction between Bax and the PTP. However, some authors have proposed an alternative specific action of Bax that is independent of the PTP. Bax has been shown to co-immunoprecipitate with other components of the PTP; specifically: the ANT in rat brain mitochondria (Marzo et al., 1998), isolated liver mitochondria and artificial PTP complexes (Marzo et al., 1998), and with porin in isolated liver mitochondria (Narita et al., 1998). These interactions induced CsA-inhibitable $\Delta\Psi_M$ collapse, cytochrome c release, and

mitochondrial swelling (Jurgensmeier et al., 1998; Marzo et al., 1998; Narita et al., 1998; Pastorino et al., 1998) indicative of a functional interaction between Bax and the PTP. A PTP independent action of Bax was proposed by Eskes et al. (Eskes et al., 1998) who demonstrated a specific Bax-induced release of cytochrome c from mitochondria in intact cells that was not inhibited by CsA, bongkrekic acid, ADP, or the Ca^{++} chelator EGTA, each of which have been shown to prevent opening of the PTP. Interestingly, the presence of Mg^{2+} ions, which are known to promote binding of HK to mitochondria (Borrebaek and Haviken, 1985) and inhibit opening of the PTP (Zoratti and Szabo, 1995), potentiated the Bax-induced cytochrome c release, further suggesting an alternative PTP-independent mode of action for Bax.

V. Conclusions

The present study provides the first in vitro demonstration of the direct toxicity of high glucose to Schwann cells. It was shown that:

1. high glucose elicited a dose-dependent reduction of PD2 and PD15 Schwann cell survival between 2 and 48 hr; and, using 2 independent markers of apoptosis (ISEL and YOYO-1 staining of fragmented DNA and condensed chromatin), that the mode of this cell death was apoptosis,

2. the anti-apoptotic compounds NAC, IGF-I, and DMD improved the survival of Schwann cells when simultaneously added with 40 mM glucose at 2 and 24 hr, suggesting that a proportion of the death observed at 2 hr was apoptotic, which either preceded or did not require oligonucleosomal DNA fragmentation,

3. the high glucose induced Schwann cell apoptosis was associated with a small production of NO in PD2 Schwann cells, and a slightly greater increase in PD15 cells. It remains to be determined whether the observed increase in NO in PD15 Schwann cells reflects an induction of NO production that is toxic,

4. $\Delta\Psi_M$ is significantly reduced by 2 hr in PD2 Schwann cells exposed to 40 mM glucose, and that this reduction is prevented by the addition of IGF-I, NAC, DMD. A smaller, but significant decrease in $\Delta\Psi_M$ was also observed in PD15 Schwann cells exposed to 40 mM glucose at 2hr,

5. using high resolution confocal imaging, the glycolytic enzyme hexokinase (Type I) was shown to co-localize with mitochondria in Schwann cells, varying linearly with $\Delta\Psi_M$. The linear relationship between mitochondrial bound

hexokinase and $\Delta\Psi_M$ was decreased in Schwann cells exposed to high glucose or the PTP opening agent atractyloside, indicated by a reduction in mitochondrial HK immunofluorescence. This suggested an involvement of the PTP. This was further confirmed by the prevention of the high glucose induced drop in $\Delta\Psi_M$ by the PTP closing agent cyclosporin A,

6. the change in mitochondrial bound hexokinase was confirmed by western blot analysis of enriched sub-cellular fractions which suggested that hexokinase protein levels were reduced in the mitochondrial fraction. Levels of the pro-apoptotic protein Bax were increased in the mitochondrial fraction in high glucose.

The demonstration of high glucose induced Schwann cell death in vitro prompts a re-evaluation of the current theories of the pathogenesis of DPN. Specifically, given the importance of Schwann cells in virtually all of the pathological and functional abnormalities associated with DPN (e.g. nerve conduction abnormalities, segmental demyelination, reduction in axonal caliber and transport, and impaired regeneration), hyperglycemia-induced Schwann cell apoptosis cannot be discounted. Moreover, if it should be demonstrated that Schwann cell apoptosis is present in human DPN, a therapeutic opportunity may be available to specifically improve Schwann cell survival independently of, or in combination with other therapies aimed at restoring the deficits in carbohydrate metabolism associated with diabetes mellitus.

VI. Future Directions

To further explore the mechanism of high glucose induced Schwann cell apoptosis, I believe that the involvement of the mitochondria, and specifically the PTP, needs to be more completely characterized. The combination of confocal imaging with western blots of sub-cellular fractions is an extremely valuable and powerful tool for examining the movement of proteins between cellular compartments. However, given the amount of protein required for the isolation of enriched nuclear, cytosolic, and particularly mitochondrial fractions, the use of primary rat Schwann cell cultures is not practical. These cultures, including PD15 Schwann cells, typically do not yield tremendous amounts of cells; therefore it may be necessary to establish an immortalized Schwann cell line to provide the tissue needed. In this case, it would need to be established that the immortalized Schwann cells responded to high glucose as the primary cells do.

In addition to whole-cell experiments, it would also be useful to utilize in vitro preparations of isolated mitochondria to characterize the dynamics of HK and Bax binding to the PTP with respect to $\Delta\Psi_M$ in the presence of glucose metabolites or ligands of the PTP such as CsA or ATR. These experiments would add the ability to directly monitor the initiation of permeability transition with respect to $\Delta\Psi_M$ using methods such as spectophotometric analysis of mitochondrial mass or the exchange of certain fluorophores that partition across the inner mitochondrial membrane according to the state of the PTP. It is also necessary to extend these findings to an in vivo model of DPN. Specifically, whether significant Schwann cell apoptosis exists and whether certain anti-

apoptotic agents can attenuate or prevent altogether the pathological and functional deficits seen.

Cy Dyes Emmision Spectra

Cy5
Ex. 650
Em. 670

Jackson ImmunoResearch
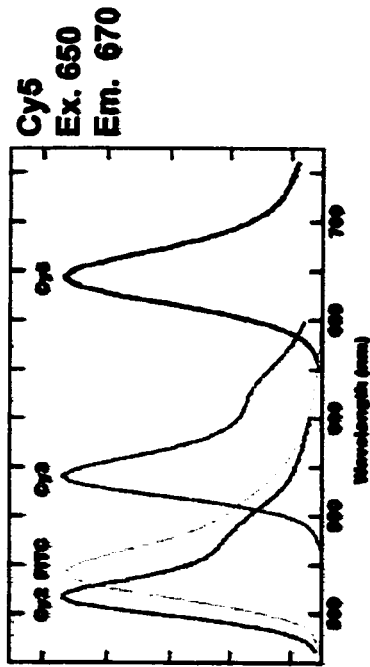
YOYO-1 Spectra
491 509
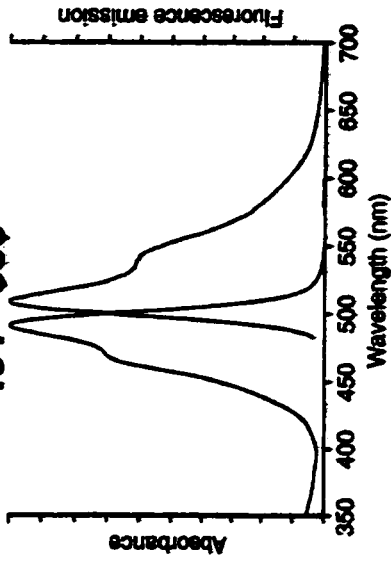
Molecular Probes

CMTMR Spectra
554 576

Appendix A.

193
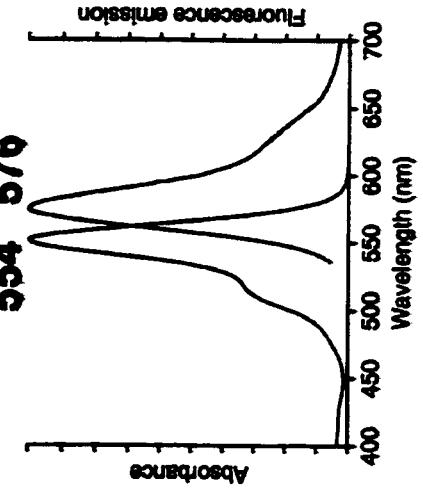
Appendix B.

Table 4. Statistical Testing of Glucose Dose Response Counts

PD2	2 hr	12 hr	24 hr	48 hr
17.5 mM	-2.85; p<0.01	-4.44; p<0.001	-4.23; p<0.001	-3.79; p<0.001
30 mM	-4.05; p<0.001	-4.51; p<0.001	-4.42; p<0.001	-3.79; p<0.001
40 mM	-4.00; p<0.001	-4.51; p<0.001	-4.42; p<0.001	-3.79; p<0.001
50 mM	-4.35; p<0.001	-4.42; p<0.001	-4.34; p<0.001	-3.79; p<0.001

PD15	2 hr	12 hr	24 hr	48 hr
17.5 mM	-1.94; p=0.056	-4.51; p<0.001	-4.23; p<0.001	-4.42; p<0.001
30 mM	-2.88; p<0.01	-4.51; p<0.001	-4.50; p<0.001	-4.51; p<0.001
40 mM	-2.26; p<0.05	-4.37; p<0.001	-4.50; p<0.001	-4.51; p<0.001
50 mM	-2.85; p<0.01	-4.51; p<0.001	-4.51; p<0.001	-4.51; p<0.001

** Mann-Whitney U (Z statistic) vs. 5.5 mM

Table 5. Statistical Testing of ISEL Counts

PD2	2 hr	12 hr	24 hr
17.5 mM	-0.936; p=0.35	-6.50; p<0.001	-5.80; p<0.001
40 mM	-0.981; p=0.36	-6.68; p<0.001	-6.82; p<0.001

PD15	2 hr	12 hr	24 hr
17.5 mM	-0.228; p=0.82	-5.27; p<0.001	-3.62; p<0.001
40 mM	-0.253; p=0.80	-6.73; p<0.001	-6.67; p<0.001

** Mann-Whitney U (Z statistic) vs. 5.5 mM

Table 6. Statistical Testing of Anti-Apoptotic Rescue Counts

PD2	2 hr	24 hr
40 mM	-2.93; p<0.01	-2.92; p<0.01
40+IGF	-2.84; p<0.01	-2.90; p<0.01
40+NAC	-2.77; p<0.01	-2.90; p<0.01
40+DMD	-2.92; p<0.01	-2.90; p<0.01

PD15	2 hr	24 hr
40 mM	-2.70; p<0.01	-2.91; p<0.01
40+IGF	-2.32; p<0.05	-2.92; p<0.01
40+NAC	-0.66; p=0.537	-2.91; p<0.01
40+DMD	-2.91; p<0.01	-2.91; p<0.01

** Mann-Whitney U
(Z statistic)
40 mM vs. 5.5 mM
40 mM+Drug vs. 40 mM

Table 7. Statistical Testing of Schwann Cell Survival With NO

PD15	24 hr
SNAP-1	-2.74; p<0.01
SNAP-10	-2.74; p<0.01
SNAP-100	-2.74; p<0.01

** Mann-Whitney U (Z statistic) vs. 5.5 mM

Table 8. Statistical Testing of NO Production by Schwann Cells

	PD2-24hr	PD15-24 hr
40 mM	-2.5; p<0.01	-5.4; p<0.001
40+DMD	-0.98; p>0.05	-2.8; p<0.01
40+NIL	-2.9; p<0.01	-2.4; p<0.01
40+SMTC	-2.9; p<0.01	-2.3; p<0.01

** Mann-Whitney U (Z statistic)
40 mM vs. 5.5 mM
DMD, NIL, SMTC vs. 40 mM alone

Table 9. Statistical Testing of NO Inhibition and Schwann Cell Survival

PD2	24 hr
40 mM	-2.89; p<0.01
40+NIL	-2.25; p<0.05
40+SMTC	0.0; p=1.00

** Mann-Whitney U
(Z statistic)
40 mM vs. 5.5 mM
NIL, SMTC vs. 40 mM

Table 10. Statistical Testing of NO Production with TNF-α/IFN-γ

PD2	24 hr
T/I-50	-2.88; p<0.01
T/I-100	-2.88; p<0.01
T/I-250	-2.88; p<0.01
T/I-500	-2.88; p<0.01
T/I+NIL4	-2.56; p<0.05
T/I+NIL6	-2.56; p<0.05

** Mann-Whitney U (Z statistic)
T/I vs. 5.5 mM
NIL vs. T/I-250

Table 11. Statistical Testing of TNF-α Production in High Glucose

PD2	24 hr
40 mM	-1.96; p<0.05
40+DMD	-.66; p=0.51
NG-S1	-1.96; p<0.05
NG-S10	-1.77; p=0.08
NG-S100	-1.33; p=0.18
HG-S1	-0.22; p=0.827
HG-S10	-1.96; p<0.05

** Mann-Whitney U (Z statistic)
40 mM vs. 5.5 mM; DMD vs. 40 mM alone
NG (5.5 mM) SNAP vs. HG (40 mM) SNAP

Table 12. Statistical Testing of High Glucose Induced Changes in $\Delta\Psi_M$

PD2	2 hr	6 hr	24 hr
40 mM	-30.07; p<0.001	-25.94; p<0.001	-31.28; p<0.001

PD15	2 hr	6 hr	24 hr
40 mM	-8.77; p<0.001	-21.40; p<0.001	-31.01; p<0.001

** Mann-Whitney U (Z statistic); 40 mM vs. 5.5 mM

Table 13. Statistical Testing of Maintenance of $\Delta\Psi_M$ by IGF-I, NAC, & DMD

PD2	2 hr	6 hr	12 hr	24 hr
40+IGF-I	-14.9; p<0.001	-22.9; p<0.001	Nd	nd
40+NAC	-9.2; p<0.001	-13.4; p<0.001	-21.3; p<0.001	-28.1; p<0.001
40+DMD	nd	-16.2; p<0.001	Nd	nd

** Mann-Whitney U (Z statistic) vs. 40 mM alone
IGF-I, NAC, DMD vs. 40 mM alone
** nd = not done

Table 14. Statistical Testing of Maintenance of $\Delta\Psi_M$ by L-NIL

	2 hr	6 hr	12 hr	24 hr
PD2-NIL	-0.95; p=0.92	-6.6; p<0.001	-18.8; p<0.001	nd
PD15-NIL	-5.1; p<0.001	Nd	nd	-3.9; p<0.001

** Mann-Whitney U (Z statistic) vs. 40 mM alone
** nd = not done
** p values in bold type denote non-significant results

Table 15. Statistical Testing of $\Delta\Psi_M$ and HK Distributions

PD2	6 hr
40 mM	-17.07; p<0.001
ATR	-18.36; p<0.001

** Mann-Whitney U (Z statistic) vs. 5.5 mM

Table 16. Regression Analysis of $\Delta\Psi_M$/HK Relationship

Y = A + B(X)
A. 5.5 mM; ANOVA, F = 128.4, p < 0.001

Parameter	Value	Sig.
A	-20.51	p = 0.15
B	0.81	p < 0.001

B. 40 mM; ANOVA, F = 50.7, p < 0.001

Parameter	Value	Sig.
A	16.2	p = 0.10
B	0.50	p < 0.001

C. ATR; ANOVA, F = 36.3, p < 0.001

Parameter	Value	Sig.
A	20.61	p < 0.05
B	0.35	p < 0.001

Table 17. Statistical Analysis of CsA Induced Survival

PD2	24 hr
40 mM	-2.75; p<0.01
40+CsA	-2.01; p<0.05
ATR	-2.75; p<0.01
ATR+CsA	-.727; p=0.485

**Mann-Whitney U
40 mM, ATR vs. 5.5 mM; CsA vs. 40 mM and ATR
**p values in bold type denote non-significant results

Table 18. Statistical Testing of Maintenance of $\Delta\Psi_M$ by CsA

	2 hr	6 hr	12 hr	24 hr
PD2-CsA	-20.3;p<0.001	-25.8;p<0.001	-29.8;p<0.001	nd
PD15-CsA	-19.4;p<0.001	-15.3;p<0.001	nd	-33.1;p<0.001

** Mann-Whitney U (Z statistic) vs. 40 mM alone
** nd = not done

A. NaNO$_2$ Standard Curve

$Y = 0.02595 + 0.011(X)$

O.D.

NaNO$_2$ (μM)

199

Appendix C.

B. TNF-α Standard Curve

Y = 0.24025 + 0.00137X

O.D.

TNF (pg/ml)
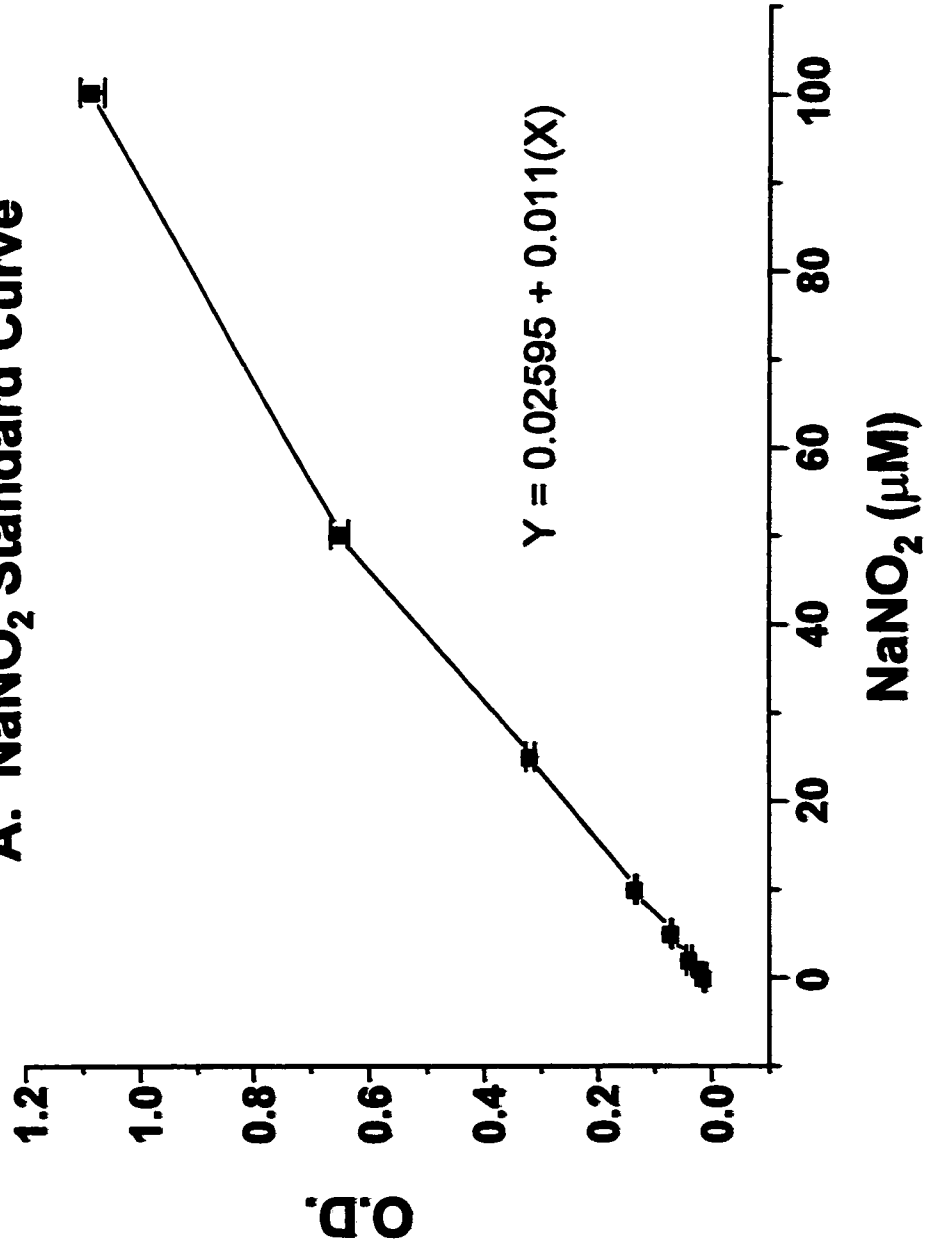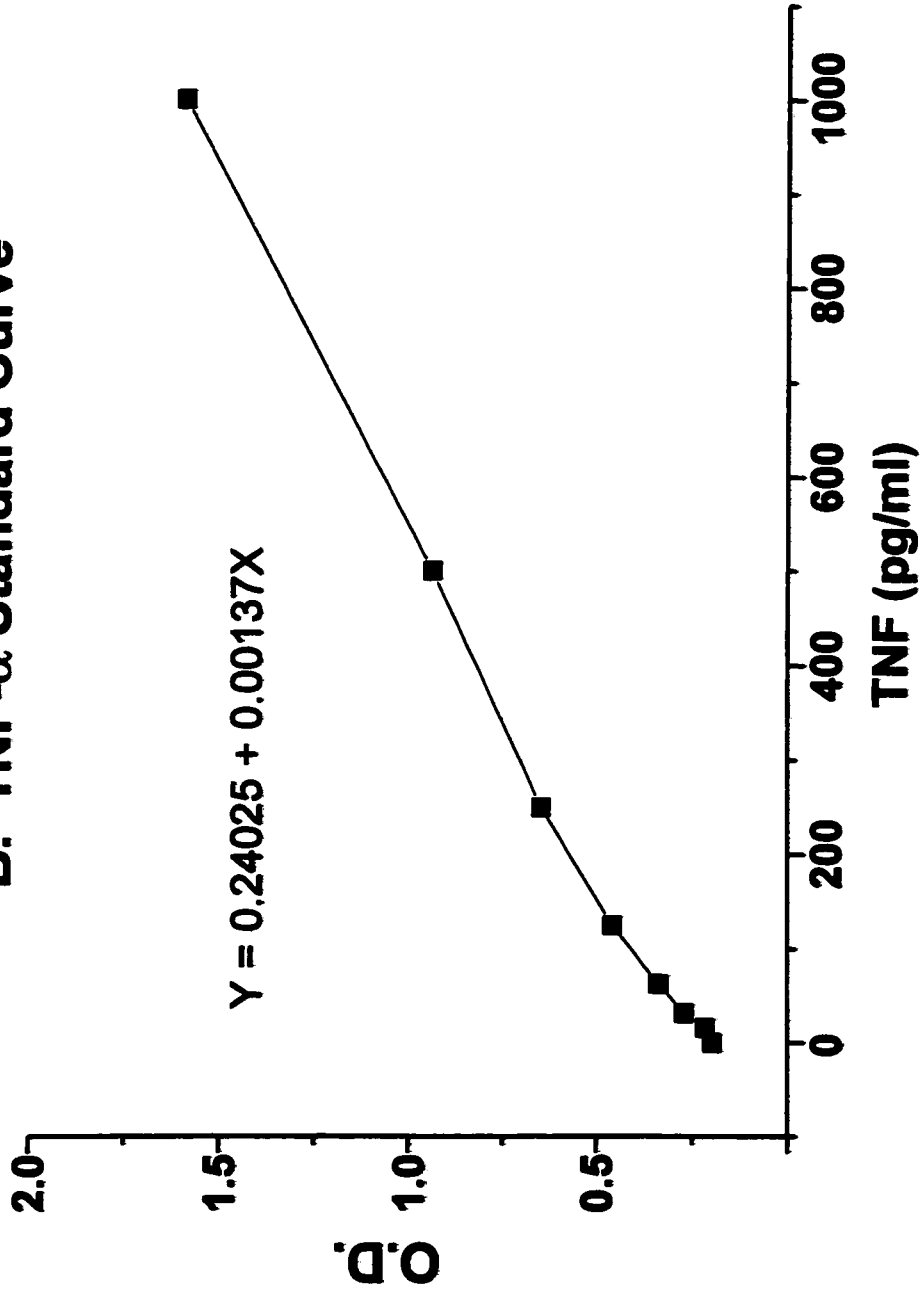
X. References

Adachi, S., Cross, A. R., Babior, B. M., and Gottlieb, R. A. (1997). Bcl-2 and the outer mitochondrial membrane in the inactivation of cytochrome c during Fas-mediated apoptosis. J Biol Chem 272, 21878-82.

Asada, T., Takakura, S., Ogawa, T., Iwai, M., and Koayashi, M. (1998). Overexpression of glucose transportor protein 5 in sciatic nerve of streptozotocin-induced diabetic rats. Neuroscience Letters 252, 111-114.

Asahina, T., Kashiwagi, A., Nishio, Y., Ikebuchi, M., Harada, N., Tanaka, Y., Takagi, Y., Saeki, Y., Kikkawa, R., and Shigeta, Y. (1995). Impaired activation of glucose oxidation and NADPH supply in human endothelial cells exposed to H2O2 in high-glucose medium. Diabetes 44, 520-6.

Assouline, J. G., Bosch, E. P., and Lim, R. (1983). Purification of rat Schwann cells from cultures of peripheral nerve: an immunoselective method using surfaces coated with anti-immunoglobulin antibodies. Brain Res 277, 389-92.

Baffy, G., Miyashita, T., Williamson, J. R., and Reed, J. C. (1993). Apoptosis induced by withdrawal of interleukin-3 (IL-3) from an IL-3-dependent hematopoietic cell line is associated with repartitioning of intracellular calcium and is blocked by enforced Bcl-2 oncoprotein production. J Biol Chem 268, 6511-9.

Ballanyi, K., and Grafe, P. (1988). Cell volume regulation in the nervous system. Ren Physiol Biochem 11, 142-57.

Basma, A. N., Heikkila, R. E., Saporito, M. S., Philbert, M., Geller, H. M., and Nicklas, W. J. (1992). 1-Methyl-4-(2'-ethylphenyl)-1,2,3,6-tetrahydropyridine-induced toxicity in PC12 cells is enhanced by preventing glycolysis. J Neurochem 58, 1052-9.

Baumgartner Parzer, S. M., Wagner, L., Pettermann, M., Grillari, J., Gessl, A., and Waldhausl, W. (1995). High-glucose--triggered apoptosis in cultured endothelial cells. Diabetes 44, 1323-7.

Beere, H. M., Chresta, C. M., Alejo Herberg, A., Skladanowski, A., Dive, C., Larsen, A. K., and Hickman, J. A. (1995). Investigation of the mechanism of higher order chromatin fragmentation observed in drug-induced apoptosis. Mol Pharmacol 47, 986-96.

Bernardi, P. (1996). The permeability transition pore. Control points of a cyclosporin A-sensitive mitochondrial channel involved in cell death. Biochim Biophys Acta 1275, 5-9.

Beutner, G., Ruck, A., Riede, B., and Brdiczka, D. (1997). Complexes between hexokinase, mitochondrial porin and adenylate translocator in brain: regulation of hexokinase, oxidative phosphorylation and permeability transition pore. Biochem Soc Trans 25, 151-7.

Beutner, G., Ruck, A., Riede, B., and Brdiczka, D. (1998). Complexes between porin, hexokinase, mitochondrial creatine kinase and adenylate translocator display properties of the permeability transition pore. Implication for regulation of permeability transition by the kinases. Biochim Biophys Acta 1368, 7-18.

Beutner, G., Ruck, A., Riede, B., Welte, W., and Brdiczka, D. (1996). Complexes between kinases, mitochondrial porin and adenylate translocator in rat brain resemble the permeability transition pore. FEBS Lett 396, 189-95.

Beyer Mears, A., and Cruz, E. (1985). Reversal of diabetic cataract by sorbinil, an aldose reductase inhibitor. Diabetes 34, 15-21.

Bolanos, J. P., Almeida, A., Stewart, V., Peuchen, S., Land, J. M., Clark, J. B., and Heales, S. J. (1997). Nitric oxide-mediated mitochondrial damage in the brain: mechanisms and implications for neurodegenerative diseases. J Neurochem 68, 2227-40.

Bolanos, J. P., Heales, S. J., Land, J. M., and Clark, J. B. (1995). Effect of peroxynitrite on the mitochondrial respiratory chain: differential susceptibility of neurones and astrocytes in primary culture. J Neurochem 64, 1965-72.

Bolanos, J. P., Peuchen, S., Heales, S. J., Land, J. M., and Clark, J. B. (1994). Nitric oxide-mediated inhibition of the mitochondrial respiratory chain in cultured astrocytes. J Neurochem 63, 910-6.

Bolin, L. M., and Shooter, E. M. (1993). Neurons regulate Schwann cell genes by diffusible molecules. J Cell Biol 123, 237-43.

Bolin, L. M., Verity, A. N., Silver, J. E., Shooter, E. M., and Abrams, J. S. (1995). Interleukin-6 production by Schwann cells and induction in sciatic nerve injury. J Neurochem 64, 850-8.

Borrebaek, B., and Haviken, J. T. (1985). Some observations on mitochondrial-bound hexokinase and creatine kinase of the heart. Biochemical Medicine 33, 170-179.

Bossy-Wetzel, E., Newmeyer, D. D., and Green, D. R. (1998). Mitochondrial cytochrome c release in apoptosis occurs upstream of DEVD-specific caspase activation and independently of mitochondrial transmembrane depolarization. EMBO J 17, 37-49.

Bradley, J. L., Thomas, P. K., King, R. H., Muddle, J. R., Ward, J. D., Tesfaye, S., Boulton, A. J., Tsigos, C., and Young, R. J. (1995). Myelinated nerve fibre regeneration in diabetic sensory polyneuropathy: correlation with type of diabetes. Acta Neuropathol Berl 90, 403-10.

Braun, N., Papadopoulos, T., and Miller-Hermelink, H. K. (1988). Cell cycle dependent distribution of the proliferation associated Ki67 antigen in human embryonic lung cells. Virchows Arch. B. 56, 25-33.

Brdiczka, D., and Wallimann, T. (1994). The importance of the outer mitochondrial compartment in regulation of energy metabolism. Mol Cell Biochem 133-134, 69-83.

Brockes, J. P., Fields, K. L., and Raff, M. C. (1979). Studies on cultured rat Schwann cells. I. Establishment of purified populations from cultures of peripheral nerve. Brain Res 165, 105-18.

Bunge, R. P. (1987). Tissue culture observations relevant to the study of axon-Schwann cell interactions during peripheral nerve development and repair. J Exp Biol 132, 21-34.

Bunge, R. P., Bunge, M. B., and Eldridge, C. F. (1986). Linkage between axonal ensheathment and basal lamina production by Schwann cells. Annu Rev Neurosci 9, 305-28.

Cameron, N. E., Cotter, M. A., and Maxfield, E. K. (1993). Anti-oxidant treatment prevents the development of peripheral nerve dysfunction in streptozotocin-diabetic rats. Diabetologia 36, 299-304.

Ceriello, A., dello Russo, P., Amstad, P., and Cerutti, P. (1996). High glucose induces antioxidant enzymes in human endothelial cells in culture. Evidence linking hyperglycemia and oxidative stress. Diabetes 45, 471-7.

Charriaut-Marlangue, C., and Ben Ari, Y. (1995). A cautionary note on the use of the TUNEL stain to determine apoptosis. Neuroreport 7, 61-4.

Cheng, H. L., and Feldman, E. L. (1998). Bidirectional regulation of p38 kinase and c-Jun N-terminal protein kinase by insulin-like growth factor-I. J Biol Chem 273, 14560-5.

Cherian, P. V., Kamijo, M., Angelides, K. J., and Sima, A. A. (1996). Nodal Na(+)-channel displacement is associated with nerve-conduction slowing in the chronically diabetic BB/W rat: prevention by aldose reductase inhibition. J Diabetes Complications 10, 192-200.

Cobuzzi, R. J., Jr., Neafsey, E. J., and Collins, M. A. (1994). Differential cytotoxicities of N-methyl-beta-carbolinium analogues of MPP+ in PC12 cells: insights into potential neurotoxicants in Parkinson's disease. J Neurochem 62, 1503-10.

Cohen, G. M., Sun, X. M., Snowden, R. T., Dinsdale, D., and Skilleter, D. N. (1992). Key morphological features of apoptosis may occur in the absence of internucleosomal DNA fragmentation. Biochem J 286, 331-4.

Collins, R. J., Harmon, B. V., Gobe, G. C., and Kerr, J. F. (1992). Internucleosomal DNA cleavage should not be the sole criterion for identifying apoptosis. Int J Radiat Biol 61, 451-3.

Conti, A. M., Malosio, M. L., Scarpini, E., Di Giulio, A. M., Scarlato, G., Mantegazza, P., and Gorio, A. (1993). Myelin protein transcripts increase in experimental diabetic neuropathy. Neurosci Lett 161, 203-6.

Conti, A. M., Scarpini, E., Malosio, M. L., Di Giulio, A. M., Baron, P., Scarlato, G., Mantegazza, P., and Gorio, A. (1996). In situ hybridization study of myelin protein mRNA in rats with an experimental diabetic neuropathy. Neurosci Lett 207, 65-9.

Daube, J. R. (1999). Electrophysiologic testing in diabetic neuropathy. In Diabetic Neuropathy, P. J. Dyck and P. K. Thomas, eds. (Philadelphia: W.B. Saunders), pp. 222-238.

de Waegh, S., and Brady, S. T. (1990). Altered slow axonal transport and regeneration in a myelin-deficient mutant mouse: the trembler as an in vivo model for Schwann cell-axon interactions. J Neurosci 10, 1855-65.

de Waegh, S. M., and Brady, S. T. (1991). Local control of axonal properties by Schwann cells: neurofilaments and axonal transport in homologous and heterologous nerve grafts. J Neurosci Res 30, 201-12.

de Waegh, S. M., Lee, V. M., and Brady, S. T. (1992). Local modulation of neurofilament phosphorylation, axonal caliber, and slow axonal transport by myelinating Schwann cells. Cell 68, 451-63.

Deckwerth, T. L., Elliott, J. L., Knudson, C. M., Johnson, E. M., Jr., Snider, W. D., and Korsmeyer, S. J. (1996). BAX is required for neuronal death after trophic factor deprivation and during development. Neuron 17, 401-11.

D'Mello, S. R., Borodezt, K., and Soltoff, S. P. (1997). Insulin-like growth factor and potassium depolarization maintain neuronal survival by distinct pathways: possible involvement of PI 3-kinase in IGF-1 signaling. J Neurosci 17, 1548-60.

Dong, Z., Brennan, A., Liu, N., Yarden, Y., Lefkowitz, G., Mirsky, R., and Jessen, K. R. (1995). Neu differentiation factor is a neuron-glia signal and regulates survival, proliferation, and maturation of rat Schwann cell precursors. Neuron 15, 585-96.

Dong, Z., Saikumar, P., Weinberg, J. M., and Venkatachalam, M. A. (1997). Internucleosomal DNA cleavage triggered by plasma membrane damage during necrotic cell death. Involvement of serine but not cysteine proteases. Am J Pathol 151, 1205-13.

Donnini, D., Zambito, A. M., Perrella, G., Ambesi Impiombato, F. S., and Curcio, F. (1996). Glucose may induce cell death through a free radical-mediated mechanism. Biochem Biophys Res Commun 219, 412-7.

Du, X. L., Sui, G. Z., Stockklauser Farber, K., Weiss, J., Zink, S., Schwippert, B., Wu, Q. X., Tschope, D., and Rosen, P. (1998). Introduction of apoptosis by high proinsulin and glucose in cultured human umbilical vein endothelial cells is mediated by reactive oxygen species. Diabetologia 41, 249-56.

Dugandzija Novakovic, S., Koszowski, A. G., Levinson, S. R., and Shrager, P. (1995). Clustering of Na+ channels and node of Ranvier formation in remyelinating axons. J Neurosci 15, 492-503.

Dyck, J. B., and Dyck, P. J. (1999). Diabetic Polyneuropathy. In Diabetic Neuropathy, P. J. Dyck and P. K. Thomas, eds. (Philadelphia: W.B. Saunders), pp. 255-278.

Dyck, P. J., and Giannini, C. (1996). Pathologic alterations in the diabetic neuropathies of humans: a review. J Neuropathol Exp Neurol 55, 1181-93.

Dyck, P. J., Karnes, J. L., Daube, J., O'Brien, P., and Service, F. J. (1985). Clinical and neuropathological criteria for the diagnosis and staging of diabetic polyneuropathy. Brain 108, 861-80.

Dyck, P. J., Karnes, J. L., and Lambert, E. H. (1989). Longitudinal study of neuropathic deficits and nerve conduction abnormalities in hereditary motor and sensory neuropathy type 1. Neurology 39, 1302-8.

Dyck, P. J., Karnes, J. L., O'Brien, P., Okazaki, H., Lais, A., and Engelstad, J. (1986). The spatial distribution of fiber loss in diabetic polyneuropathy suggests ischemia. Ann Neurol 19, 440-9.

Dyck, P. J., Kratz, K. M., Karnes, J. L., Litchy, W. J., Klein, R., Pach, J. M., Wilson, D. M., PC, O. B., Melton, L. J. d., and Service, F. J. (1993). The prevalence by staged severity of various types of diabetic neuropathy,

retinopathy, and nephropathy in a population-based cohort: the Rochester Diabetic Neuropathy Study. Neurology *43*, 817-24.

Dyck, P. J., Kratz, K. M., Lehman, K. A., Karnes, J. L., Melton, L. J. d., PC, O. B., Litchy, W. J., Windebank, A. J., Smith, B. E., Low, P. A., and et al. (1991). The Rochester Diabetic Neuropathy Study: design, criteria for types of neuropathy, selection bias, and reproducibility of neuropathic tests. Neurology *41*, 799-807.

Dyck, P. J., Lais, A., Karnes, J. L., O'Brien, P., and Rizza, R. (1986). Fiber loss is primary and multifocal in sural nerves in diabetic polyneuropathy. Ann Neurol *19*, 425-39.

Dyck, P. J., Zimmerman, B. R., Vilen, T. H., Minnerath, S. R., Karnes, J. L., Yao, J. K., and Poduslo, J. F. (1988). Nerve glucose, fructose, sorbitol, myo-inositol, and fiber degeneration and regeneration in diabetic neuropathy. N Engl J Med *319*, 542-8.

Ekstrom, A. R., Kanje, M., and Skottner, A. (1989). Nerve regeneration and serum levels of insulin-like growth factor-I in rats with streptozotocin-induced insulin deficiency. Brain Res *496*, 141-7.

Elias, K. A., Cronin, M. J., Stewart, T. A., and Carlsen, R. C. (1998). Peripheral neuropathy in transgenic mice: Restoration of C-fiber function with human recombinant nerve growth factor. Diabetes *47*, 1637-1642.

Ellerby, L. M., Ellerby, H. M., Park, S. M., Holleran, A. L., Murphy, A. N., Fiskum, G., Kane, D. J., Testa, M. P., Kayalar, C., and Bredesen, D. E. (1996). Shift of the cellular oxidation-reduction potential in neural cells expressing Bcl-2. J Neurochem *67*, 1259-67.

Enari, M., Talanian, R. V., Wong, W. W., and Nagata, S. (1996). Sequential activation of ICE-like and CPP32-like proteases during Fas-mediated apoptosis. Nature *380*, 723-6.

Eskes, R., Antonsson, B., Osen-Sand, A., Montessuit, S., Richter, C., Sadoul, R., Mazzei, G., Nichols, A., and Martinou, J.-C. (1998). Bax-induced cytochrome c release from mitochondria is independent of the permeability transition pore but highly dependent on Mg++ ions. J of Cell Biol *143*, 217-224.

Estevez, A. G., Radi, R., Barbeito, L., Shin, J. T., Thompson, J. A., and Beckman, J. S. (1995). Peroxynitrite-induced cytotoxicity in PC12 cells: evidence for an apoptotic mechanism differentially modulated by neurotrophic factors. J Neurochem *65*, 1543-50.

Fernyhough, P., Diemel, L. T., Hardy, J., Brewster, W. J., Mohiuddin, L., and Tomlinson, D. R. (1995). Human recombinant nerve growth factor replaces deficient neurotrophic support in the diabetic rat. Eur J Neurosci 7, 1107-10.

Ferrari, G., Yan, C. Y., and Greene, L. A. (1995). N-acetylcysteine (D- and L-stereoisomers) prevents apoptotic death of neuronal cells. J Neurosci 15, 2857-66.

Fiek, C., Benz, R., Roos, N., and Brdiczka, D. (1982). Evidence for identity between the hexokinase-binding protein and the mitochondrial porin in the outer membrane of rat liver mitochondria. Biochim Biophys Acta 688, 429-40.

Filipski, J., Leblanc, J., Youdale, T., Sikorska, M., and Walker, P. R. (1990). Periodicity of DNA folding in higher order chromatin structures. EMBO J 9, 1319-27.

Forcier, N. J., Mizisin, A. P., Rimmer, M. A., and Powell, H. C. (1991). Cellular pathology of the nerve microenvironment in galactose intoxication. J Neuropathol Exp Neurol 50, 235-55.

Friedman, B., Scherer, S. S., Rudge, J. S., Helgren, M., Morrisey, D., McClain, J., Wang, D. Y., Wiegand, S. J., Furth, M. E., Lindsay, R. M., and et al. (1992). Regulation of ciliary neurotrophic factor expression in myelin-related Schwann cells in vivo. Neuron 9, 295-305.

Fukuda, K., Kojiro, M., and Chiu, J. F. (1993). Demonstration of extensive chromatin cleavage in transplanted Morris hepatoma 7777 tissue: apoptosis or necrosis? Am J Pathol 142, 935-46.

Funakoshi, H., Frisen, J., Barbany, G., Timmusk, T., Zachrisson, O., Verge, V. M., and Persson, H. (1993). Differential expression of mRNAs for neurotrophins and their receptors after axotomy of the sciatic nerve. J Cell Biol 123, 455-65.

Gandhi, D., Matthews, C. C., and Feldman, E. L. (1995). IGF-I rescues neurons from hyperglycemic, hyperosmotic, injury. In Diabetic Neuropathy: New Concepts and Insights, N. Hotta, D. A. Greene, J. D. Ward, A. A. F. Sima and A. J. M. Boulton, eds. (Amsterdam: Elsevier), pp. 183-189.

Gardiner, S. M., Kemp, P. A., March, J. E., and Bennett, T. (1995). Cardiac and regional haemodynamics, inducible nitric oxide synthase (NOS) activity, and the effects of NOS inhibitors in conscious, endotoxaemic rats. Br J Pharmacol 116, 2005-16.

Gerbitz, K. D., Gempel, K., and Brdiczka, D. (1996). Mitochondria and diabetes. Genetic, biochemical, and clinical implications of the cellular energy circuit. Diabetes 45, 113-26.

Giannini, C., and Dyck, P. J. (1996). Axoglial dysjunction: a critical appraisal of definition, techniques, and previous results. Microsc Res Tech 34, 436-44.

Giannini, C., and Dyck, P. J. (1999). Pathological alterations in human diabetic polyneuropathy. In Diabetic Neuropathy, P. J. Dyck and P. K. Thomas, eds. (Philadelphia: W.B. Saunders), pp. 279-295.

Giannini, C., and Dyck, P. J. (1994). Ultrastructural morphometric abnormalities of sural nerve endoneurial microvessels in diabetes mellitus. Ann Neurol 36, 408-15.

Ginsberg, B. J., and Mazze, R. (1994). Clinical consequences of the Diabetes Control and Complications Trial. N J Med 91, 221-4.

Gold, R., Zielasek, J., Kiefer, R., Toyka, K. V., and Hartung, H. P. (1996). Secretion of nitrite by Schwann cells and its effect on T-cell activation in vitro. Cell Immunol 168, 69-77.

Goping, I. S., Gross, A., Lavoie, J. N., Nguyen, M., Jemmerson, R., Roth, K., Korsmeyer, S. J., and Shore, G. C. (1998). Regulated targeting of bax to mitochondria. J Cell Biol 143, 207-215.

Graier, W. F., Grubenthal, I., Dittrich, P., Wascher, T. C., and Kostner, G. M. (1995). Intracellular mechanism of high D-glucose-induced modulation of vascular cell proliferation. Eur J Pharmacol 294, 221-9.

Green, D., and Kroemer, G. (1998). The central executioners of apoptosis: Caspases or mitochondria? TICB 8, 267-271.

Green, D. R., and Reed, J. C. (1998). Mitochondria and apoptosis. Science 281, 1309-1312.

Greene, D. A., and Winegrad, A. I. (1979). In vitro studies of the substrates for energy production and the effects of insulin on glucose utilization in the neural components of peripheral nerve. Diabetes 28, 878-87.

Grosse, F., and Manns, A. (1993). Terminal deoxyrinonucleotidyl transferase. Methods in Molecular Biology 16, 95-105.

Gunter, T. E., and Pfeiffer, D. R. (1990). Mechanisms by which mitochondria transport calcium. Am J Physiol 258, C755-86.

Guy, R. J., Clark, C. A., Malcolm, P. N., and Watkins, P. J. (1985). Evaluation of thermal and vibration sensation in diabetic neuropathy. Diabetologia 28, 131-7.

Hara, S., Halicka, H. D., Bruno, S., Gong, J., Traganos, F., and Darzynkiewicz, Z. (1996). Effect of protease inhibitors on early events of apoptosis. Exp Cell Res 223, 372-84.

Harris, M., Eastman, R., and Cowie, C. (1993). Symptoms of sensory neuropathy in adults with NIDDM in the U.S. population. Diabetes Care 16, 1446.

Hellweg, R., and Hartung, H. D. (1990). Endogenous levels of nerve growth factor (NGF) are altered in experimental diabetes mellitus: a possible role for NGF in the pathogenesis of diabetic neuropathy. J Neurosci Res 26, 258-67.

Hellweg, R., Raivich, G., Hartung, H. D., Hock, C., and Kreutzberg, G. W. (1994). Axonal transport of endogenous nerve growth factor (NGF) and NGF receptor in experimental diabetic neuropathy. Exp Neurol 130, 24-30.

Heneka, M. T., Loschmann, P. A., Gleichmann, M., Weller, M., Schulz, J. B., Wullner, U., and Klockgether, T. (1998). Induction of nitric oxide synthase and nitric oxide-mediated apoptosis in neuronal PC12 cells after stimulation with tumor necrosis factor-alpha/lipopolysaccharide. J Neurochem 71, 88-94.

Hermenegildo, C., Raya, A., Roma, J., and Romero, F. J. (1993). Decreased glutathione peroxidase activity in sciatic nerve of alloxan-induced diabetic mice and its correlation with blood glucose levels. Neurochem Res 18, 893-6.

Hortelano, S., Dallaporta, B., Zamzami, N., Hirsch, T., Susin, S. A., Marzo, I., Bosca, L., and Kroemer, G. (1997). Nitric oxide induces apoptosis via triggering mitochondrial permeability transition. FEBS Lett 410, 373-7.

Hsu, Y. T., Wolter, K. G., and Youle, R. J. (1997). Cytosol-to-membrane redistribution of bax and bcl-xl during apoptosis. PNAS 94, 3668-3672.

Hunt, J. V., Dean, R. T., and Wolff, S. P. (1988). Hydroxyl radical production and autoxidative glycosylation. Glucose autoxidation as the cause of protein damage in the experimental glycation model of diabetes mellitus and ageing. Biochem J 256, 205-12.

Ishii, D. N., Glazner, G. W., and Pu, S. F. (1994). Role of insulin-like growth factors in peripheral nerve regeneration. Pharmacol Ther 62, 125-44.

Ishii, D. N., and Lupien, S. B. (1995). Insulin-like growth factors protect against diabetic neuropathy: effects on sensory nerve regeneration in rats. J Neurosci Res 40, 138-44.

Ishitani, R., Sunaga, K., Tanaka, M., Aishita, H., and Chuang, D. M. (1997). Overexpression of glyceraldehyde-3-phosphate dehydrogenase is involved in low

K+-induced apoptosis but not necrosis of cultured cerebellar granule cells. Mol Pharmacol *51*, 542-50.

Ishitani, R., Tanaka, M., Sunaga, K., Katsube, N., and Chuang, D. M. (1998). Nuclear localization of overexpressed glyceraldehyde-3-phosphate dehydrogenase in cultured cerebellar neurons undergoing apoptosis. Mol Pharmacol *53*, 701-7.

Itoga, M., Tsuchiya, M., Ishino, H., and Shimoyama, M. (1997). Nitric oxide-induced modification of glyceraldehyde-3-phosphate dehydrogenase with NAD+ is not ADP-ribosylation. J Biochem Tokyo *121*, 1041-6.

Jaffey, P. B., and Gelman, B. B. (1996). Increased vulnerability to demyelination in streptozotocin diabetic rats. J Comp Neurol *373*, 55-61.

Jessen, K. R., Brennan, A., Morgan, L., Mirsky, R., Kent, A., Hashimoto, Y., and Gavrilovic, J. (1994). The Schwann cell precursor and its fate: a study of cell death and differentiation during gliogenesis in rat embryonic nerves. Neuron *12*, 509-27.

Jessen, K. R., and Mirsky, R. (1991). Schwann cell precursors and their development. Glia *4*, 185-94.

Jessen, K. R., and Mirsky, R. (1992). Schwann cells: early lineage, regulation of proliferation and control of myelin formation. Curr Opin Neurobiol *2*, 575-81.

Jung Testas, I., Schumacher, M., Robel, P., and Baulieu, E. E. (1994). Actions of steroid hormones- and growth factors on glial cells of the central and peripheral nervous system. J Steroid Biochem Mol Biol *48*, 145-54.

Jurgensmeier, J. M., Xie, Z., Deveraux, Q., Ellerby, L., Bredesen, D., and Reed, J. C. (1998). Bax directly induces cytochrome c release from isolated mitochondria. PNAS *95*, 4997-5002.

Kabir, F., and Wilson, J. E. (1994). Mitochondrial hexokinase in brain: coexistence of forms differing in sensitivity to solubilization by glucose-6-phosphate on the same mitochondria. Arch Biochem Biophys *310*, 410-6.

Kacem, K., Lacombe, P., Seylaz, J., and Bonvento, G. (1998). Structural organization of the perivascular astrocyte endfeet and their relationship with the endothelial glucose transporter: a confocal microscopy study. Glia *23*, 1-10.

Kalichman, M. W., Powell, H. C., and Mizisin, A. P. (1998). Reactive, degenerative, and proliferative Schwann cell responses in experimental galactose and human diabetic neuropathy. Acta Neuropathol Berl *95*, 47-56.

Kamijo, M., Merry, A. C., Akdas, G., Cherian, P. V., and Sima, A. A. (1996). Nerve fiber regeneration following axotomy in the diabetic biobreeding Worcester rat: the effect of ARI treatment. J Diab Comp 10, 183-91.

Kane, D. J., Sarafian, T. A., Anton, R., Hahn, H., Gralla, E. B., Valentine, J. S., Ord, T., and Bredesen, D. E. (1993). Bcl-2 inhibition of neural death: decreased generation of reactive oxygen species. Science 262, 1274-7.

Karihaloo, A. K., Joshi, K., and Chopra, J. S. (1997). Effect of sorbinil and ascorbic acid on myo-inositol transport in cultured rat Schwann cells exposed to elevated extracellular glucose. J Neurochem 69, 2011-8.

Kashiwagi, A., Asahina, T., Ikebuchi, M., Tanaka, Y., Takagi, Y., Nishio, Y., Kikkawa, R., and Shigeta, Y. (1994). Abnormal glutathione metabolism and increased cytotoxicity caused by H2O2 in human umbilical vein endothelial cells cultured in high glucose medium. Diabetologia 37, 264-9.

Kerr, J. F., Wyllie, A. H., and Currie, A. R. (1972). Apoptosis: a basic biological phenomenon with wide-ranging implications in tissue kinetics. Br J Cancer 26, 239-57.

Khodarev, N. N., Sokolova, I. A., and Vaughan, A. T. (1998). Mechanisms of induction of apoptotic DNA fragmentation. Int J Radiat Biol 73, 455-67.

Kluck, R. M., Bossy Wetzel, E., Green, D. R., and Newmeyer, D. D. (1997). The release of cytochrome c from mitochondria: a primary site for Bcl-2 regulation of apoptosis. Science 275, 1132-6.

Komiyama, A., and Suzuki, K. (1992). Age-related differences in proliferative responses of Schwann cells during Wallerian degeneration. Brain Res 573, 267-75.

Korsmeyer, S. J., Shutter, J. R., Veis, D. J., Merry, D. E., and Oltvai, Z. N. (1993). Bcl-2/Bax: a rheostat that regulates an anti-oxidant pathway and cell death. Semin Cancer Biol 4, 327-32.

Krajewski, S., Tanaka, S., Takayama, S., Schibler, M. J., Fenton, W., and Reed, J. C. (1993). Investigation of the subcellular distribution of the bcl-2 oncoprotein: residence in the nuclear envelope, endoplasmic reticulum, and outer mitochondrial membranes. Cancer Res 53, 4701-14.

Kroemer, G., Petit, P., Zamzami, N., Vayssiere, J. L., and Mignotte, B. (1995). The biochemistry of programmed cell death. FASEB J 9, 1277-87.

Krueger, K. E. (1991). Peripheral-type benzodiazepine receptors: a second site of action for benzodiazepines. Neuropsychopharm 4, 237-44.

Lemke, G. (1996). Neuregulins in development. Mol Cell Neurosci 7, 247-62.

Li, X. M., Qi, J., Juorio, A. V., and Boulton, A. A. (1997). Reciprocal regulation of the content of aromatic L-amino acid decarboxylase and tyrosine hydroxylase mRNA by NGF in PC12 cells. J Neurosci Res 47, 449-54.

Linden, M., Gellerfors, P., and Nelson, B. D. (1982). Pore protein and the hexokinase-binding protein from the outer membrane of rat liver mitochondria are identical. FEBS Lett 141, 189-92.

Llewelyn, J. G., Gilbey, S. G., Thomas, P. K., King, R. H., Muddle, J. R., and Watkins, P. J. (1991). Sural nerve morphometry in diabetic autonomic and painful sensory neuropathy. A clinicopathological study. Brain 114, 867-92.

Low, P. A., and Nicklander, K. K. (1991). Oxygen free radical effects in sciatic nerve in experimental diabetes. Diabetes 40, 873.

Lynch, R. M., Carrington, W., Fogarty, K. E., and Fay, F. S. (1996). Metabolic modulation of hexokinase association with mitochondria in living smooth muscle cells. Am J Physiol 270, C488-99.

Lynch, R. M., Fogarty, K. E., and Fay, F. S. (1991). Modulation of hexokinase association with mitochondria analyzed with quantitative three-dimensional confocal microscopy. J Cell Biol 113, 385-395.

Macho, A., Decaudin, D., Castedo, M., Hirsch, T., Susin, S. A., Zamzami, N., and Kroemer, G. (1996). Chloromethyl-X-Rosamine is an aldehyde-fixable potential-sensitive fluorochrome for the detection of early apoptosis. Cytometry 25, 333-40.

Magnani, P., Cherian, P. V., Gould, G. W., Greene, D. A., Sima, A. A., and Brosius, F. C., 3rd (1996). Glucose transporters in rat peripheral nerve: paranodal expression of GLUT1 and GLUT3. Metabolism 45, 1466-73.

Mahajan, N. P., Linder, K., Berry, G., Gordon, G., Heim, R., and Herman, B. (1998). Bcl-2 and bax interactions in mitochondria probed with green fluorescent protein and fluorescence resonance energy transfer. Nature Biotech 16, 547-552.

Marchetti, P., Castedo, M., Susin, S. A., Zamzami, N., Hirsch, T., Macho, A., Haeffner, A., Hirsch, F., Geuskens, M., and Kroemer, G. (1996). Mitochondrial permeability transition is a central coordinating event of apoptosis. J Exp Med 184, 1155-60.

Marzo, I., Brenner, C., Zamzami, N., Jurgensmeier, J., Susin, S., Vieira, H., Prevost, M.-C., Xie, Z., Matsuyama, S., Reed, J. C., and Kroemer, G. (1998). Bax and adenine nucleotide translocator cooperate in the mitochondrial control of apoptosis. Science 281, 2027-2031.

Marzo, I., Brenner, C., Zamzami, N., Susin, S. A., Beutner, G., Brdiczka, D., Remy, R., Xie, Z. H., Reed, J. C., and Kroemer, G. (1998). The permeability transition pore complex: a target for apoptosis regulation by caspases and bcl-2-related proteins. J Exp Med 187, 1261-71.

Matthews, R. T., Yang, L., Jenkins, B. G., Ferrante, R. J., Rosen, B. R., Kaddurah Daouk, R., and Beal, M. F. (1998). Neuroprotective effects of creatine and cyclocreatine in animal models of Huntington's disease. J Neurosci 18, 156-63.

McCabe, E. R. B. (1994). Microcompartmentation of energy metabolism at the outer mitochondrial membrane: Role in diabetes mellitus and other diseases. J of Bioenerg Biomem 26, 317-325.

McEnery, M. W., Snowman, A. M., Trifiletti, R. R., and Snyder, S. H. (1992). Isolation of the mitochondrial benzodiazepine receptor: association with the voltage-dependent anion channel and the adenine nucleotide carrier. PNAS 89, 3170-4.

Medori, R., Autilio Gambetti, L., Jenich, H., and Gambetti, P. (1988). Changes in axon size and slow axonal transport are related in experimental diabetic neuropathy. Neurology 38, 597-601.

Memon, S. A., Moreno, M. B., Petrak, D., and Zacharchuk, C. M. (1995). Bcl-2 blocks glucocorticoid- but not Fas- or activation-induced apoptosis in a T cell hybridoma. J Immunol 155, 4644-52.

Metivier, D., Dallaporta, B., Zamzami, N., Larochette, N., Susin, S., Marzo, I., and Kroemer, G. (1998). Cytofluorometric detection of mitochondrial alterations in early CD95/Fas/APO-1-triggered apoptosis of Jurkat T lymphoma cells. Comparison of seven mitochondrion-specific fluorochromes. Immunology Letters 61, 157-163.

Michaelidis, T. M., Sendtner, M., Cooper, J. D., Airaksinen, M. S., Holtmann, B., Meyer, M., and Thoenen, H. (1996). Inactivation of bcl-2 results in progressive degeneration of motoneurons, sympathetic and sensory neurons during early postnatal development. Neuron 17, 75-89.

Mirsky, R., and Jessen, K. R. (1996). Schwann cell development, differentiation and myelination. Curr Opin Neurobiol 6, 89-96.

Mitrovic, B., Ignarro, L. J., Montestruque, S., Smoll, A., and Merrill, J. E. (1994). Nitric oxide as a potential pathological mechanism in demyelination: its differential effects on primary glial cells in vitro. Neuroscience 61, 575-85.

Mizisin, A. P., Li, L., Perello, M., Freshwater, J. D., Kalichman, M. W., Roux, L., and Calcutt, N. A. (1996). Polyol pathway and osmoregulation in JS1 Schwann cells grown in hyperglycemic and hyperosmotic conditions. Am J Physiol 270, F90-7.

Mizisin, A. P., and Powell, H. C. (1997). Schwann cell changes induced as early as one week after galactose intoxication. Acta Neuropathol Berl 93, 611-8.

Mizisin, A. P., Shelton, G. D., Wagner, S., Rusbridge, C., and Powell, H. C. (1998). Myelin splitting, Schwann cell injury and demyelination in feline diabetic neuropathy. Acta Neuropathol Berl 95, 171-4.

Moore, S. A., Peterson, R. G., Felten, D. L., and O'Connor, B. L. (1980). A quantitative comparison of motor and sensory conduction velocities in short- and long-term streptozotocin- and alloxan-diabetic rats. J Neurol Sci 48, 133-52.

Morgan, L., Jessen, K. R., and Mirsky, R. (1991). The effects of cAMP on differentiation of cultured Schwann cells: progression from an early phenotype (04+) to a myelin phenotype (P0+, GFAP-, N-CAM-, NGF-receptor-) depends on growth inhibition. J Cell Biol 112, 457-67.

Muona, P., Sollberg, S., Peltonen, J., and Uitto, J. (1992). Glucose transporters of rat peripheral nerve. Differential expression of GLUT1 gene by Schwann cells and perineural cells in vivo and in vitro. Diabetes 41, 1587-96.

Mytilineou, C., Radcliffe, P. M., and Olanow, C. W. (1997). L-(-)-desmethylselegiline, a metabolite of selegiline [L-(-)-deprenyl], protects mesencephalic dopamine neurons from excitotoxicity in vitro. J Neurochem 68, 434-6.

Narita, M., Shimizu, S., Ito, T., Chittenden, T., Lutz, R., Matsuda, H., and Tsujimoto, Y. (1998). Bax interacts with the permeability transition pore to induce permeability transition and cytochrome c release in isolated mitochondria. PNAS 95, 14681-14686.

Nicolay, K., Rojo, M., Wallimann, T., Demel, R., and Hovius, R. (1990). The role of contact sites between inner and outer mitochondrial membrane in energy transfer. Biochimica et Biophysica Acta 1018, 229-233.

Nomura, Y., Uehara, T., and Nakazawa, M. (1996). Neuronal apoptosis by glial NO: involvement of inhibition of glyceraldehyde-3-phosphate dehydrogenase. Hum Cell 9, 205-14.

Oberhammer, F., Fritsch, G., Schmied, M., Pavelka, M., Printz, D., Purchio, T., Lassmann, H., and Schulte Hermann, R. (1993). Condensation of the chromatin at the membrane of an apoptotic nucleus is not associated with activation of an endonuclease. J Cell Sci 104, 317-26.

Oberhammer, F., Wilson, J. W., Dive, C., Morris, I. D., Hickman, J. A., Wakeling, A. E., Walker, P. R., and Sikorska, M. (1993). Apoptotic death in epithelial cells: cleavage of DNA to 300 and/or 50 kb fragments prior to or in the absence of internucleosomal fragmentation. EMBO 12, 3679-84.

O'Gorman, E., Beutner, G., Dolder, M., Koretsky, A. P., Brdiczka, D., and Wallimann, T. (1997). The role of creatine kinase in inhibition of mitochondrial permeability transition. FEBS Lett 414, 253-7.

Pastorino, J. G., Chen, S. T., Tafani, M., Snyder, J. W., and Farber, J. L. (1998). The overexpression of Bax produces cell death upon induction of the mitochondrial permeability transition. J Biol Chem 273, 7770-5.

Paterson, I. A., Zhang, D., Warrington, R. C., and Boulton, A. A. (1998). R-deprenyl and R-2-heptyl-N-methylpropargylamine prevent apoptosis in cerebellar granule neurons induced by cytosine arabinoside but not low extracellular potassium. J Neurochem 70, 515-23.

Penso, J., and Beitner, R. (1998). Clotrimazole and bifonazole detach hexokinase from mitochondria of melanoma cells. Eur J Pharmacol 342, 113-7.

Petit, P. X., Goubern, M., Diolez, P., Susin, S. A., Zamzami, N., and Kroemer, G. (1998). Disruption of the outer mitochondrial membrane as a result of large amplitude swelling: the impact of irreversible permeability transition. FEBS Lett 426, 111-6.

Petronilli, V., Nicolli, A., Costantini, P., Colonna, R., and Bernardi, P. (1994). Regulation of the permeability transition pore, a voltage-dependent mitochondrial channel inhibited by cyclosporin A. Biochim Biophys Acta 1187, 255-9.

Pfanner, N., Rassow, J., Wienhues, U., Hergersberg, C., Sollner, T., Becker, K., and Neupert, W. (1990). Contact sites between inner and outer membranes: Structure and role in protein translocation into the mitochondria. Biochimica et Biophysica Acta 1018, 239-242.

Pfeifer, M. A., and Schumer, M. P. (1995). Clinical trials of diabetic neuropathy: past, present, and future. Diabetes 44, 1355-61.

Pittenger, G. L., Liu, D., and Vinik, A. I. (1997). The apoptotic death of neuroblastoma cells caused by serum from patients with insulin-dependent diabetes and neuropathy may be Fas-mediated. J Neuroimmunol 76, 153-60.

Polla, B. S., Kantengwa, S., Francois, D., Salvioli, S., Franceschi, C., Marsac, C., and Cossarizza, A. (1996). Mitochondria are selective targets for the protective effects of heat shock against oxidative injury. PNAS 93, 6458-63.

Poot, M., Gibson, L. L., and Singer, V. L. (1997). Detection of apoptosis in live cells by MitoTracker red CMXRos and SYTO dye flow cytometry. Cytometry 27, 358-64.

Poot, M., Zhang, Y. Z., Kramer, J. A., Wells, K. S., Jones, L. J., Hanzel, D. K., Lugade, A. G., Singer, V. L., and Haugland, R. P. (1996). Analysis of mitochondrial morphology and function with novel fixable fluorescent stains. J Histochem Cytochem 44, 1363-72.

Porte, D., and Halter, J. B. (1999). The clinical syndrome of diabetes mellitus. In Diabetic Neuropathy, P. J. Dyck and P. K. Thomas, eds. (Philadelphia: W.B. Saunders), pp. 1-28.

Porter, S., Glaser, L., and Bunge, R. P. (1987). Release of autocrine growth factor by primary and immortalized Schwann cells. PNAS 84, 7768-72.

Portera Cailliau, C., Price, D. L., and Martin, L. J. (1997). Non-NMDA and NMDA receptor-mediated excitotoxic neuronal deaths in adult brain are morphologically distinct: further evidence for an apoptosis-necrosis continuum. J Comp Neurol 378, 88-104.

Pulselli, R., Amadio, L., Fanciulli, M., and Floridi, A. (1996). Effect of lonidamine on the mitochondrial potential in situ in Ehrlich ascites tumor cells. Anticancer Res 16, 419-23.

Quignon, F., De Bels, F., Koken, M., Feunteun, J., Ameisen, J., and de The, H. (1998). PML induces a novel caspase-independent death process. Nature Genetics 20, 259-265.

Rassow, J., Guiard, B., Wienhues, U., Herzog, V., Hartl, F. U., and Neupert, W. (1989). Translocation arrest by reversible folding of a precursor protein imported into mitochondria. A means to quantitate translocation contact sites. J Cell Biol 109, 1421-8.

Ratych, R. E., Chuknyiska, R. S., and Bulkley, G. B. (1987). The primary localization of free radical generation after anoxia/reoxygenation in isolated endothelial cells. Surgery 102, 122-31.

Rinner, W. A., Pifl, C., Lassmann, H., and Hortnagl, H. (1997). Induction of apoptosis in vitro and in vivo by the cholinergic neurotoxin ethylcholine aziridinium. Neuroscience 79, 535-42.

Riparbelli, M. G., Callaini, G., Tripodi, S. A., Cintorino, M., Tosi, P., and Dallai, R. (1995). Localization of the Bcl-2 protein to the outer mitochondrial membrane by electron microscopy. Exp Cell Res 221, 363-9.

Rodriguez-Pena, A., Botana, M., Gonzalez, M., and Requejo, F. (1995). Expression of neurotrophins and their receptors in sciatic nerve of experimentally diabetic rats. Neurosci Lett 200, 37-40.

Romero, F. J., Monsalve, E., Hermenegildo, C., Puertas, F. J., Higueras, V., Nies, E., Segura Aguilar, J., and Roma, J. (1991). Oxygen toxicity in the nervous tissue: comparison of the antioxidant defense of rat brain and sciatic nerve. Neurochem Res 16, 157-61.

Romero, F. J., Segura Aguilar, J., Monsalve, E., Hermenegildo, C., Nies, E., Puertas, F. J., and Roma, J. (1990). Antioxidant and glutathione-related enzymatic activities in rat sciatic nerve. Neurotoxicol Teratol 12, 603-5.

Russell, J. W., Karnes, J. L., and Dyck, P. J. (1996). Sural nerve myelinated fiber density differences associated with meaningful changes in clinical and electrophysiologic measurements. J Neurol Sci 135, 114-7.

Russell, J. W., Sullivan, K., Herrmann, D., and Feldman, E. L. (1998). IGF-I prevents loss of mitochondrial integrity in hyperglycemic neuronal cell death. In Soc Neurosci Abstr, pp. 276.

Sagara, M., Satoh, J., Wada, R., Yagihashi, S., Takahashi, K., Fukuzawa, M., Muto, G., Muto, Y., and Toyota, T. (1996). Inhibition of development of peripheral neuropathy in streptozotocin-induced diabetic rats with N-acetylcysteine. Diabetologia 39, 263-9.

Said, G., Goulon Goeau, C., Lacroix, C., and Moulonguet, A. (1994). Nerve biopsy findings in different patterns of proximal diabetic neuropathy. Ann Neurol 35, 559-69.

Salzer, J. L., and Bunge, R. P. (1980). Studies of Schwann cell proliferation. I. An analysis in tissue culture of proliferation during development, Wallerian degeneration, and direct injury. J Cell Biol 84, 739-52.

Sattler, M., Liang, H., Nettesheim, D., Meadows, R. P., Harlan, J. E., Eberstadt, M., Yoon, H. S., Shuker, S. B., Chang, B. S., Minn, A. J., Thompson, C. B., and

Fesik, S. W. (1997). Structure of Bcl-xL-Bak peptide complex: recognition between regulators of apoptosis. Science 275, 983-6.

Saunders, P. A., Chalecka Franaszek, E., and Chuang, D. M. (1997). Subcellular distribution of glyceraldehyde-3-phosphate dehydrogenase in cerebellar granule cells undergoing cytosine arabinoside-induced apoptosis. J Neurochem 69, 1820-8.

Saura, J., MacGibbon, G., and Dragunow, M. (1997). Etoposide-induced PC12 cell death: apoptotic morphology without oligonucleosomal DNA fragmentation or dependency upon de novo protein synthesis. Brain Res Mol Brain Res 48, 382-8.

Schulz, J. B., Beinroth, S., Weller, M., Wullner, U., and Klockgether, T. (1998). Endonucleolytic DNA fragmentation is not required for apoptosis of cultured rat cerebellar granule neurons. Neurosci Lett 245, 9-12.

Seniuk, N., Altares, M., Dunn, R., and Richardson, P. M. (1992). Decreased synthesis of ciliary neurotrophic factor in degenerating peripheral nerves. Brain Res 572, 300-2.

Shaw, P. (1994). Deconvolution in 3-D optical microscopy. Histochem J 26, 687-94.

Siesjo, B. K. (1988). Hypoglycemia, brain metabolism, and brain damage. Diabetes Metab Rev 4, 113-44.

Sima, A. A. (1996). Metabolic alterations of peripheral nerve in diabetes. Semin Neurol 16, 129-37.

Sima, A. A., Greene, D. A., Brown, M. B., Hohman, T. C., Hicks, D., Graepel, G. J., Bochenek, W. J., Beg, M., and Gonen, B. (1993). Effect of hyperglycemia and the aldose reductase inhibitor tolrestat on sural nerve biochemistry and morphometry in advanced diabetic peripheral polyneuropathy. The Tolrestat Study Group. J Diabetes Complications 7, 157-69.

Sima, A. A., Lattimer, S. A., Yagihashi, S., and Greene, D. A. (1986). Axo-glial dysjunction. A novel structural lesion that accounts for poorly reversible slowing of nerve conduction in the spontaneously diabetic bio-breeding rat. J Clin Invest 77, 474-84.

Sima, A. A., Nathaniel, V., Bril, V., McEwen, T. A., and Greene, D. A. (1988). Histopathological heterogeneity of neuropathy in insulin-dependent and non-insulin-dependent diabetes, and demonstration of axo-glial dysjunction in human diabetic neuropathy. J Clin Invest 81, 349-64.

Singleton, J. R., Dixit, V. M., and Feldman, E. L. (1996). Type I insulin-like growth factor receptor activation regulates apoptotic proteins. J Biol Chem 271, 31791-31794.

Sirover, M. A. (1997). Role of the glycolytic protein, glyceraldehyde-3-phosphate dehydrogenase, in normal cell function and in cell pathology. J Cell Biochem 66, 133-40.

Sobue, G., and Pleasure, D. (1985). Adhesion of axolemmal fragments to Schwann cells: a signal- and target-specific process closely linked to axolemmal induction of Schwann cell mitosis. J Neurosci 5, 379-87.

Sondell, M., Fex-Svenningsen, A., and Kanje, M. (1997). The insulin-like growth factors I and II stimulate proliferation of different types of Schwann cells. Neuroreport 8, 2871-6.

Srinivasan, S., and Wiley, J. W. (1997). Evidence for altered mitochondrial function in an insulin deficient model of diabetes mellitus. Soc Neurosci Abstr, pp. 395.

Starr, R., Attema, B., DeVries, G. H., and Monteiro, M. J. (1996). Neurofilament phosphorylation is modulated by myelination. J Neurosci Res 44, 328-37.

Stemple, D. L., and Anderson, D. J. (1992). Isolation of a stem cell for neurons and glia from the mammalian neural crest. Cell 71, 973-85.

Stewart, H. J., Morgan, L., Jessen, K. R., and Mirsky, R. (1993). Changes in DNA synthesis rate in the Schwann cell lineage in vivo are correlated with the precursor–Schwann cell transition and myelination. Eur J Neurosci 5, 1136-44.

Stoll, G., Trapp, B. D., and Griffin, J. W. (1989). Macrophage function during Wallerian degeneration of rat optic nerve: clearance of degenerating myelin and Ia expression. J Neurosci 9, 2327-35.

Strange, K., and Morrison, R. (1992). Volume regulation during recovery from chronic hypertonicity in brain glial cells. Am J Physiol 263, C412-9.

Sugimura, K., and Dyck, P. J. (1982). Multifocal fiber loss in proximal sciatic nerve in symmetric distal diabetic neuropathy. J Neurol Sci 53, 501-9.

Sui, D., and Wilson, J. E. (1997). Structural determinants for the intracellular localization of the isozymes of mammalian hexokinase: intracellular localization of fusion constructs incorporating structural elements from the hexokinase isozymes and the green fluorescent protein. Arch Biochem Biophys 345, 111-25.

Susin, S. A., Zamzami, N., Castedo, M., Hirsch, T., Marchetti, P., Macho, A., Daugas, E., Geuskens, M., and Kroemer, G. (1996). Bcl-2 inhibits the mitochondrial release of an apoptogenic protease. J Exp Med *184*, 1331-41.

Syroid, D., Maycox, P., Burrola, P., Liu, N., Wen, D., Lee, K., Lemke, G., and Kilpatrick, T. (1996). Cell death in the Schwann cell lineage and its regulation by neuregulin. PNAS *93*, 9229-9234.

Syroid, D., Zorick, T., Arbet-Engels, C., Kilpatrick, T., Eckhart, W., and Lemke, G. (1999). A role for insulin-like growth factor-I and the regulation of Schwann cell survival. J Neurosci *19*, 2059-2068.

Tanabe, H., Eguchi, Y., Kamada, S., Martinou, J. C., and Tsujimoto, Y. (1997). Susceptibility of cerebellar granule neurons derived from Bcl-2-deficient and transgenic mice to cell death. Eur J Neurosci *9*, 848-56.

Tanaka, S., Seino, H., Satoh, J., Fujii, N., Rikiishi, H., Zhu, X. P., Takahashi, K., Sagara, M., Nobunaga, T., and Toyota, T. (1992). Increased in vivo production of tumor necrosis factor after development of diabetes in nontreated, long-term diabetic BB rats. Clin Immunol Immunopathol *62*, 258-63.

Tatton, N. A., and Kish, S. J. (1997). In situ detection of apoptotic nuclei in the substantia nigra compacta of 1-methyl-4-phenyl-1,2,3,6-tetrahydropyridine-treated mice using terminal deoxynucleotidyl transferase labelling and acridine orange staining. Neuroscience *77*, 1037-48.

Tatton, N. A., Maclean-Fraser, A., Tatton, W. G., Peral, D. P., and Olanow, C. W. (1998). A fluorescent double-labeling method to detect and confirm apoptotic nuclei in Parkinson's disease. Ann Neurol *44*, S142-S148.

Tatton, W. G., and Chalmers Redman, R. M. (1996). Modulation of gene expression rather than monoamine oxidase inhibition: (-)-deprenyl-related compounds in controlling neurodegeneration. Neurology *47*, S171-83.

Tatton, W. G., Chalmers Redman, R. M., Ju, W. Y., Wadia, J., and Tatton, N. A. (1997). Apoptosis in neurodegenerative disorders: potential for therapy by modifying gene transcription. J Neural Transm Suppl *49*, 245-68.

Tatton, W. G., Ju, W. Y., Holland, D. P., Tai, C., and Kwan, M. (1994). (-)-Deprenyl reduces PC12 cell apoptosis by inducing new protein synthesis. J Neurochem *63*, 1572-5.

Tesfaye, S., Stevens, L. K., Stephenson, J. M., Fuller, J. H., Plater, M., Ionescu Tirgoviste, C., Nuber, A., Pozza, G., and Ward, J. D. (1996). Prevalence of diabetic peripheral neuropathy and its relation to glycaemic control and potential

risk factors: the EURODIAB IDDM Complications Study. Diabetologia 39, 1377-84.

Thomas, P. K., Beamish, N. G., Small, J. R., King, R. H., Tesfaye, S., Ward, J. D., Tsigos, C., Young, R. J., and Boulton, A. J. (1996). Paranodal structure in diabetic sensory polyneuropathy. Acta Neuropathol Berl 92, 614-20.

Trapp, B. D., Andrews, S. B., Cootauco, C., and Quarles, R. (1989). The myelin-associated glycoprotein is enriched in multivesicular bodies and periaxonal membranes of actively myelinating oligodendrocytes. J Cell Biol 109, 2417-26.

Troni, W., Carta, Q., Cantello, R., Caselle, M. T., and Rainero, I. (1984). Peripheral nerve function and metabolic control in diabetes mellitus. Ann Neurol 16, 178-83.

Uehara, T., Kikuchi, Y., and Nomura, Y. (1999). Caspase activation accompanying cytochrome c release from mitochondria is possibly involved in nitric oxide-induced neuronal apoptosis in SH-SY5Y cells. Journal of Neurochemistry 72, 196-205.

Vabnick, I., Novakovic, S. D., Levinson, S. R., Schachner, M., and Shrager, P. (1996). The clustering of axonal sodium channels during development of the peripheral nervous system. J Neurosci 16, 4914-22.

Wadia, J. S., Chalmers Redman, R. M. E., Ju, W. J. H., Carlile, G. W., Phillips, J. L., Fraser, A. D., and Tatton, W. G. (1998). Mitochondrial membrane potential and nuclear changes in apoptosis caused by serum and nerve growth factor withdrawal: time course and modification by (-)-deprenyl. J Neurosci 18, 932-47.

Wagner, R., and Myers, R. R. (1996). Schwann cells produce tumor necrosis factor alpha: expression in injured and non-injured nerves. Neuroscience 73, 625-9.

Walker, P. R., and Sikorska, M. (1997). New aspects of the mechanism of DNA fragmentation in apoptosis. Biochem Cell Biol 75, 287-99.

Watkins, P. J., Gayle, C., Alsanjari, N., Scaravilli, F., Zanone, M., and Thomas, P. K. (1995). Severe sensory-autonomic neuropathy and endocrinopathy in insulin-dependent diabetes. QJM 88, 795-804.

Webster, H., Martin, R., and O'Connell, M. (1973). The relationship between interphase Schwann cells and axons before myelination: A quantitative electron microscopic study. Developmental Biology 32, 401-416.

Weiler, U., Riesinger, I., Knoll, G., and Brdiczka, D. (1985). The regulation of mitochondrial-bound hexokinases in the liver. Biochem Med 33, 223-35.

Weis, J., Dimpfel, W., and Schroder, J. M. (1995). Nerve conduction changes and fine structural alterations of extra- and intrafusal muscle and nerve fibers in streptozotocin diabetic rats. Muscle Nerve 18, 175-84.

Whitworth, I. H., Terenghi, G., Green, C. J., Brown, R. A., Stevens, E., and Tomlinson, D. R. (1995). Targeted delivery of nerve growth factor via fibronectin conduits assists nerve regeneration in control and diabetic rats. Eur J Neurosci 7, 2220-5.

Wicker, U., Bucheler, K., Gellerich, F. N., Wagner, M., Kapischke, M., and Brdiczka, D. (1993). Effect of macromolecules on the structure of the mitochondrial inter-membrane space and the regulation of hexokinase. Biochim Biophys Acta 1142, 228-39.

Williamson, J. R., Chang, K., Frangos, M., Hasan, K. S., Ido, Y., Kawamura, T., Nyengaard, J., Van Den Enden, M., Kilo, C., and Tilton, R. G. (1993). Hyperglycemic pseudohypoxia and diabetic complications. Diabetes 42, 801-813.

Wilson, J. E. (1998). Distinguishing the Type I and Type II isozymes of hexokinase. Diabetes 47, 1544-1548.

Wilson, J. E. (1997). Homologous and heterologous interactions between hexokinase and mitochondrial porin: evolutionary implications. J Bioenerg Biomembr 29, 97-102.

Windebank, A. J., Wood, P., Bunge, R. P., and Dyck, P. J. (1985). Myelination determines the caliber of dorsal root ganglion neurons in culture. J Neurosci 5, 1563-9.

Wink, D. A., Grisham, M. B., Mitchell, J. B., and Ford, P. C. (1996). Direct and indirect effects of nitric oxide in chemical reactions relevant to biology. Methods Enzymol 268, 12-31.

Wolter, K. G., Hsu, Y. T., Smith, C. L., Nechushtan, A., Xi, X. G., and Youle, R. J. (1997). Movement of Bax from the cytosol to mitochondria during apoptosis. J Cell Biol 139, 1281-92.

Wolvetang, E. J., Johnson, K. L., Krauer, K., Ralph, S. J., and Linnane, A. W. (1994). Mitochondrial respiratory chain inhibitors induce apoptosis. FEBS Lett 339, 40-4.

Wu, R. M., Murphy, D. L., and Chiueh, C. C. (1995). Neuronal protective and rescue effects of deprenyl against MPP+ dopaminergic toxicity. J Neural Transm Gen Sect 100, 53-61.

Wyllie, A. H., Kerr, J. F. R., and Currie, A. R. (1980). Cell death: The significance of apoptosis. Int Rev Cytology 68, 251-306.

Xia, Z., Dickens, M., Raingeaud, J., Davis, R. J., and Greenberg, M. E. (1995). Opposing effects of ERK and JNK-p38 MAP kinases on apoptosis. Science 270, 1326-31.

Xie, G., and Wilson, J. E. (1990). Tetrameric structure of mitochondrially bound rat brain hexokinase: a crosslinking study. Arch Biochem Biophys 276, 285-93.

Yagihashi, S. (1995). Pathology and pathogenetic mechanisms of diabetic neuropathy. Diabetes Metab Rev 11, 193-225.

Yang, J., Liu, X., Bhalla, K., Kim, C. N., Ibrado, A. M., Cai, J., Peng, T. I., Jones, D. P., and Wang, X. (1997). Prevention of apoptosis by Bcl-2: release of cytochrome c from mitochondria blocked. Science 275, 1129-32.

Zamzami, N., Brenner, C., Marzo, I., Susin, S., and Kroemer, G. (1998). Subcellular and submitochondrial mode of action of bcl-2-like oncoproteins. Oncogene 16, 2265-2282.

Zamzami, N., Marchetti, P., Castedo, M., Decaudin, D., Macho, A., Hirsch, T., Susin, S. A., Petit, P. X., Mignotte, B., and Kroemer, G. (1995). Sequential reduction of mitochondrial transmembrane potential and generation of reactive oxygen species in early programmed cell death. J Exp Med 182, 367-77.

Zamzami, N., Marchetti, P., Castedo, M., Hirsch, T., Susin, S. A., Masse, B., and Kroemer, G. (1996). Inhibitors of permeability transition interfere with the disruption of the mitochondrial transmembrane potential during apoptosis. FEBS Lett 384, 53-7.

Zamzami, N., Marchetti, P., Castedo, M., Zanin, C., Vayssiere, J. L., Petit, P. X., and Kroemer, G. (1995). Reduction in mitochondrial potential constitutes an early irreversible step of programmed lymphocyte death in vivo. J Exp Med 181, 1661-72.

Zamzami, N., Susin, S. A., Marchetti, P., Hirsch, T., Gomez Monterrey, I., Castedo, M., and Kroemer, G. (1996). Mitochondrial control of nuclear apoptosis. J Exp Med 183, 1533-44.

Zhu, W., Cowie, A., Wasfy, G. W., Penn, L. Z., Leber, B., and Andrews, D. W. (1996). Bcl-2 mutants with restricted subcellular location reveal spatially distinct pathways for apoptosis in different cell types. EMBO J 15, 4130-41.

Zhuang, H. X., Snyder, C. K., Pu, S. F., and Ishii, D. N. (1996). Insulin-like growth factors reverse or arrest diabetic neuropathy: effects on hyperalgesia and impaired nerve regeneration in rats. Exp Neurol *140*, 198-205.

Zoratti, M., and Szabo, I. (1995). The mitochondrial permeability transition. Biochim Biophys Acta *1241*, 139-76.